STUDY OF POLYSTYRENE-ALUMINA AND POLYSTYRENE-TITANIA COMPOSITES AS SUBSTRATE FOR MICROSTRIP LINE AND RESONATOR IN C- AND X- BANDS

THESIS SUBMITTED TO

TEZPUR UNIVERSITY

IN FULFILLMENT OF THE REQUIREMENTS

FOR THE DEGREE OF

DOCTOR OF PHILOSOPHY

JUTI RANI DEKA

**DEPARTMENT OF PHYSICS
TEZPUR UNIVERSITY
ASSAM 784028**

DECEMBER, 2004

To

My Beloved Parents

Mr. Parikshit Deka

And

Mrs. Binapani Deka

whose encouragement, strength and support is the prime inspiration behind this work

Department of Physics
Tezpur University

Napaam, Tezpur 784 028
Assam, India
Phone : +91-3712-267006/7/9
Extn. 5555 (O)
: +91-3712-267083 (R)
Fax : +91-3712-267005/6
e-mail : nidhi@tezu.ernet.in
nidhi_tu@yahoo.com

Dr. Nidhi S. Bhattacharyya
Reader

CERTIFICATE

This is to certify that the thesis entitled **"Study of Polystyrene-Alumina and Polystyrene-Titania Composites as Substrate for Microstrip Line and Resonator in C- and X- Bands"** being submitted by **Juti Rani Deka** to Tezpur University, Tezpur, Assam in fulfillment of the requirements for the award of the degree of Doctor of Philosophy, is a record of original bonafide research work carried out by her. She has worked under my guidance and supervision and has fulfilled the requirements for the submission of this thesis. The results contained in the thesis have not been submitted in part or full to any other university or institute for award of any degree or diploma.

Dated : December 20, 2004

(Nidhi Saxena Bhattacharyya)

DECLARATION

I hereby declare that the thesis entitled **"Study of Polystyrene-Alumina and Polystyrene-Titania Composites as Substrate for Microstrip Line and Resonator in C- and X- Bands"** being submitted to the Department of Physics, Tezpur University, Tezpur, Assam in fulfillment of the requirements for the award of the degree of Doctor of Philosophy, has previously not formed the basis for the award of any degree, diploma, associateship, fellowship or any other similar title or recognition.

Dated: 20.12.2004.

(Juti Rani Deka)

Department of Physics,
Tezpur University,
Tezpur-784 028 (Assam)

PREFACE

Major new applications for terrestrial and satellite communication technology using composite materials are springing up at an ever increasing pace. Development of composite material has become an important aspect. The purpose of the present investigation was to fabricate and study application of polystyrene-alumina and polystyrene-titania composites for microwave devices. Properties of polymer composite can be tailored by varying shape, size, dielectric properties and volume fractions of the constituents in the composite. It is impossible to develop a composite material with the entire ideal characteristic, an attempt has been made to develop and examine composite material encompassing all the desired properties.

Chapter I of the thesis introduces the subject giving a general insight to various polymer composites and its microwave device application. Chapter II deals with the various steps involved in developing the automation of microwave measurement system. Chapter III depicts with the composites preparation technique and concentrates on the essential properties -physical, thermal and microstructural of the composite system. Permittivity and loss factor, which is the most important parameter for microwave devices, have been studied in Chapter IV. Chapter V concentrates on the theoretical modeling of the microstrip line on composite substrate. Chapter VI and VII essentially devote to the study of composite material prepared in the present investigation, for device applications. The design problems of two such devices are considered and its behaviors associated to various phenomenons at microwave frequencies are studied. It highlights two different fabrication techniques giving easy, cost effective and accurate results. Finally Chapter VIII gives concluding remarks of the thesis.

(Juti Rani Deka)

CONTENTS

CHAPTER VII   DESIGN AND FABRICATION OF MICROSTRIP REFLECTION TYPE RADIAL STUB RESONATOR

CHAPTER VIII   ACHIEVEMENTS, LIMITATIONS AND FUTURE DIRECTIONS

CHAPTER I

INTRODUCTION AND HISTORICAL PERSPECTIVE

1.1 Introduction

1.2 Particulate Composites as Substrate in Microwave Integrated Circuit

1.2.1 Composites in general

1.2.2 Present scenario in microwave application

1.2.3 Requirements of composites as microwave integrated circuit substrate

1.3 Present Investigation and Thesis Organization

References

1.1 INTRODUCTION

Microwave frequencies are the mainstay in the present day wireless communication systems. In the last few decades miniaturization of the systems and components have become imperative. The need is for development of better performing planar structures including interconnecting lines and passive components. Microwave circuits are making enormous strides in regard to their performance and other characteristics.

Substrates play a pre-eminent role in the design of devices in microwave circuits like printed circuit board (PCB), monolithic microwave integrated circuits (MMICs) and microwave integrated circuits (MICs). The characteristics which enhance performance of these circuits are high permittivity, low loss etc. Other properties, which can make a material suitable for such applications are higher thermal conductivity, lower thermal expansion coefficient, high quality surface adhesion for metallization, smooth surface finish and flatness of the material.

The recent strides in polymer technology have spawned enormous application possibilities of polymers as microwave substrate materials. Customized fabrication of polymer composite materials with characteristics and controlled parameters are finding new applications in areas of aeronautics, space and telecommunications technology and are evolving at an ever-increasing pace.

Polymers as substrate materials have advantages of design flexibility, lightweight, low cost, good surface adhesion for metallization, corrosion resistance and high strength to stiffness ratio [1]. However, It suffers from poor microwave dielectric properties apart from having poor dimensional stability and heat dissipation when compared with other microwave material choices viz. ceramics and ferrites [2-3]. In conventional engineering thermoplastics, polymers are reinforced with fillers to form composites, which modify other specific functional properties [4-9]. Fillers are also used to tailor specific microwave properties [10-11].

1

Particle-filled polymer composites have currently generated a great deal of technological interest as by simply altering the quantity, distribution and microstructure of the reinforcing phase, the desired microwave characteristics can be controlled. Moreover, the process for mass production of such particle filled composites is efficient and economical [12].

Study of propagation of electromagnetic waves in these composites, provide an insights in the optimization of these materials for a given microwave application. The effective electromagnetic properties of the composite materials depend on dielectric properties and intrinsic microscopic properties of each phase and homogeneity of distribution of filler in polymer matrix [10].

1.2 PARTICULATE COMPOSITES AS SUBSTRATES IN MICROWAVE INTEGRATED CIRCUITS

In adapting filled composites for microwave applications it is important to understand composites and to control and optimize them to get the best performance at microwave frequencies.

1.2.1 Composites in General

Composites are combinations of two materials in which one of the materials, called the reinforcing phase, is in the form of fiber sheets or particles embedded in the other material called the matrix phase. The reinforcing material and the matrix material can be metal, ceramic or polymer. Typically, reinforcing materials are strong with low densities while the matrix is usually a ductile and tough material. The strength of the composite depends primarily on the amount, arrangement and type of particles used as reinforcers in the polymer. In addition, the composite is often formulated with fillers and additives that change processing or performance parameters. Thus the composite can achieve a

combination of desirable properties which are not available in any single conventional material.

Composites could be characterized as [13]

• Particle-reinforced composites

• Fiber-reinforced composites

• Structural composites

Particle Reinforced Composites

In particle reinforced composites, particles used for reinforcing include ceramics, glasses e.g small mineral particles, metal particles e.g aluminum, and amorphous materials, including polymers and carbon black. Particles are used to increase the modulus of the matrix but decreases permeability and ductility of the matrix. The effective utilization of the particle reinforced polymers depends strongly on the ability to disperse the particles homogenously throughout the matrix. Interfacial properties strongly affect the characteristic and performance of the composite.

One of the most attractive features of these particulate composite is that their dielectric properties can be varied over a wide range by the choice of the shape, size and connectivity of the constituents in the polymer matrix. The use of particle in polymer matrix can produce inexpensive composites.

Fiber-Reinforced Composites

Reinforcing fibers can be made of metals, ceramics, glasses or polymers and carbon fibers. Fibers increase the modulus of the matrix material. The strong covalent bonds along the fiber's length give them a very high modulus in this direction. Fibers are difficult to process into composites, which makes fiber-reinforced composites relatively expensive.

Structural Composites

The properties of structural composites depend on constituents and geometrical design. Common structural composite types are laminar and sandwich panel. Laminar is composed of two-dimensional sheets or panels that have a preferred high strength direction. Sandwich panel consists of two strong outer sheets, which are called face sheets and may be made of aluminum alloys, fiber reinforced plastics, titanium alloys or steel. Face sheets carry most of the loading and stresses.

1.2.2 Present Scenario in Microwave Applications

Polytetrafluroethylene (PTFE), glass reinforced polystyrene, polyphenyleneoxide (PPO) and air filled polyethylene, find wide uses in microwave circuits, antennas in satellite-broadcast receivers and linear amplifiers in mobile telephones [14-18]. From the wide group of polymers - PTFE which is also commonly known as RT/Duroid® is the first grade of fiber reinforced polymer composite developed in 1949 by M/s Rogers Corporation. In 1953, glass micro-fiber and ceramic fiber reinforced PTFE materials were developed. Fiber reinforced polymer entered into the domain of space technology with the use of Duroid ® 5600 in Jupiter Space vehicle in1955 [19].

In 1970, a low noise microstrip mixer at 6.0 GHz on polyolefin board with copper/aluminium metal cladding was reported [20]. Some patent publications of fabrication [21-24] on inorganic fillers in polymer matrix for PCBs are found. A simplified fabrication technique for insulated metal substrate with insulating layer of polymer filled with inorganic fillers was published by Shin'chiro Asai et al.[25]. Nakatsugawa and Nishikawa [26] successfully proposed 1: N multiport power dividers using series and parallel division of transmission lines on polyamide/alumina ceramic structure.

A thin film microstrip line (TFMSL) model for practical circuit designed on benzocyclobutene was reported in reference [27]. Marcello Pesare et al. gave analytical

modeling of multilayer structure electronic devices for electro-thermal layout optimization [28].

Due to high mechanical strength and low conductivity as compared to ferrites and other dielectrics, thin 'substrates on plastics materials find ample use in monolithic microwave integrated circuits (MMICs) and also as miniaturized microstrip lines [29].

Applications of the composite polymers at microwave frequencies require microwave characterization. Clausius and Mossotti [30] performed some of the earliest theoretical work on the dielectric properties of composite materials. The application of EM theories for analysis of the particulate composites first appeared in 1935 [31]. Theoretical approaches for microwave characterization for particle filled composite materials, in the last decade [31-37], have met with different degrees of success as their predictions are often contradictory and not adequately supported by experimental evidences.

Baziard et. al. investigated the dielectric properties of aluminium powder-epoxy resin composite [38]. Studies of physicochemical properties and mesostructure in carbon black filled polymer composites were reported in references [39-41]. Lagarkov et al. published experimental studies on dielectric properties of fiber filled composites and proposed scale dependent effective medium theory [42]. Microwave characterization of carbon black and silica in polyethelene matrix was published by Brosseau et al. [43]. A simple theoretical model based on Bruggeman's and Jonscher's model is presented.

Reports have been found on effects of various coupling agents such as silanes, titanates etc. in reducing viscosity of the polymer matrix, with the possibility of increase of filler contents in the composite [44]. Todd and Shi investigated and characterized the effect of chemical coupling agents on the interphase regions at polymer filler interfaces [45]. A molecular basis of interphase dielectric properties with experimental evidence was reported by the same authors [46].

A flexible electromagnetic crystal of ceramic powder (BaTiO$_3$) filled thermoplastic elastomer (EPDM TPE) having high dielectric constant (approximately 9) and low loss

tangent (less than 0.01) [47] was reported. Recently, Moulart et al. published work on the dielectric and conductive properties of thermoplastic (ABS) composites filled with ceramic powder (barium titanate), conductive powders (carbon black, copper) and conductive fibers (carbon, steel) for use in electromagnetic crystals and microwave devices [48].

1.2.3 Requirements of Composites as Microwave Integrated Circuit Substrate

As mentioned in section 1.1, for a material to be used as substrate for MIC applications, the crucial parameters to be considered are complex permittivity and thermal properties of the material. In addition, design flexibility, high quality surface adhesion for metallization, smooth surface finish and uniformity, lightweight and low cost of production of materials, are important considerations.

Most polymers consist of very long non-polar molecules which have minimal dielectric response and therefore low permittivity. Loss in most polymers results primarily from defects due to free radicals [50]. Low loss materials usually have low permanent dipole moment. Although they may possess an appreciable induced dipole moment. As low loss material possess high Q factor, device attenuation of the device on composite substrates should be low in comparison to the ceramic.

For choosing composites for microwave applications important properties to be examined are,

(i) insertion loss of the device

(ii) phase velocity of the transmitted signal

(iii) quality factor and

(iv) attenuation.

It is important that the composite system is useful over a broad microwave frequency range of interest. The insertion loss characteristic reflects the ability to transmit

percentage of microwave power at the designed frequency. Higher the permittivity of the material, higher is the transmitted power [49]. Higher value of dielectric constant reduces the guided wavelength which increases the phase velocity. It is desirable for the materials to have good thermal conductivity and low coefficient of thermal expansion.

1.3 PRESENT INVESTIGATION AND THESIS ORGANIZATION

With a view to optimize most of the desirable properties of the composite system for microwave device applications, the following polymer –particle filled composite systems

(i)   Polystyrene – alumina

(ii)   Polystyrene – titania

are investigated. Polystyrene is used as matrix in the composite systems because of the ease with which it bonds with metals apart from having low dielectric loss at radio frequencies [51]. To improve the dielectric, thermal and mechanical properties of polystyrene, alumina/titania is added in different volume fractions. Surfactant is added to the composite systems to enhance physical wetting and reduce the interphase region.

Studied of microwave, thermal, mechanical and microstructural properties of the composite systems with varying content of filler particles are conducted. The investigation on composite systems has shown an enhancement in dielectric properties, dimensional stability and thermal properties in comparison to polymer matrix. The materials are used in devices to ascertain their utility as substrate materials. A broad outline of contents of each chapter is presented in the following paragraphs.

To measure the insertion loss of the device and carry out microwave characterization more precisely and accurately with less time, the existing manual microwave measurement setup is completely computerized including development of both hardware and software. This has not only enhanced the repeatability and accuracy of the results but also facilitated the obtaining of large amount of experimental data with ease

and speed. **Chapter II** describes different steps involved in automation of the microwave measurement setup in X-band.

In the present investigation polystyrene is used as the parent material to which alumina and titania are added in different volume fraction. Preparation technique of the two composite systems has been discussed in **Chapter III**. The chapter also includes microstructural studies viz. XRD, SEM, optical micrographs, to determine the shape, size and distribution of the constituents in the composite. IR studies are performed to examine any chance of chemical bonding between polymer and filler. Densification, thermal conductivity, and thermal expansion coefficient studies are conducted on these materials to analyze their device applicability at microwave frequencies.

For any microwave application, it is of utmost importance to measure the permittivity and dielectric loss of the material at microwave frequencies. Determination of microwave properties of the composites is done using different measurement techniques viz. cavity resonator technique, waveguide or double minima method and resonance method to minimize errors and enhance reliability of experimental results. As frequency dependence of dielectric constant gives rise to 'material dispersion' in which the wave velocity is frequency dependent, the dispersive permittivity of the two composite systems are also measured with the waveguide and resonator method. Effective medium theory is applied to analytical interpretation of experimental results. **Chapter IV** portrays experimental investigation of microwave permittivity of the composites.

Microwave devices are designed and fabricated using the substrate material developed. In **Chapter V**, Spectral Domain Technique (SDT) is applied on the composite substrates. This technique presents straightforward algebraic solutions of the homogenous equations for the spectral domain Green's function and quite accurate results for the propagation constant [52-57]. Galerkin's method is used to yield homogenous systems of equations. The behavior of a microstrip transmission line is investigated using SDT. Instead of taking composite material as single layer with uniform permittivity value, it is

considered as two layers consisting of polymer and filler in one unit cell. The whole structure is considered to be having such many polymer-filler unit cells. The size and distribution of these cells are determined from micro-structural studies conducted in chapter III.

Chapter VI and VII essentially devotes to the study of composite materials prepared in the present investigation for device applications. Microwave integrated circuit on the composite materials is realized in C- and X-bands. Insertion loss and propagation constant measurements are carried out. The results obtained are analyzed with the Spectral Domain Technique Modified for Composite (MSDTC) materials, developed in chapter V and the conventional SDT approach.

A microstrip reflection-type radial stub resonator (RRSR) is designed and fabricated on the two composite systems and its resonance behavior is studied in the X-band. Radial stubs on the circumference of circular disc resonators not only influence the resonance frequency but significantly reduces the dimensions. The fabrication is done with hot press method, which gives an easy, cheap and quite accurate method to transfer the computer artwork on metallized composite substrates. The resonator is center fed and scattering parameters (S_{11}) are measured shorting the stubs at $\lambda_g/2$, $\lambda_g/3$ and coupling adjacent stubs. The results are presented in chapter VII of the dissertation.

Chapter VIII, the last chapter gives a summary of the suitability of the new composite materials as substrates in microwave applications. It also highlights the limitations and improvements that can be incorporated and unfolds the prospect of the studies conducted in this investigation.

References:

[1] V. R. K. Murthy, S. Sunderam and B. Viswanathan, "Materials and Technology for Microwave Integrated Circuits," Microwave Materials, pp- 30, Narosa Publishing House, New Delhi, 1993.

[2] S. Harold, "Applications of Integrated Circuit Technology to Microwave Frequencies," Proc. IEEE, vol. 59, pp- 1200, 1971.

[3] N. Afser, "Precision Dielectric Measurements of Nonpolar Polymers in the Millimeter Wavelength Range," IEEE Trans Microwave Theory and Techniques, vol. 33, pp- 1410, 1985.

[4] M. Xanthos, "MICA: Filler/ Reinforcement in Flake Form," Plastic Compounding (July/August), 1979.

[5] M. J. Balow and D. C. Fuccella, "Hybridization of Reinforcement to Optimize Part Performance and Molding in Reinforced Thermoplastics," Polymer-Plastic Technology Engineering, vol. 20, pp-13, 1983.

[6] J. R. Copeland and W. O. Rush, "Wollastonite: Short – Fiber Filler/ Reinforcement," Plastic Compounding", vol. 1, pp- 26, 1978.

[7] G. J. L. Griffin, "Orientation Effects in Filled Plastics Bearing Materials," ASLE Trans, vol. 15, pp- 171, 1972.

[8] J. Runt and C. E. Galgoci, "Polymer Piezoelectric Ceramic Composites: Polystyrene and Poly(methyl metharylate) with PZT," Journal of Applied Polymer Science, vol. 29, pp- 611, 1984.

[9] J. Runt and C. E. Galgoci, "Piezoelectric Composite of PZT and Some Semicrystalline Polymers," Materisal Research Bulletin, vol. 19, pp- 253, 1984.

[10] C. A. Brebbia, "The Boundary Element method for Engineers," Pentech Press, London, 1978.

[11] S. Akhtarzad and P. B. Johns, "Three-Dimensional Transmission-Line Matrix Computer Analysis of Microstrip Resonators," IEEE Trans Microwave Theory and Techniques, vol. 23, pp- 990, 1975.

[12] J. B. Donnet, R. C. Bansal and M. J. Wang, "Carbon Black, Science and Technology," edited by Marcel Dekker, New York, 1983.

[13] E. K. Sichel, "Carbon Black- Polymer Composites," Marcel Dekker, New York, 1982.

[14] H. Howe Jr, "Microwave Integrated Circuits-an Historical Perspective," IEEE Trans Microwave Theory and Techniques, vol. 32, pp- 991, 1984.

[15] R. J. Bonfield, "A Modified PTFE Microwave Circuit Substrate," MSN Communication Technology, pp- 36, 1988.

[16] S. Maeda, T. Koseki, T. Horiuchi, M. Itoh and T. Sakamoto, "Polyphenyleneoxide Kei Sekisouban no Kaiha-tsu," Printo Kairogakkai dai3 kai gakujyutsu Kouen Taikai, (in Japanese), pp- 113, 1988.

[17] T. Sakamoto, M. Itoh and S. Maeda, "Kousyuuha Kairo You Doubariban," Densi-Zairyou Besusatsu Jissougijyutsu Shiriizu, (in Japanese), vol. 9, pp- 42, 1988.

[18] T. Sugawara, S. Tazaki and Y. Yamaguchi, "Low Transmission Loss Copper Clad Laminates for Flat Antenna MCL-100S," Hitachi Kasei Tech Report (in Japanese) no 12, pp- 25, 1989.

[19] Report on History of Rogers Corporation, 2002.

[20] B. R. Hallford, "Low-Noise Microstrip Mixer on a Plastic Substrate," IEEE Trans Microwave Theory and Techniques, vol. 16, pp- 1178, 1970.

[21] S. Fujikawa, "Fossojyoshi Sekisou Ban," Japan Kokai (open system) Patent, Syou 62 (1987)-19450, 1987.

[22] H. Misawa and S. Maeda, "Sekisouban," Japan Kokai (open system) Patent Hei 2 (1990)- 50832, 1990.

[23] K. Hasegawa, "Kouyuudenritu Douhari Seki- Souban No Sizouhour," Japan Kokai (open system) Patent Hei 3 (1991)- 221448, 1991.

[24] G. M. Herunandesu, "Kouyuudenritue Nanshitu Shi-to-Zairyou," Japan Kokai (open system) Patent Hei 3 (1991)- 501426, 1991.

[25] S. Asai, M. Funaki, H. Sawa and K. Kato, "Fabrication of an Insulated Metal Substrate (IMS), Having an Insulating Layer with A High Dielectric Constant," IEEE Trans. Comp. Hybrids Mfg. Technology, vol. 16, pp- 499, 1993.

[26] M.I. Nagatsugawa and K. Nishikawa, "A Novel Configuration for 1:N Multiport Power Dividers Using Series/Parallel Transmission-Line Division and A Polyimide/Alumina-Ceramic Structure for HPA Module Implementation," IEEE Trans Microwave Theory and Techniques, vol. 49, pp- 1187, 2001.

[27] F. Schnieder and W. Heinrich, "Model of Thin-Film Microstrip Line for Circuit Design," IEEE Trans Microwave Theory and Technique, vol. 49, pp- 21, 2001.

[28] M. Pesare, A. Giorgio and A. G. Perri, "Analytical Modelling of Multilayer Structure Electronic Devices for Electro-thermal Layout Optimization," International Journal of Numerical Modeling: Electronic Networks, Devices and Fields, vol. 14, pp- 395, 2001.

[29] R. S. Tahim, G. M. Hayashibara and K. Chang, "Design and Performance of W-Band Broadband Integrated Circuit Mixers," IEEE Trans Microwave Theory and Techniques, vol. 31, pp- 277, 1983.

[30] A. Issacs, J. Dainith and E. Martin, "A Dictionary of Science," Oxford University Press, Market House Books Limited, 1999.

[31] D. A. G. Bruggeman, "The Calculation of Various Physical Constants of Heterogeneous Substances. I. The Dielectric Constants and Conductivities of Mixtures Composed of Isotropic Substances," Annalen der Physik (Berlin, Germany) vol. 24, pp- 636, 1935.

[32] D. J. Bergman and D. Stroud, "The Physical Properties of Macroscopically Inhomogeneous Media," Solid State Physics, vol. 46, pp- 148, 1992.

[33] C. Nan, "Physics of Inhomogeneous Inorganic Materials," Progress in Material Science, vol. 37, pp- 1, 1993.

[34] A. Priou, "Dielectric Properties of Heterogeneous Materials," Progress in Electromagnetics Research, Elsevier, New York, 1992.

[35] A. K. Jonscher, "Dielectric Relaxation in Solids," Chelsea Dielectric, London, 1987

[36] A. K. Jonscher, "Universal Relaxation Law," Chelsea Dielectric, London, 1996.

[37] A. K. Jonscher, "Dielectric Relaxation in Solids," Journal of Physics D: Applied Physics, vol. 32, R57,1999.

[38] Y. Baziard, S. Breton, S. Toutain and A. Gourdenne, "Dielectric Properties of Aluminium Powder-Epoxy Resin Composites," European Polymer Journal, vol. 24, pp- 521, 1988.

[39] J. Yacubowicz and M. Narkis, "Dielectric Behavior of Carbon Black Filled Polymer Composites," Polymer Engineering Science, vol. 26, pp- 1568, 1986.

[40] C. Brosseau, F. Boulic, P. Queffelec, C. Bourbigot, Y. Le Mest and J. Loaeca, "Dielectric and Microstructure Properties of Polymer Carbon Black Composites," Journal of Applied Physics, vol. 81, pp- 882, 1997.

[41] F. Boulic, C. Brosseau and Y. L. Mest, "Absorbency Properties and Electron Paramagnetic Resonance Characterization of Polymeric Carbon Black Composites," Journal of Physics D: Applied Physics, vol. 31, pp- 1904, 1998.

[42] A. N. Lagarkov, S. M. Matytsin, K. N. Rozanov, and A. K. Sarychev, "Dielectric Properties of Fiber-filled Composites," Journal of Applied Physics, vol. 84, pp- 3806, 1998.

[43] C. Brosseau, P. Queffelec and P. Talbot, "Microwave Characterization of Filled Polymer," Journal of Applied Physics, vol. 89, pp- 4532, 2001.

13
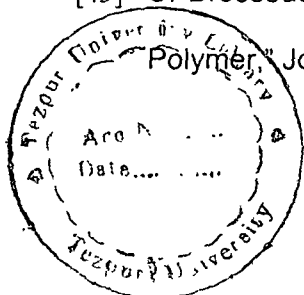
[44] K. L Mittal, "Silanes and Other Coupling Agents," Adhesion Society, vol. 2, 2000.

[45] M. G. Todd and F. G. Shi, "Characterizing the Interphase Dielectric Constant of Polymer Composite Materials: Effect of Chemical Coupling Agents," Journal of Applied Physics, vol. 94, pp- 4551, 2003.

[46] M. G. Todd and F. G. Shi, "Molecular Basis of the Interphase Dielectric Properties of Microelectronic and Opto-Electronic Packaging Materials," IEEE Trans on Components and Packaging Technologies, vol. 26, pp- 667, 2003.

[47] C. Marrett, A. Moulart, J. Colton, and A. Tcharkhtchi, "Flexible Polymer Composite Electromagnetic Crystals," Polymer Engineering and Science, vol. 43, pp- 822, 2003.

[48] A. Moulart, C. Marretta and J. Colton, "Polymeric Composites for use in Electronic and Microwave Devices," Polymer Engineering and Science, vol. 44, pp-588, 2004.

[49] P. A. Rizzi, "Microwave Engineering Passive Circuits," Prentice Hall of India, 1999.

[50] J. B. Jarvis, R. G. Geyer, J. H. Grosvenor, M. D. Janezic, C. A. Jones, B. Riddle and C. M Weil, " Dielectric Characterization of Low-loss Materials A Comparison Technique," IEEE Trans on Dielectrics and Electrical Insulations, vol. 5, pp- 571, 1998.

[51] E. N. Torgow, and J. W. E. Griemamann, "Miniature Strip Transmission Line for Microwave Applications," IEEE Trans Microwave Theory and Techniques, vol. 3, pp. 57, 1955.

[52] E. J. Denlinger, "A Frequency Dependent Solution for Microstrip Transmission Lines," IEEE Trans Microwave Theory and Techniques, vol. 19, pp- 30, 1971.

[53] T. Itoh and R. Mittra, "A Technique for Computing Dispersion Characteristics of Shielded Microstrip Lines," IEEE Trans Microwave Theory and Techniques, vol. 22, pp- 896, 1974.

[54] G. Mur, "A Finite Difference Method for the Solution of Electromagnetic Waveguide Discontinuity Problems," IEEE Trans Microwave Theory and Techniques, vol. 22, pp- 54, 1974.

[55] A. F. Thomson and A. Gopinath, "Calculation of Microstrip Discontinuity Inductances," IEEE Trans Microwave Theory and Techniques, vol. 23, pp- 648, 1975.

[56] N. K. Das, and D. M. Pozar, "A Generalized Spectral Domain Greens Function for Multilayer Dielectric Substrates with Application to Multilayer Transmission Lines," IEEE Trans Microwave Theory and Techniques, vol. 35, pp- 326, 1987.

[57] R. H. Jansen, "A Novel Cad Tool and Concept Compatible with the Requirement of Multilayer GaAs MMIC Technology," IEEE MTT-S Int Microwave Symp. Digest, St. Luis, pp-711, 1985.

CHAPTER II

AUTOMATION OF MICROWAVE MEASUREMENT SETUP

2.1 Introduction

2.2 Insertion Loss Measurement Setup

2.2.1 Microwave source

2.2.2 Microwave bench

2.3 Automation

2.3.1 Sweep measurement and calibration of Gunn oscillator

2.3.2 Driver circuit

2.3.3 Computer interfacing of power meter

2.4 Software Development

2.4.1 Initialization

2.4.2 Main measurement module

2.5 Results

2.1 INTRODUCTION

The X-band insertion loss measurement setup in the laboratory was a manual one and it was tedious and time consuming to carry out measurements. The experimental setup is automated to overcome these limitations.

The design approach and final implementation of both the software and hardware components are detailed in the subsections. There were constraints in the form of paucity of funds and unavailability of components locally. This, on occasions, dictated choice of components and circuit design leading to concepts which otherwise had scope for optimization.

This chapter begins with a brief description of the manual setup followed by detailed discussion on both the software and hardware developed for automation. The automated setup is thoroughly tested for accuracy and repeatability, results of which one included towards the end of this chapter. It is only after detailed evaluation of the system performance that devices and circuits designed and fabricated is tested using this automated system.

2.2 INSERTION LOSS MEASUREMENT SETUP

The setup broadly consists of a microwave power source with frequency range of 8.4GHz-12.0GHz, a microwave bench which guides the microwave power to the device under test and a sensor connected to a power meter to measure the microwave power. The shaded blocks in figure 2.1 are components of the manual measurement setup. These are described in the following sub-sections.

2.2.1 Microwave Source

The vital elements in the gunn diode microwave source are the gunn power supply, gunn oscillator and pin modulator.

16

Gunn power supply (X 110)

The gunn power supply consists of a voltage regulating circuit, which supplies D.C. voltage variable from 0 to 10V and a stable multivibrator, which supplies 1 kHz square wave voltage to the pin modulator. Peak value of the square wave voltage can be varied from 0 to 10V by means of a potentiometer. A Darlington pair increases the current output of D.C. voltage from 100 to 750V maximum. Four zener diodes are used for over voltage protection.

Gunn oscillator (X 2151)

The oscillator has a gunn diode mounted in a cavity WR 90 of high Q that is tuned to the transit time frequency of the gunn diode. The resonant frequency of the cavity is changed by means of a micrometer-controlled plunger. The tuning range of the oscillator is 8.4 to 12.0 GHz. The lead voltage standing wave ratio (VSWR) is maximum 1.5.

PIN modulator (X 451)

The PIN modulator is a transmission line having wave-guide shunted with PIN diode. For negative or zero bias the diode presents very low impedance, thus reflecting the signal. At positive bias the diode presents very high impedance and therefore doesn't affect the signal propagating along the transmission line.The frequency range of operation of the PIN modulator is 8.4 to 12.0 GHz. Maximum radio frequency power is 1 watt. The flange and the wave guide type used are UG- 39 /U and WR- 90 respectively.

2.2.2 Microwave Bench

The power output from the Gunn Oscillator passes through a high power ferrite isolator (model X6021) with the average power handling capacity of about 8 watts. An attenuator is used to vary the power. The attenuated power is fed to the device under test (DUT) via a circulator. The received power through the other port of the circulator is detected by a power sensor (HP 8478B) which is subsequently fed to the power meter.

Calibration of gunn oscillator

The gunn oscillator can be tuned in a broad frequency range from 8.4 to 12.0GHz. This is done by adjusting the micrometer position attached to the plunger in the gunn cavity.

2.3 AUTOMATION

The setup for insertion loss measurement has a Gunn source in X-band where the micrometer has to be adjusted to tune to different frequencies. The adjustment depends on the operator's astute measurement ability, which affected the repeatability and accuracy of the readings. Moreover, no sweep measurement was available and the number of readings was limited because of practical constraints. This also resulted in missing intermediate data between consecutive measurement points and hence potentially critical information. To obtain good repeatability of measured data in the manual set-up, averaging of a number of readings was essential, which required a lot of time and effort. The time for manual measurement extended up to 3-4 hours per set of data and required constant operator intervention. A completely computerized setup is thus developed to overcome these problems. Figure 2.1 gives the block diagram of the automated setup. Final processing of the data can easily be carried out once it is already in the computer which otherwise would have required manual feeding of data.

A PMH stepper motor is used for tuning the Gunn diode in the automated setup. Calibration of the motor steps with the tuning frequency is made through the calibration of micrometer position with frequency meter reading. The output power is picked up from the power meter LED display (ICL 7106). The software is developed in C language. Gear attached to the motor in the automated system could read a minimum discrete frequency of 0.005 GHz, which can simulate an almost continuous sweep. The continuous sweep measurements reduced the measurement time to about 3 minutes. The closer data points provide better details.

This automated system gave excellent repeatability and improved accuracy
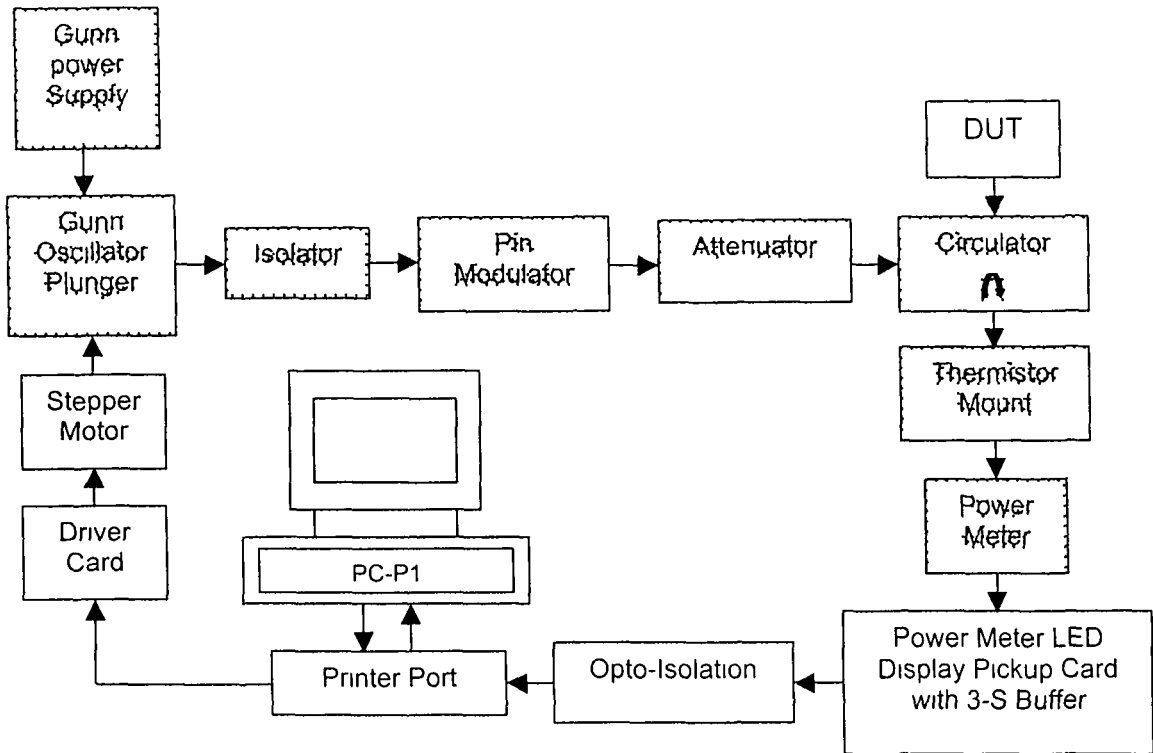
Figure 2.1: PC - Interfaced automated microwave X band set-up
(shaded blocks are components associated with the manual measurement setup)

Micrometer reading (mm)
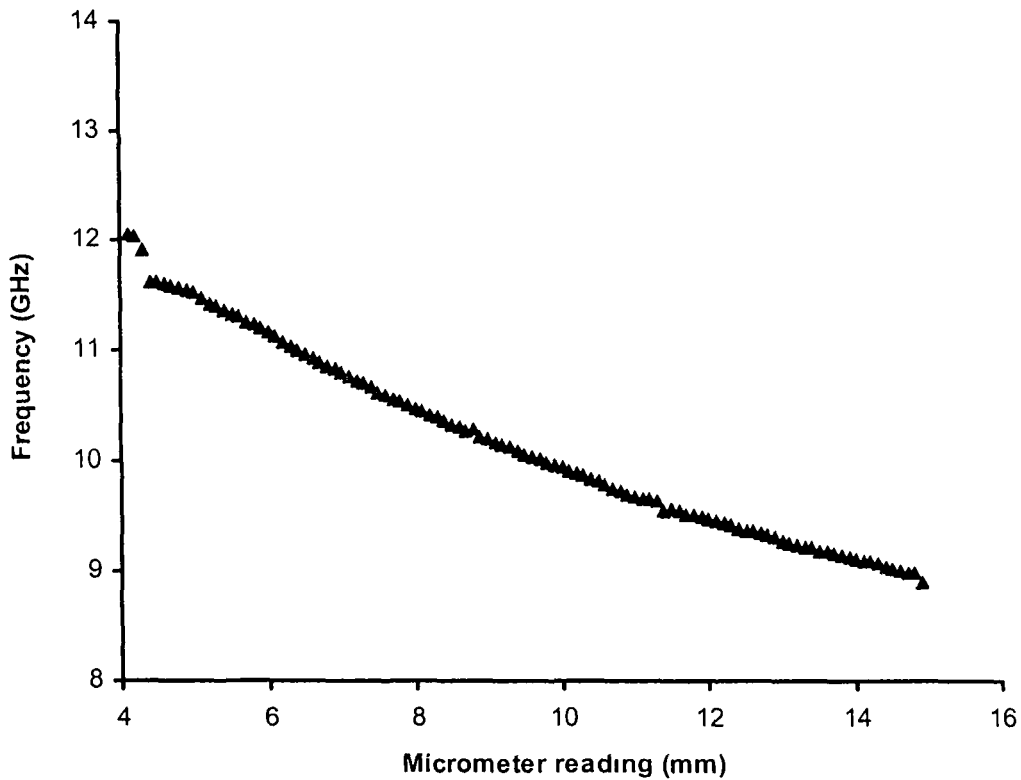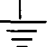
Figure 2.2: Calibration graph of micrometer reading and frequency

19

The LPT1 port of a PC is used as the I/O port obviating the need for purchase of any I/O card. Moreover, the data is picked up from the 7-segment display of the power meter. No additional A/D-D/A card is, therefore, necessary. The approach is to make maximum use of the existing/available hardware although it required customized design of the additional circuitry involving manipulation of the corresponding voltage levels of the segment states of the 7-segment display. The details of the pin configuration of LPT1 are given in table 2.1.

A simple but efficient driver card for stepper motor is designed and fabricated in the laboratory. The power meter digit pick-up card is also designed in the laboratory. The overall cost of automation, excluding the existing equipment, is very low (Approximately Rupees 1500/- about US $33).

Table 2.1: Details of LPT1 pin configuration

LPT1 Pin number	Signal name	Direction 10-13,15	Address
1	Strobe	→ To printer	37A
2-9	Data bit	→ To printer	378H
10-13,15	Acknowledge, Busy, out of paper, select, error	← From printer	379H
14,16,17	Auto line feed, initialize, select-up	→ To printer	37A
18-25	Ground	⏚ From printer	-----

2.3.1 Sweep Measurement and Calibration of Gunn Oscillator

A PMH stepper motor of torque 1.0 kg-cm has been used to rotate the micrometer system attached to the Gunn diode for tuning at different X-band frequencies. Gear attachments with ratio of 85:16, give a frequency setting resolution of 0.005GHz and sufficient torque to rotate the micrometer. Calibration of readings of micrometer to

20
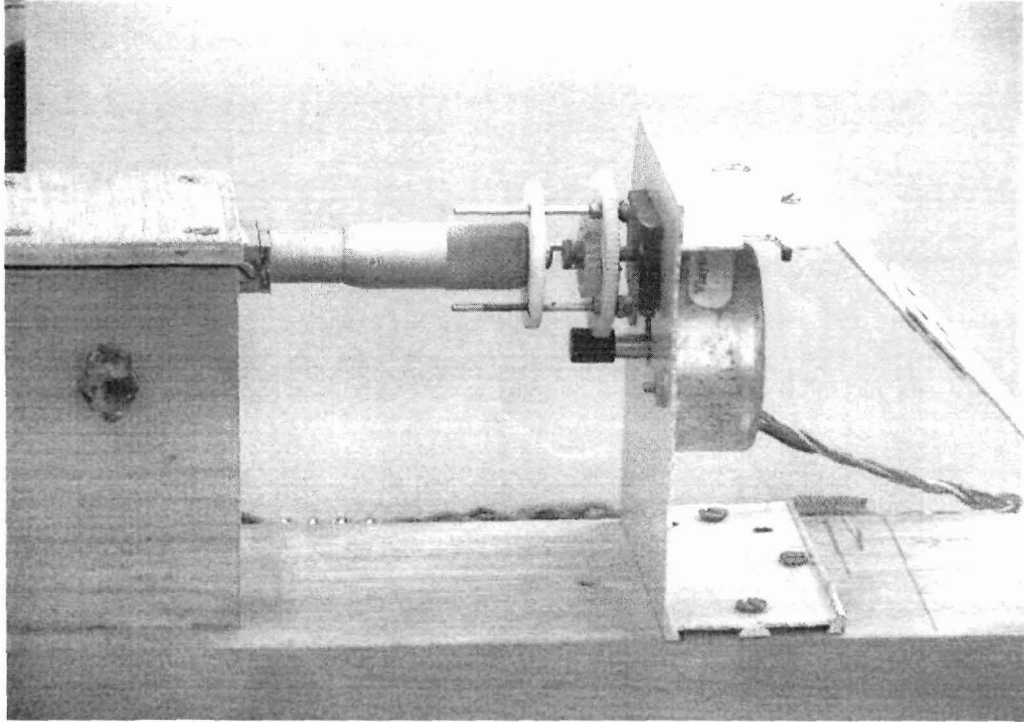
Figure 2.3a: Photograph of the stepper motor attachment with the mount attached to Gunn source.

corresponding frequencies is made as shown in figure 2.2. Then number of steps the motor must be moved to tune the frequency from 8.4-12.0 GHz is calculated using the data which is put in a look-up table data file. The arrangement is shown in figure 2.3a. The relation between number of steps and micrometer reading is found as,

Step angle = 3.75° (in an 8 step sequence)

Total steps for one rotation (of the circular scale of the micrometer)

$$\frac{360°}{3.75°} \times \text{gear ratio} = \frac{360°}{3.75°} \times \frac{85}{16} = 510 \text{ steps}$$

510 steps $\cong$0.5mm (linear micrometer reading traversed in one rotation)

If stepper motor traverses 'N' steps then

21

$$N \text{ steps} = \frac{N \times 0.5}{510} mm$$

By using bisection method on the calibrated frequency-micrometer data the corresponding frequency is evaluated.

2.3.2 Driver Circuit

For excitation of phases of the stepper motor, control signals have to be given in the form of digital pulses, which is converted into precise incremental motion. The circuit diagram of the driver circuit designed is given in figure 2.3b

IRF540 MOSFET is used to as motor winding switches. IRF540 allows fast switching and has very low on-state-resistance. The source is grounded and the drain is connected to a 14V supply via the windings A1, B1, A2 and B2 of the stepper motor. Gates of the MOSFETs are connected to 4 of the 8 bit output pins at port address 0X378 of the printer port LPT1. Details of motor specification are given in table 2.2.
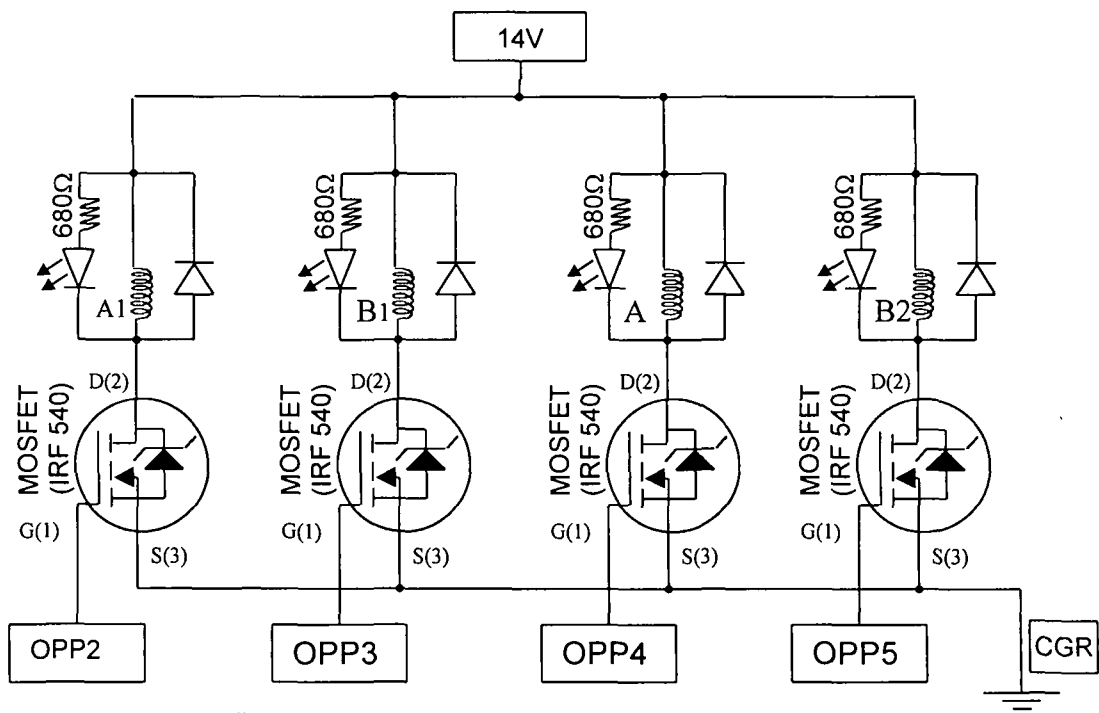
Figure 2.3b: Circuit diagram of the stepper motor driver card
(OPP = Out put of LPT1; CGR = Computer Ground)

22

Table 2.2: Motor specification

Motor type	PMH
Resistance of motor windings	48Ω
Current passing through each winding	0.5A
Torque	1 kg-cm

2.3.3 Interfacing Power Meter Reading to Computer

Figure 2.4 shows the block diagram of power meter LED display pickup card with 3-S buffer. The display had 4 seven segments and three dots.
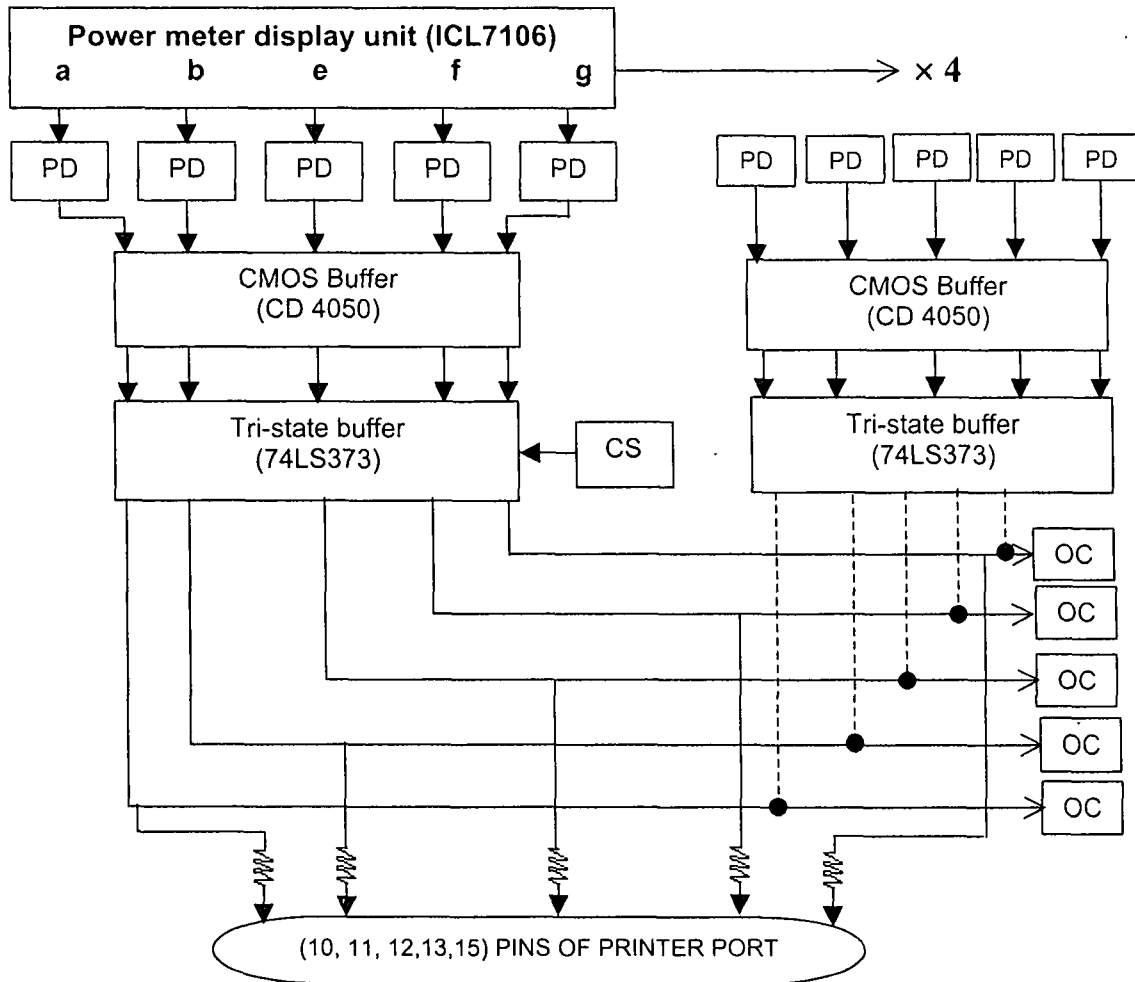
Figure 2.4: Block diagram of power meter LED display pickup card with 3-S Buffer
(PD = Potential divider, OC = Opto-coupler, CS = Chip selection circuit)

23

Chip select circuit of figure 2.5 is designed to eliminate the possibility of more than one tristate buffer (74LS373) getting selected at the same time. Two output pins (6 and 7) of LPT1 port are used for this purpose. The chip selection logic table is given in table2.3.

To identify the digits 0-9, states of only 5 segments (a, b, e, f and g) are needed out of seven segments. Table 2.4a gives the equivalent hexadecimal for the digit read. Hexadecimal equivalent of minus sign and one of the fourth segment and the three dots are given in table 2.4b. An octal 74LS373 tri-state buffer is initially used to pick-up the signal. The TTL tristate buffer inputs are found to load the display ICL 7106 when the segments are read. To overcome the problem, an additional buffer CMOS CD 4050 compatible with the display and which could drive TTL levels is used to pick-up the signals. The transition voltage of the buffer (CD 4050) is 2.6V. A potential divider circuit for proper scaling of the voltage for state transition is done which is 2.4V for low and 4.0V for high. The final outputs from the 74LS373 are 0.02V for low and 4.99V for high. To avoid the computer printer port from picking up stray signals an isolation of computer ground is mandatory. To accomplish this, opto-coupler MCT2E is used. MCT2E is compatible with standard TTL ICs. When the LED segments driven by ICL7106 glows the printer port finally picks it up as high and vice versa.
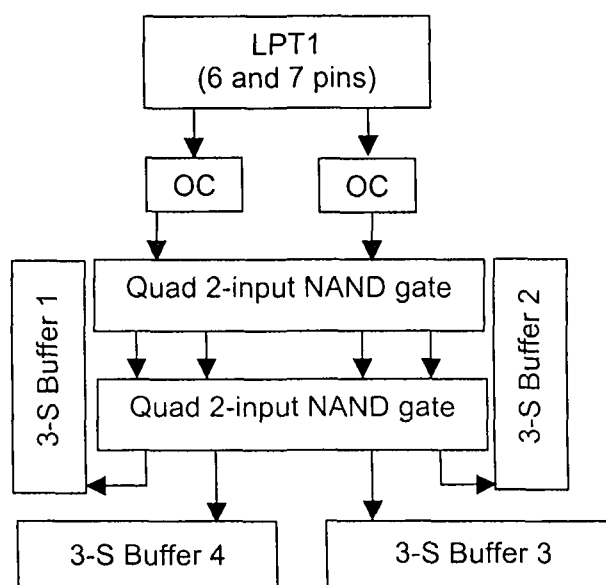
Figure 2.5: Block diagram of chip select circuit

24

The photograph of the PCB for the power meter digital display pick-up card and stepper motor driver card is shown in figure 2.6.

Table 2.3: Chip selection table from LPT1 pins 6and 7

Chip selection address						Decimal Equivalent .
MSB					LSB	
1	1	0	0	0	0	48
1	0	0	0	0	0	32
0	1	0	0	0	0	16
0	0	0	0	0	0	0
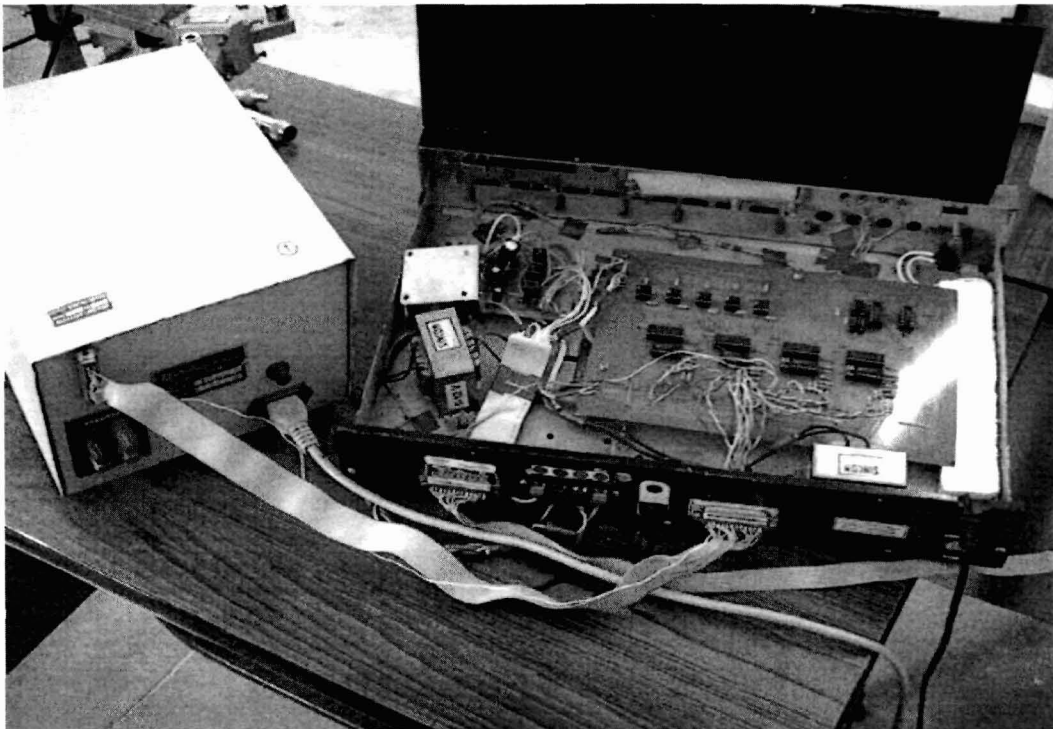
Figure 2.6: Photograph of the PCB ef (mounted) digit pickup and the stepper motor driver card

2.4 SOFTWARE DEVELOPMENT

A program is developed to acquire the transmitted power versus frequency for DUT. An additional module is developed to directly compute the insertion loss and the reflected power. Flowchart of the software developed is shown in figure 2.8. The modules developed are briefly discussed in the following sub-sections.

2.4.1 Initialization

The LPT1 input and output port addresses are 379H and 378H respectively. The frequency-micrometer calibration data are read from the data file (*calf1.dat*). Measured data are stored in a data file (*power1.dat*). The 8 -step motor sequences are written in this section. The micrometer is set only once manually (after the system is developed) at

Table 2.4 a: Hexadecimal equivalent of LED segment

Display	Logical State of the Segment					Hexadecimal Code
	a	b	e	f	g	
0	1	1	1	1	0	0XC70
1	0	1	0	0	0	0XC00
2	1	1	1	0	1	0XC68
3	1	1	0	0	1	0XC48
4	0	1	0	1	1	0XC18
5	1	0	0	1	1	0XCD8
6	1	0	1	1	1	0XCF8
7	1	1	0	0	0	0XC40
8	1	1	1	1	1	0XC78
9	1	1	0	1	1	0XC58

Table 2.4b: Hexadecimal equivalent of minus, one and dots display

Minus	One(digit4)	$D_3(1/1000)$	D_2 (1/100)	D_1 (1/10)	Hex value
1	1	1	0	0	0XCB8
1	1	0	1	0	0XC18
1	1	0	0	1	0XCD8
1	0	1	0	0	0XCA8
1	0	0	1	0	0XC08
1	0	0	0	1	0XCC8
0	1	1	0	0	0XCB0
0	1	0	1	0	0XC10
0	1	0	0	1	0XCD0
0	0	1	0	0	0XCA0
0	0	0	1	0	0XC00
0	0	0	0	1	0XCC0

Figure 2.7.Photograph of fully computerized Microwave X-band measurement Setup

16.5 mm position which corresponds to frequency 8.4 GHz, the subsequent measurement sets then automatically takes this position. The commencing (*fstart*) and the ending values (*fend*) of frequency range and frequency increment step (*fincr*) to be used in experimentation is furnished by the operator. Numbers of motor steps equivalent to the start frequency value are computed and the motor is given instruction to move from the initial value to the *fstart* value.

2.4.2 Main Measurement Module

The four display units of ICL7106 is selected using the out port 378H with chip select valued of address as 48, 32, 16 and 0 (as shown in table 2.3) respectively. The power meter display is then read from the input port 379H. When the first chip is selected, the first digit is read and so on. The last chip selects the sign and the position of the decimal point as well as the fourth digit. A lookup table finally identifies the displayed value on power meter (table 2.4a and 2.4b). The frequency and the power meter readings are written in the output data file. Necessary software delays are given for stabilization of the power meter reading. The motor is moved to the next incremented frequency position and similarly the next power meter reading is acquired. This data acquisition continues till the end frequency value is reached. The output data file is closed.

During measurement, a counter keeps track of the number of steps moved. Once, the set is completed, this counter is used to move the micrometer to its original position making it ready for the next measurement. All windings are de-energized to avoid unnecessary consumption of power and heating of the motor. It may be noted that the micrometer need not be positioned manually a second time even unless there is power failure during measurement or the motor is stalled due to some reason.

28
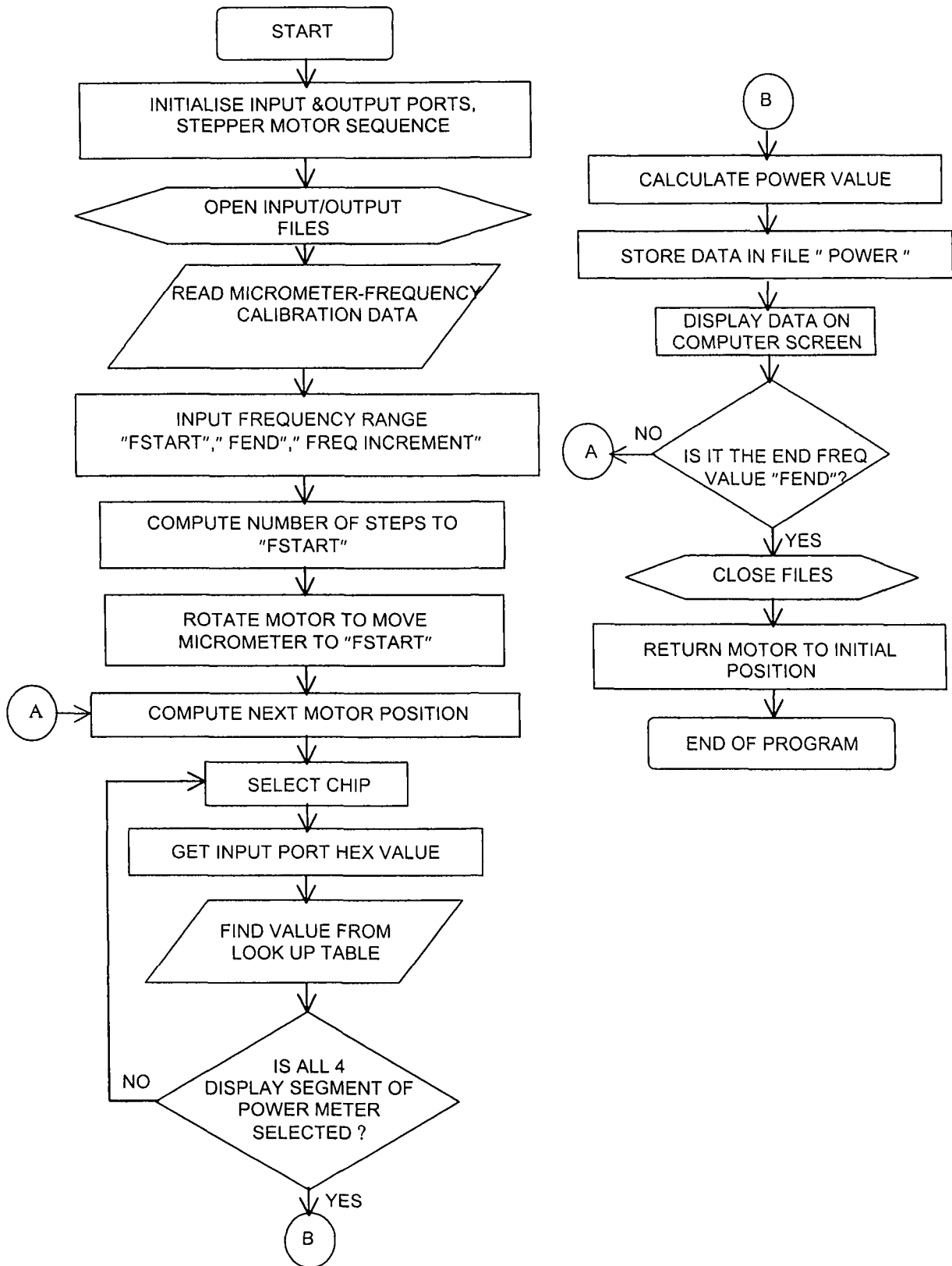
Figure 2.8: Flow chart of software developed for PC- based X band setup

2.5 RESULTS

The program is developed in C language. Figure 2.9 shows the plot for the same sample measured at two different times which shows excellent repeatability of data. Figure 2.10 shows a comparison of manual and automated data for the same DUT. As can be seen from the plot, that some important information's are left out, as the frequency steps are larger in manual reading.
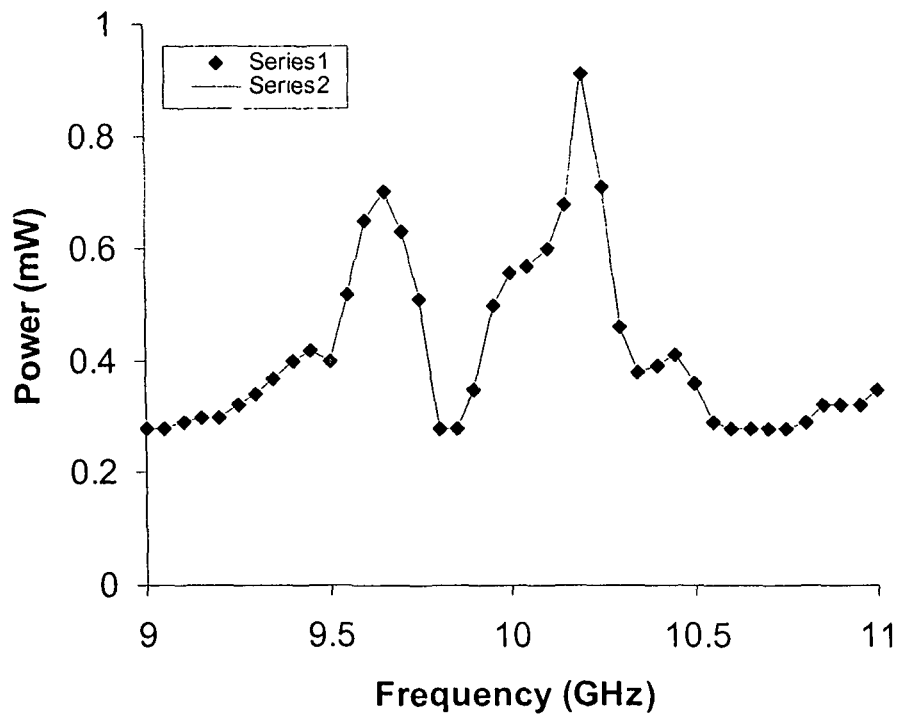
Figure 2.9: Repeatability of data within the frequency range 9.0 - 11.0GHz with 0.01 GHz increment in frequency
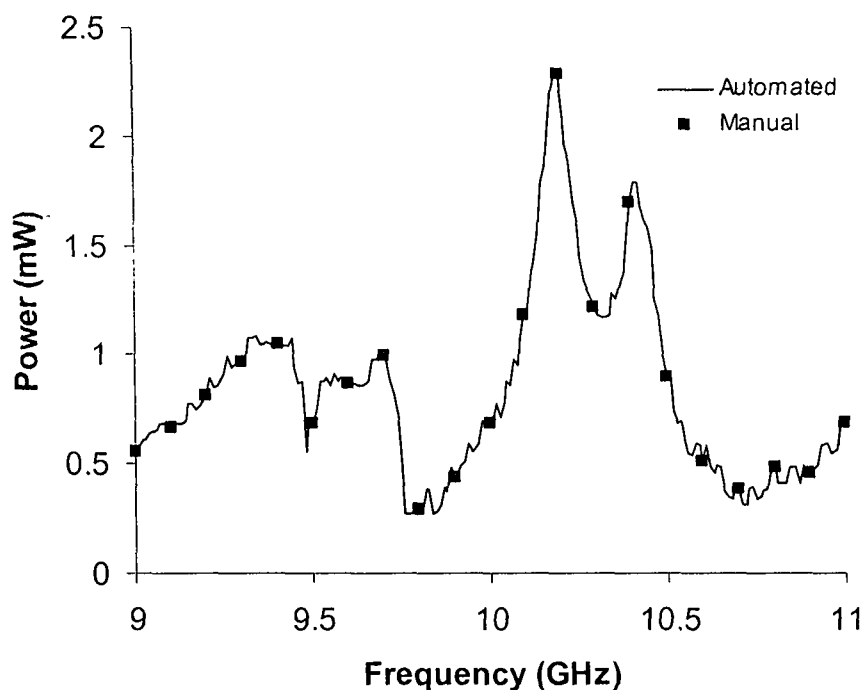
Figure 2.10: Plot of automated and manual measurement data

Comparison of automated and manual measurement facility is given in table 2.5. The optimized listing of the program developed is attached as Appendix-I at the end of the thesis.

Table 2.4: Comparison of automated and manual measurement setup

Performance	Automated setup	Manual setup
Repeatability	Excellent (Average difference of two data taken at different times <1%)	Good (after averaging three sets)
Time (for one complete set of data including averaging)	3 minutes	3-4 hours
Number of data points	201	20
Minimum Measurable Frequency Increment	0.005 GHz	0.1 GHz

31

CHAPTER III

COMPOSITE - PREPARATION, MICROSTRUCTURAL AND THERMAL PROPERTIES STUDIES

3.1 INTRODUCTION

With rapid expansion of technology, especially at high frequencies, material development has become an important aspect. With polymer-composites finding a wide application in different facets of modern technology, it is very important to optimize the properties of the composites according to designer's application.

Polymers are stronger, more durable, light weight and have good surface adhesion for metallization. They suffer from poor microwave dielectric properties, feeble dimensional stability and poor heat dissipation when compared with other microwave material choices viz. ceramics and ferrites [1-3]. Improvements in properties of polymers can be done by reinforcing it with additional materials. Such a reinforced physical mixture is called composite [4]. Particle filled composite shows greater fabrication flexibility in getting the desired properties by simply altering shape, size and distribution of reinforcing particle in the composite. For microwave applications it is important to choose the rein-forcers which will enhance the microwave properties.

This chapter, initially discuss the choice of rein-forcers and matrix phases, the preparation techniques of the polymer composite and the correlated factors which play a significant part in the present investigation. As properties of the particulate composite are highly sensitive to microstructural properties of the reinforced particle [5-8], XRD, optical micrograph, SEM of the samples prepared are obtained and studied. Fourier transform infrared (FTIR) spectroscopy studies are conducted to ensure absence of chemical interaction between the filler particle and the polymer.

The main objective of the present investigation is to study these composites as substrate in microstrip device applications. To ascertain good circuit performance, it is important to examine the physical and thermal properties of the composites. Therefore thermal and physical properties of the composites are conducted. The results of this investigation are described in the later part of the present chapter.

32

3.2 MATERIAL PREPARATION TECHNIQUE

Polystyrene is used as matrix, because of the ease with which it could bond itself

and to the metals [9]. Moreover, dielectric loss of

polystyrene (PS) at radio frequencies is found to be

quite low ($\sim10^{-4}$) at 9.68 GHz. PS is a rigid material

that can be formed or shaped only when heated. The

structural formula is given in figure 3.1.
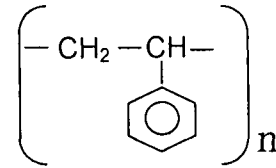
Figure 3.1: Structural formula of Polystyrene

To increase the dielectric constant and mechanical strength of the polystyrene various quantities of alumina and titania are mixed into polystyrene as reinforcing phase. Although the dielectric constant of alumina is low in comparison to the titania but its thermal properties are better than that of alumina. The microwave, physical and thermal properties of alumina and titania along with polystyrene are tabulated in table 3.1

Table 3.1: Microwave, physical and thermal properties of the composite constituents

Materials	Microwave property		Physical property		Thermal property	
	Dielectric constant 10GHz	Dielectric loss	Density (gm/cc)	Average Size of filler(μm)	Thermal conductivity (W/cm K)	CTE ($10^{-6} \times$ K^{-1})
*Polystyrene	2.5	0.0002	1.05	-	0.001-0.013	30-210
**Alumina	9.6-10.4	0.0001	3.75	3	0.37	6.3
**Titania	85	0.004	1.70	1	0.05	7.5

*Goodfellow- Material Information Polystyrene PS
** Microwave Material, "V R K Murthy, S Sundaram, B Viswanathan", Narosa Publishing House

The polymer is dissolved in cyclohexane. Tetraethyl orthotitanate or titanium ethoxide [$Ti(OC_2H_5)_4$] is used as surfactant. Coupling agents and surfactants are added in order to reduce the viscosity of the solution so as the quantity of filler can be increased. Additionally coupling agents reduce the molecular polarizability in the filler-polymer

"interphase" region by enhancing "physical wetting" between the polymer and the filler particles [10-11].

Alumina/ titania is grounded and sieved several times to get particle size less than the probing wavelength (which is ~36×10^3 μm at the lower X-band range). Thus, for the probing wave the material will appear homogeneous having negligible scattering attenuation. The small size of the filler particles can be approximated as spherical. Different percentage volume fraction (VF) of filler is added and a heterogeneous mixture is obtained. The mixture is placed in a homogenizer for half an hour. This homogenous mixture is casted in rectangular shape and allowed to dry at room temperature. The preparation and environmental conditions are kept same for one batch of samples. The processing chart is shown in figure 3.2.

```
                    ┌─────────────────────────────┐
                    │      2gm Polystyrene         │
                    └─────────────────────────────┘
                                  │
                                  ▼
                    ┌─────────────────────────────┐
                    │      50ml Cyclohexane        │
                    └─────────────────────────────┘
                                  │  Stirring for 30 minutes
                                  ▼
                ┌─────────────────────────────────────┐
                │   2 ml Surfactant (Orthotitanate)    │
                └─────────────────────────────────────┘
                                  │
                                  ▼
              ┌─────────────────────────────────────────┐
              │   (100mg- 1gm)Alumina & Titania          │
              └─────────────────────────────────────────┘
                                  │  Homogenizing for ½hours
                                  ▼
              ┌─────────────────────────────────────────┐
              │     Homogeneous viscous solution         │
              └─────────────────────────────────────────┘
                                  │
                                  ▼
              ┌─────────────────────────────────────────┐
              │     Casting in rectangular shape         │
              └─────────────────────────────────────────┘
```
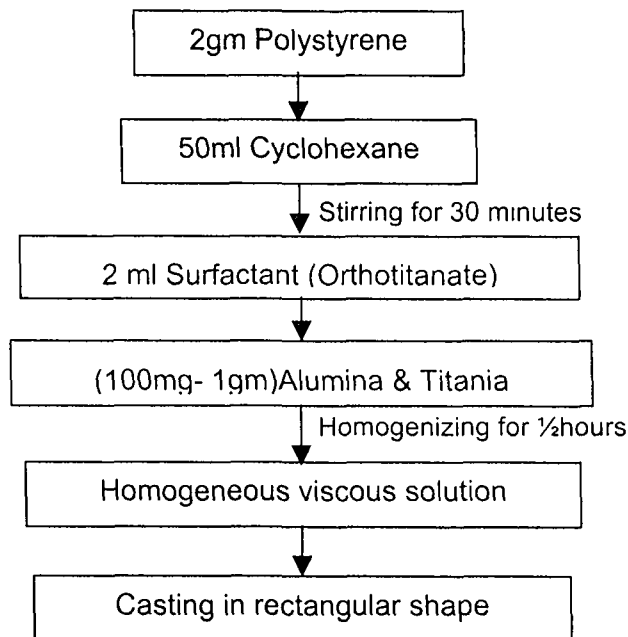
Figure 3.2: Schematic of preparation technique of polymer composite

3.3 MICROSTRUCTURAL STUDIES

Propagation of electromagnetic wave inside the composite material depends on the distribution of filler in the composite matrix, the size of the filler particles and any change in structural configuration of the filler particles after its formation into composite phase.

34

Microstructural analysis gives complete insight of the composite deciding its utility as substrate in microwave technology. Various techniques used for micro-structural studies are described subsequently.

3.3.1 X-Ray Diffraction

X-ray diffraction patterns of the samples are recorded at 2θ values from 3° to 100° using a Philips X'pert Pro diffractometer. In general, polystyrene is amorphous and does not show any peak. Figures 3.3 (a-d) shows the XRD patterns of PS-alumina composite with different concentrations. Alumina is crystalline in nature and shows distinct peaks at 17°, 20°, 38°, 45°, 65°, 68° and 78° [12]. XRD of PS-alumina system shows six peaks at Bragg angles 17.5°, 21.5°, 27°, 46°, 66.5° and 77° confirming that the alumina particles filled polymer matrix does not loose its crystalline properties. Figures 3.4(a-e) show the XRD spectra of pure titania and PS-titania composite with increase in volume fraction of TiO_2. This system shows peaks at 26°, 38.5°, 44.5°, 48°, 54° and 63°. These peaks are that of titania [13] which shows that titania also retains its crystalline properties in the composite.
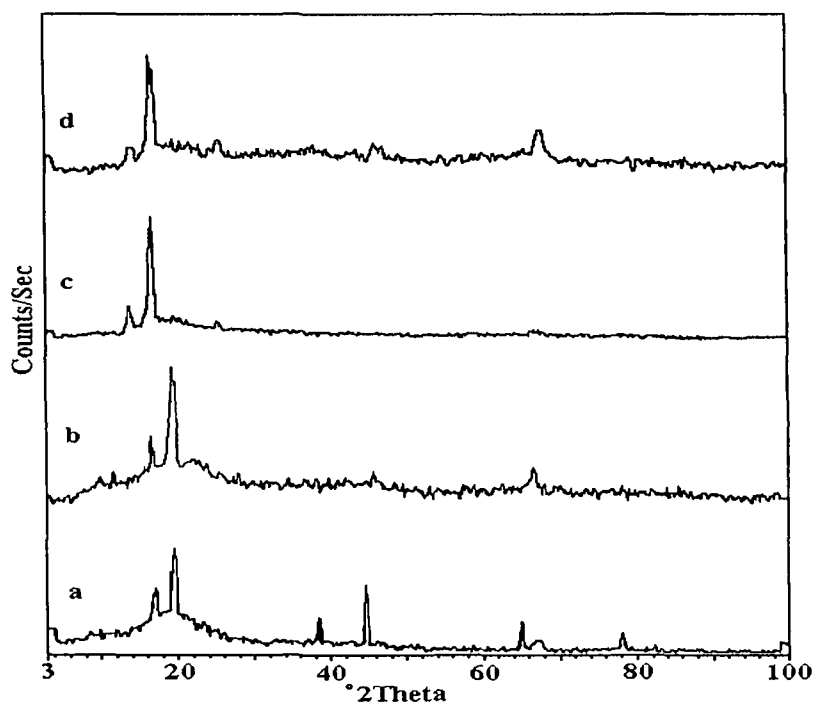
Figure 3.3: XRD pattern of PS-Alumina composite with a) 1% b) 2% c) 3% and d) 4% alumina filler percentage by volume fraction

35
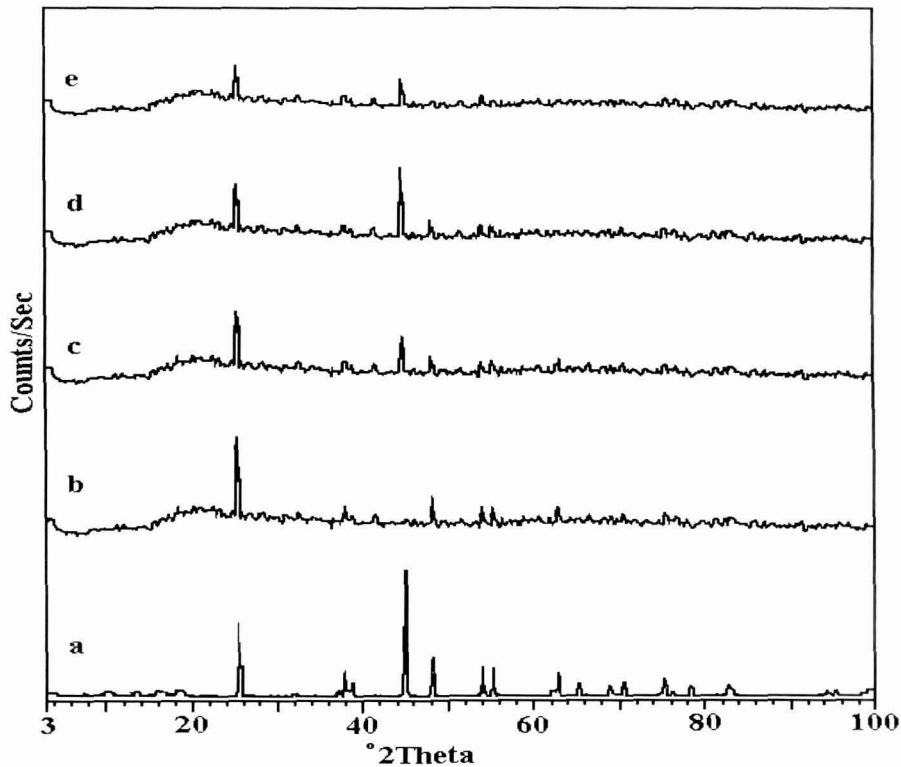
Figure 3.4: XRD pattern of PS –Titania composite a) pure TiO$_2$, b) 1% c) 2% d) 3% and e) 4% TiO$_2$ filler percentage by volume fraction

3.3.2 Optical Micrographs

The distribution and size of the alumina/titania particles in the composites are investigated by optical microscope (LEICA 2000). The specimen [1cm × 1cm] is placed on a glass slide and observed at 40X resolution. The distribution and morphology of PS-alumina and PS-titania are photographed using KODAK film. The micrographs of 1 and 4%VF of alumina and titania samples are shown in figure 3.5 a-b and 3.6 a-b respectively.
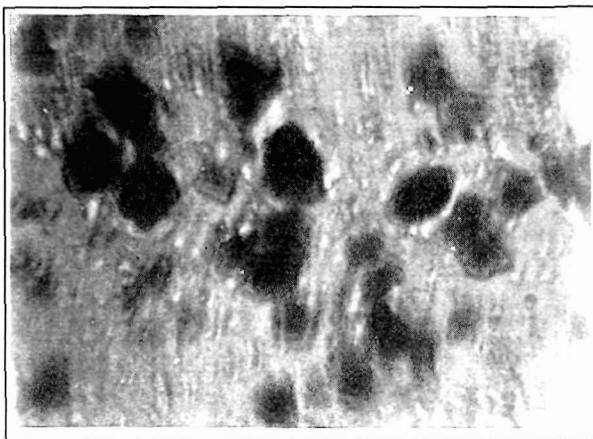
Figure 3.5 a) 1%VF Alumina distribution
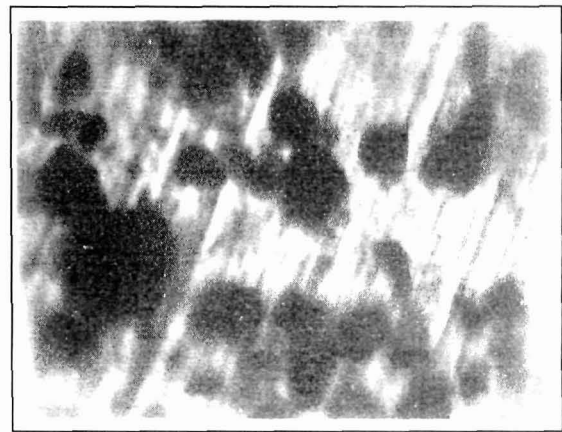
Figure 3.5 b) 4%VF Alumina distribution

36
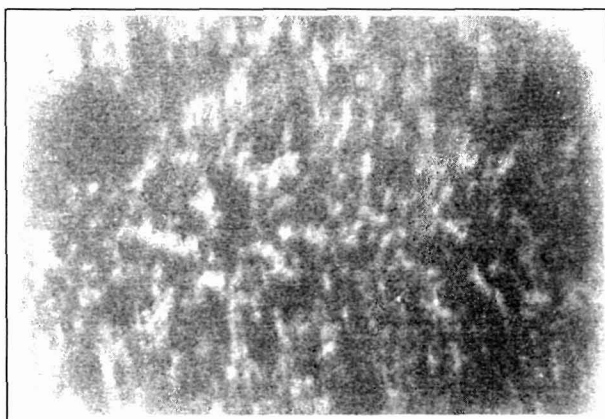
Figure 3.6 a) 1%VF Titania distribution   **Figure3.6 b) 4%VF Titania distribution**

3.3.3 Scanning Electron Micrographs

Scanning electron microscopy (SEM) is a very sensitive technique for studying the size and distribution pattern of the filler in the polymer matrix. SEM has been taken by JEOL JSM-35CF. It is based on the principle of irradiating the specimen with finally focused electron beam. The electron beam on striking the surface releases secondary electrons, back scattered electrons, Auger electrons, characteristic X-rays and several other types of radiation from small part of the specimen. In the surface SEM secondary electrons are generally collected to form the image. The surface of each samples are gold coated using a sputtering unit before taking the micrographs. The micrographs are taken at 10^{-11}A probe current and 20 KV accelerating voltage at 3000X. Figure 3.7(a–b) and 3.8 (a-b) show the SEM micrographs of 1%VF and 4%VF of alumina and titania respectively. The samples are studied with increase in filler percentage. The volume faction, average particle size and average number of particles of alumina and titania in 1mm^2 area are given in table 3.2.

The distribution of alumina and titania particles in the polymer matrix is homogeneous. From SEM and optical micrograph the average particle size for alumina is found to be 3 micron and that for titania as 1 micron. The shape of filler particles as seen from optical micrographs and SEM can be approximated as spherical.
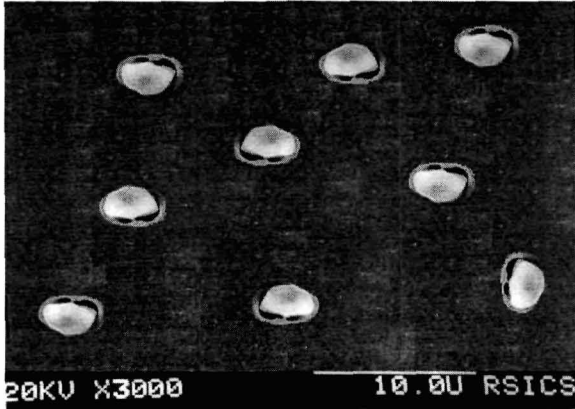
3.7 a) 1%VF Alumina distribution
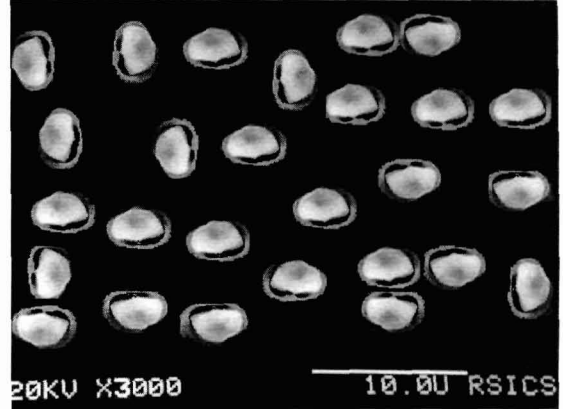
3.7 b) 4%VF Alumina distribution
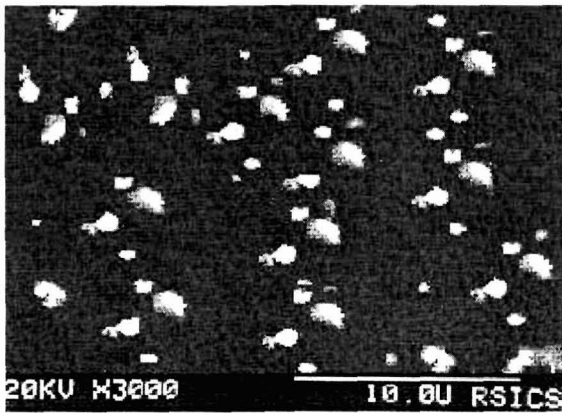
3.8 a) 1%VF Titania distribution
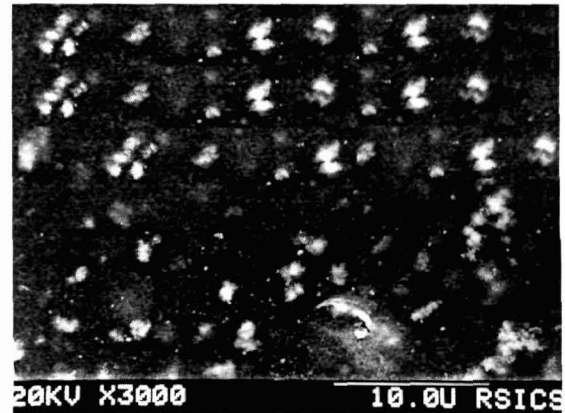
3.8 b) 4%VF Titania distribution

Table 3.2: Average distribution and effective surface area of particles in 1mm^2 area

% VF	PS-Alumina		PS-Titania	
	Number of particles	Effective surface area of particle (mm^2)	Number of particles	Effective surface area of particle (mm^2)
1	28	79×10^{-5}	40	12.5×10^{-5}
2	46	130×10^{-5}	62	19.4×10^{-5}
3	65	183×10^{-5}	90	28.2×10^{-5}
4	85	240×10^{-5}	120	37.6×10^{-5}
5	106	299×10^{-5}	152	46.5×10^{-5}
6	128	361×10^{-5}	169	53.0×10^{-5}
7	151	426×10^{-5}	190	59.6×10^{-5}

38

3.4 DENSITY AND WATER ABSORBANCE

It is essential to reduce the size and weight of microwave electronic parts for space and telecommunication applications [14]. Moreover, the water absorbance of the composite material prepared appraises the porosity of the material, which is an important parameter to be observed. Density and porosity of the composite gives an idea of the compactness of the material and its applicability as alternate light- weight material. The density of a material is equal to its weight per unit volume.

$$d_s = \frac{W}{V}$$

where

d_s = Density in gm/cc

W = Weight in gms

V = Volume in cm^3

The densities of the samples are measured with Archimedes's principle. The samples are cut into rectangular shape of 1cm^2 area and tied with a thin inelastic thread. Its weight in air is measured using digital balance. The specimen is then completely dipped in water and weighed. Since the buoyancy force is equal to the difference between these two weights, the volume of the sample is equal to the weight difference divided by the density of water. The weight of the thread is also taken and duly subtracted to get the correct weight of the sample in air. If,

W_{air} = Weight of the sample in air + weight of thread (gm)

W_{water} = Weight of the sample in water + weight of thread (gm)

W_{thread} = Weight of thread (gm)

D_{water} = Density of water (=1 gm/cc)

Then

$$d_s = \frac{W_{air} - W_{thread}}{W_{air} - W_{water}} \times D_{water}$$

39

For samples of uniform shape, the density can also be estimated from its mass and volume. The volume is being estimated from dimensions of the samples. The method is suitable for highly dense samples only. The results of density determination is tabulated in table 3.3.

It is observed that both the set of samples do not absorb water. An increase in density of 22.3% is observed in alumina reinforced composite and an increase of 2.39% is also observed in titania reinforced composites for the 1 to 10% increase in volume fraction.

Table 3.3: Densities of two composites with increasing volume fraction

%Volume fraction	Alumina filled composite		Titania filled composite	
	Density (gm/cc)	Water absorbance	Density (gm/cc)	Water absorbance
0	1.10	0	1.10	0
1	1.15	0	1.102	0
2	1.27	0	1.104	0
3	1.285	0	1.11	0
4	1.302	0	1.115	0
5	1.325	0	1.118	0
6	1.352	0	1.12	0
7	1.375	0	1.122	0
8	1.398	0	1.123	0
9	1.406	0	1.125	0
10	1.417	0	1.127	0

3.5 FOURIER TRANSFORM INFRARED SPECTROSCOPY

Fourier transform infrared (FTIR) spectroscopy is a powerful analytical tool for characterizing and identifying organic molecules. Using the IR spectrum, chemical bonds and the molecular structure of organic compounds can be identified. The wavelength of light absorbed is characteristic to the chemical bond. By interpreting the infrared absorption spectrum, the chemical bonds in a molecule can be determined. FTIR spectra of pure compounds are generally so unique that they are like a molecular "fingerprint".

FTIR spectra of composite samples are studied using a Nicolet Impact 410 spectrophotometer. The resolution of spectrophotometer is 1 cm^{-1}. Spectra are scanned in the spectral range 4000 – 500 cm^{-1} in order to determine if any chemical interaction between PS matrix and alumina/titania filler particle in the composite has taken place. No difference between the IR spectra of the pure and filled PS is observed indicating that the chemical composition of the PS matrix remains unchanged on adding filler alumina/titania and the surfactant titanium ethoxide. Thus it indicates that interaction between polymer and filler is physical in nature. Figure 3.9 shows the FTIR spectra of PS-Alumina composite.
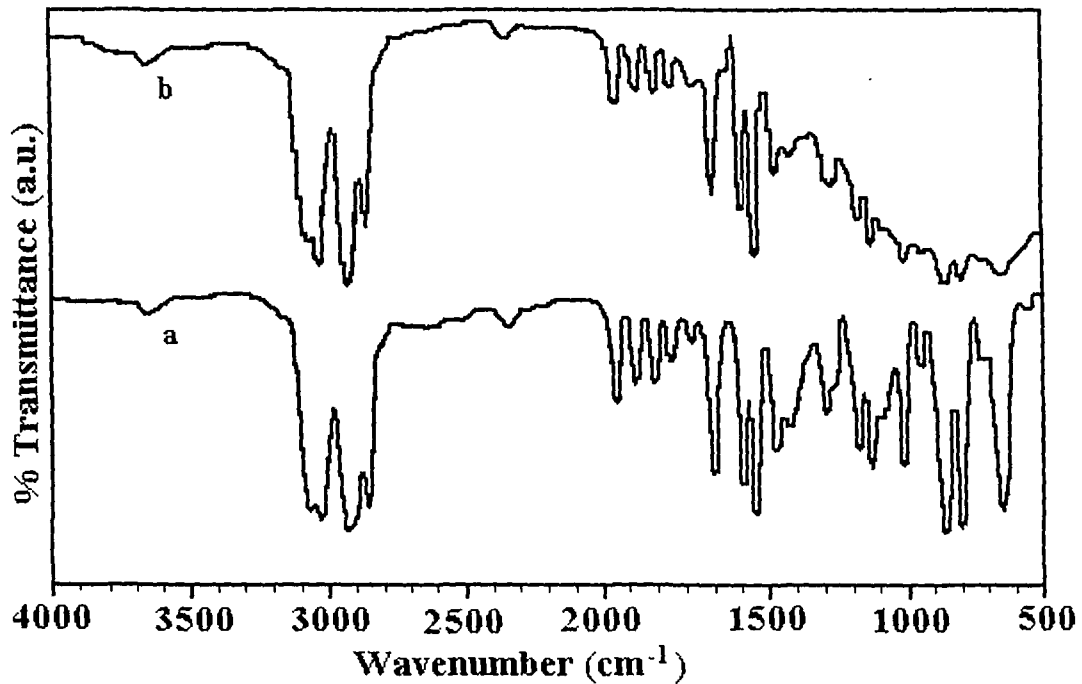
Figure 3.9: IR spectra of a) PS and b) 4% Volume Fraction PS-alumina composite

3.6 STUDIES OF THERMAL PROPERTIES

Thermal conductivity and thermal expansion coefficients are the important parameters to be measured for applications of composite materials in devices. Dimensional stability with the change in temperature and heat dissipation of the composite material is the major findings of these observations. Set-ups are developed in the

41

laboratory to measure the thermal conductivity and thermal expansion coefficient of the samples and are described below.

3.6.1 Thermal Conductivity – Set up Fabrication and Measurement

There are different techniques for thermal conductivity measurements in insulators. Lee's method is the most popular one, but it suffers from the need of bulky steam system for heating and high possibility of radial heat flow. There are other advanced methods (e.g NPL's (UK) Guarded Hot Plate Method) which are very accurate but expensive. The set up is indigenously designed and fabricated in the laboratory by using more robust components: guarded hot plate, solid state transducer and amplifier. The theory of the instrument is based on Lee's method.

Design of Modified Lee's Method

The instrument consists of two brass slabs where one acts as heat source and other as sink. The sample to be tested is placed between the source and sink. The exposed portion of the source and sink is covered with heat insulating-seal to ensure no radial heat flow. A thermostatic electric heater is used to heat the source and sink is kept at room temperature. A spring system is attached to the other end of sink to ensure good contact between source, sample and sink with advantage of easy placement of the sample. A non-conducting casing is used for mounting the system. The schematic diagram of the instrument is shown in figure 3.10.
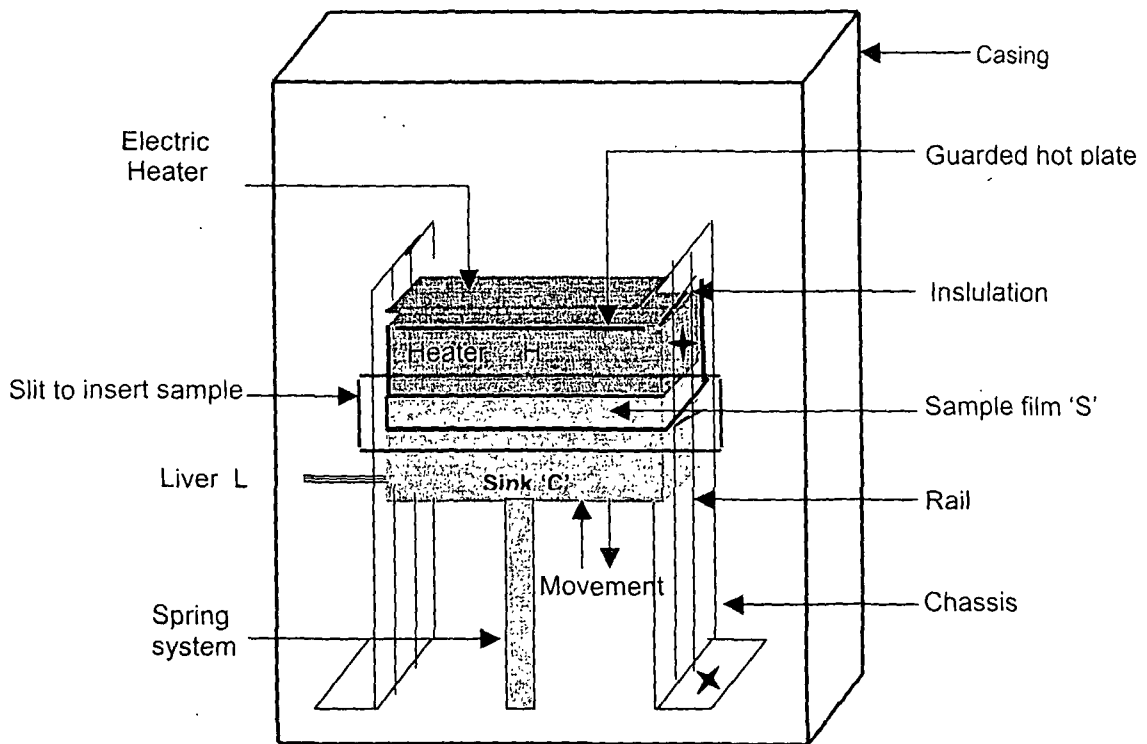
Figure 3.10 Schematic diagram of thermal conductivity measurement set -up

Transducer element

Temperature of the slabs is measured by a transducer element, transistor. It works on the principle of Peltier effect. The schematic of the transducer system is shown in figure 3.11.
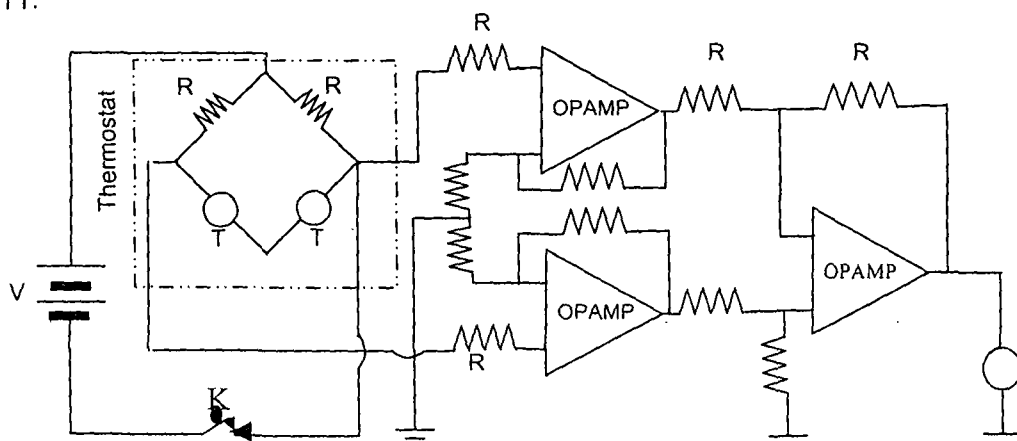
Figure 3.11 Circuit diagram of the transducer system
OPAMP = Operational Amplifier, R = Resistance=1KΩ, T = Transistor

43

The system can measure both absolute and relative temperatures of the slabs using a switch.

Working principle

The experimental sample S is trapped between the source and sink. The area of sample is kept same as the area of the slab. The source is heated and heat conducts through the sample to the sink. The rate at which heat (Q) conducts through the specimen is equal to the rate at which the sink losses heat

$$Q = \frac{KA(\theta_1 - \theta_2)}{d} \qquad\qquad 3.1$$

where

K is the coefficient of thermal conductivity of the specimen

A is the area of sample

d is thickness of sample

θ_1 and θ_2 are temperatures of the source and sink at steady state

If M is the mass of the slab, 's' is specific heat of the slab material, the rate of cooling of the sink at θ_2 is

$$Q = MS\left(\frac{d\theta}{dt}\right)_{\theta=\theta_2} \qquad\qquad 3.2$$

where $d\theta/dt$ is the rate of fall of temperature at θ_2

From equation 3.1 and 3.2

$$\frac{KA(\theta_1 - \theta_2)}{d} = MS\left(\frac{d\theta}{dt}\right)_{\theta=\theta_2} \qquad\qquad 3.3$$

$$K = \frac{dMs\left(\frac{d\theta}{dt}\right)_{\theta=\theta_2}}{A(\theta_1 - \theta_2)} \qquad\qquad 3.4$$

The rate of cooling is found by heating the sink to a temperature above θ_2. The sample is then placed between the source and sink and source is heated. The temperature of the source is allowed to reach an equilibrium temperature with the sink. 't', the time of fall of temperature of the sink is noted at regular intervals. The slope of the tangent drawn to this plot gives the value of rate of fall of temperature.

3.6.2. Coefficient of Thermal Expansion – Setup Development and Measurement

Thermal expansion coefficients of the prepared samples are measured with Comparator method. The experimental setup, developed in the laboratory is shown in figure 3.12. The setup consists of a glass cavity containing inlet and outlet for steam. A glass rod is used as holder to place the sample inside the cavity. A thermometer is placed near the sample to measure its temperature. A traveling microscope of least count 0.01 mm monitors the change in dimension of the sample.

The length of the sample is made manifolds than the cross sectional dimensions so as the change can be taken linearly. Prior to placing the sample the change in length of the
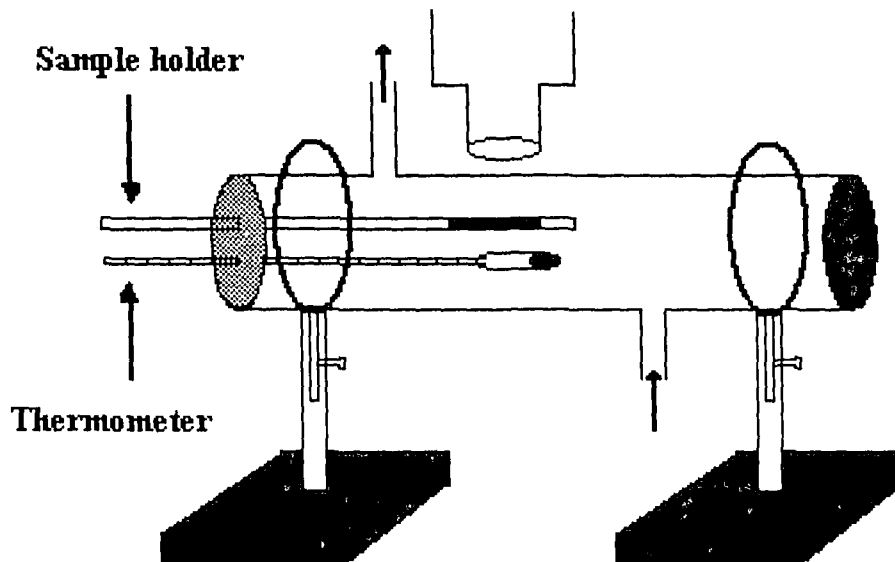
Figure 3.12: Setup for thermal expansion coefficient measurement

glass for the same increase in temperature is observed which is found to be negligible as compared to the change in the sample length.

The initial length of the sample is L_1 (say) at room temperature, $t_1°C$. After passing steam at 100°C through the cavity the temperature reaches steady value ($t_2°C$) and the new linear dimension is L_2 The thermal expansion coefficient (α) can be determined as

$$\alpha = \frac{L_2 - L_1}{L_1 \times (t_2 - t_1)} \quad \text{per } °C$$

3.6.3 Thermal Conductivity and Thermal Expansion Coefficient Measurement Results

The thermal conductivity and thermal expansion coefficient of the prepared samples measured with the above two techniques are tabulated in table 3.4.

Table 3.4: Thermal conductivity and thermal expansion coefficient of two composites

%Volume fraction	PS + Alumina		PS + Titania	
	K (W/cm°K)	$\alpha \times 10^{-6}$ (K^{-1})	K (W/cm°K)	$\alpha \times 10^{-6}$ (K^{-1})
0	0.00728	30.1	0.00728	30.1
1	0.0109	29.87	0.0076	29.88
2	0.0145	29.57	0.0081	29.65
3	0.0181	29.39	0.0085	29.43
4	0.0217	29.157	0.0089	29.20
5	0.0254	28.91	0.0093	28.97
6	0.0290	28.68	0.0098	28.75
7	0.0326	28.44	0.0106	28.52

3.7 DISCUSSION AND CONCLUSION

Investigations of microstructural properties show that PS-alumina and PS-titania composite systems are homogeneous and the size of the reinforced particles are smaller than the probing wavelength (corresponding to 10 GHz) hence, the scattering losses can be assumed to be negligible. In the composites, the alumina/titania particles are homogenously distributed in the polystyrene matrix and the particles are isolated from each other. However, when the volume fraction of particles in the mixture becomes large, complete wetting of the particles in the mixture may be frustrated due to inter particle interactions. In the present investigation, when the filler particles in the composites crosses 7%VF agglomeration of particles produces a region where the particle materials forms a semi contiguous geometry. The composite becomes brittle and fragile at higher concentration of filler particles.

The density measurement shows that compactness of both composite system increases with percentage increase in volume fraction. As titania density is less than alumina, PS-titania is lighter than PS-alumina composite for the same change in volume fraction. FTIR studies on both the composite systems show that there is no chemical interaction between the matrix and filler phase.

Higher thermal conductivity permits better heat dissipation in circuit, especially for circuits operating at high microwave power levels. An improved thermal conductivity of about 4.47 times for PS-alumina and 1.456 times for PS-titania composites for 7 % VF, as compared to PS is observed as shown in figure 3.13. The effective thermal properties of composite materials depend on the intrinsic microscopic properties of the filler dielectrics, homogeneity of distribution and compactness of the composite [15]. Filler particles reinforced in polymer matrix forms an interacting interface. Increase in number of filler particles with increasing % volume fraction increases the effective area of interaction between filler-phase and polymer-phase. Heat transfer in such composites probably takes place via the polymer-filler interface.

47
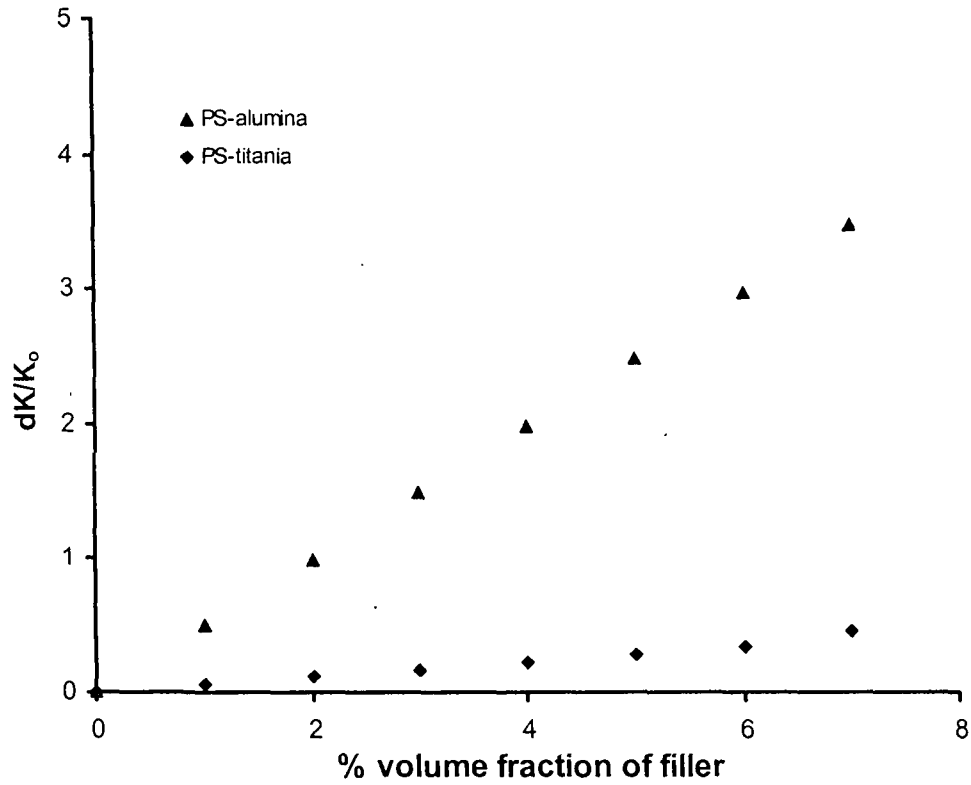
Figure 3.13: Relative enhancement of thermal conductivity for of two composites
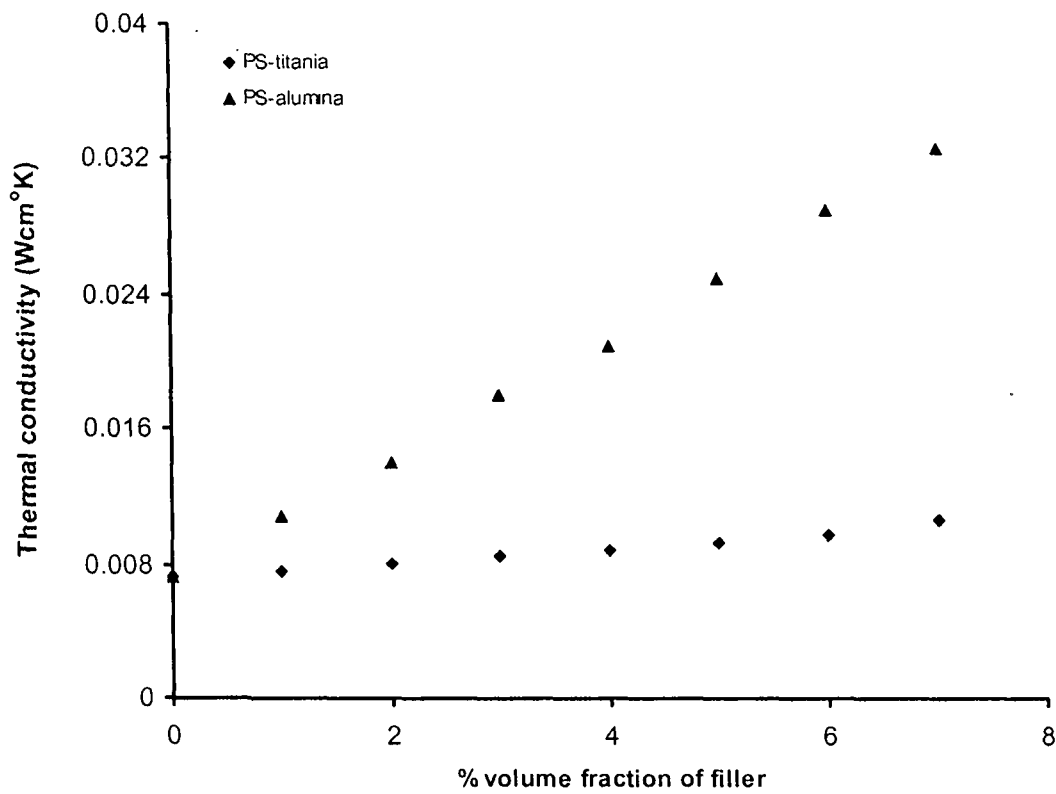
Figure 3.14: Thermal conductivity Vs % VF of PS-alumina and PS-titania composite

An enhanced thermal conductivity is expected with the increase in number of reinforced particles. Figure 3.14 shows the change in thermal conductivity with % volume fraction of filler. Thermal conductivity of alumina is 7.4 times that of titania (table 3.1). Although the number of titania particles in the same area is more than alumina, the particle size of alumina is larger than that of titania. So the effective surface area of interaction of alumina is more than titania in the polystyrene matrix system (for same %volume fraction).

The other requirement for microwave device application is dimensional stability over the operating temperature range. The plot of effective surface area of filler and its
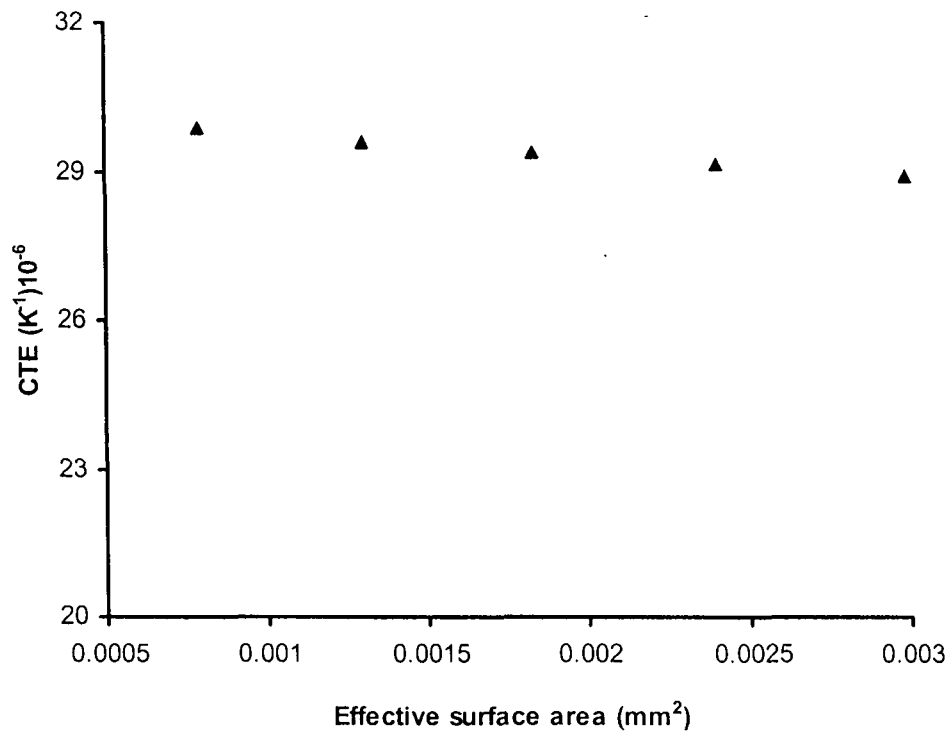
Figure 3.15 a: Effective surface area in 1mm^2 area vs CTE of PS-alumina composite
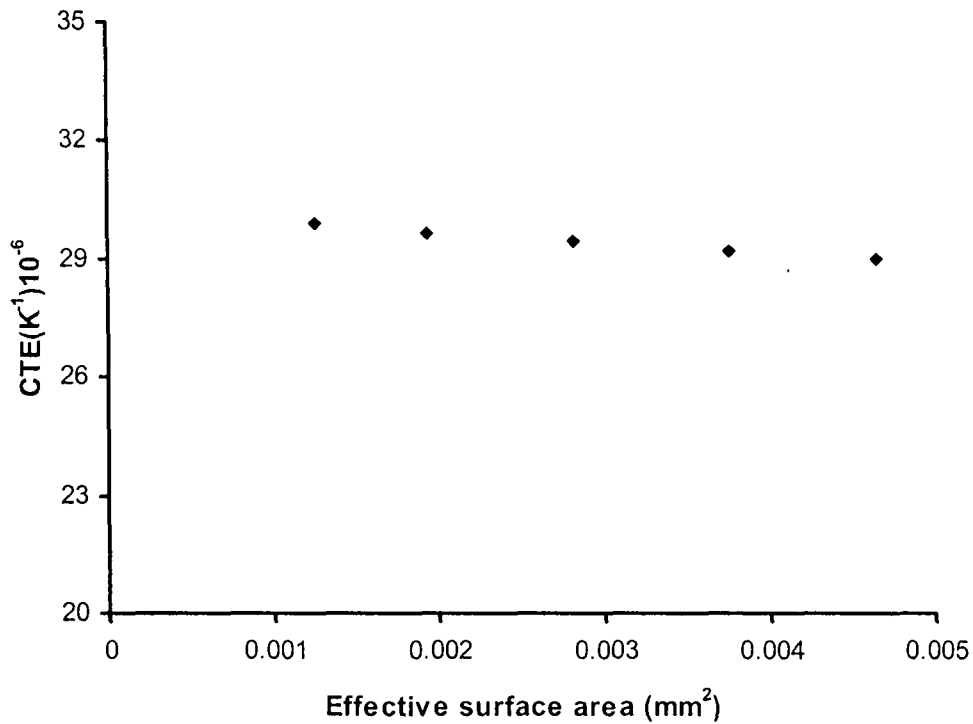
Figure 3.15b: Effective surface area in 1mm^2 area Vs CTE of PS-titania composite

corresponding CTE are given in figure 3.15(a-b). An improved thermal stability of the PS-alumina and PS-titania systems with respect to the pure PS matrix is observed. The glass transition temperature (T_g) of the PS is 80°C. On heating PS to temperatures above T_g, a negative coefficient of thermal expansion (CTE) of pure PS sample is observed due to scission of weak bonds [15]. An intermolecular chain transfer reaction with formation of primary free radicals at the chain end also takes place leading to thermal degradation of PS. PS segment attached to titania and alumina filler particles in the composite restricts the chain transfer reaction rendering altered molecular mobility and improved stability. The CTE of alumina is less than that of titania (table 3.1) thus reducing the mobility of PS-alumina segment more than that of PS-titania and rendering better dimensional stability for PS-alumina composites.

References:

[1] V. R. K. Murthy, S. Sunderam and B. Viswanathan, "Materials and Technology for Microwave Integrated Circuits," Microwave Materials, pp- 30, Narosa Publishing House, New Delhi, 1993.

[2] I. Bahl and K. Ely, "Modern Microwave Substrate Materials," Microwave Journal, vol. 33, pp -131, 1990.

[3] G. R. Traut, "Clad Laminates of PTFE Composites for Microwave Antennas," Microwave Journal, vol. 23, pp- 47, 1980.

[4] E. K. Sichel, "Carbon Black- Polymer Composites," Edited by Marcel Dekker, New York, 1982.

[5] C. Brossaeu, P. Queffelec and P. Talbot, "Microwave Characterization of Filled Polymer," Journal of Applied Physics, vol. 89, pp- 4532, 2001.

[6] H. M. Musal Jr., H. T. Hahn and G. G. Bush, "Validation of Mixture Equation for Dielectric-Magnetic Composite," Journal of Applied Physics, vol. 63, pp-3768, 1988.

[7] T. Nakamura, T. Tsutaoka and K. Hatakeyama, "Frequency Dispersion of Permeability in Ferrite Composite Materials," Journal of .Magnetism and Magnetic Materials, vol.138, pp-319, 1994.

[8] J. P. Ganne, M. Pate, B. Grammaticos, A. Ramani and T. Robin," Microwave Permeability of Ferrite Loaded Composites: Comparison Between Model and Experiment, "ICF 7, Bordeaux, 1996.

[9] E. N. Torgow and W. E. John Griemamann, "Miniature Strip Transmission Line for Microwave Applications," IEEE Trans Microwave Theory and Techniques, vol. 3, pp - 57, 1955.

[10] K. L. Mittal, "Silanes and Other Coupling Agents", Adhesion Society, vol. 2, 2000

[11] M. G. Todd and F. G. Shi, "Characterizing the Interphase Dielectric Constant of Polymer Composite Materials: Effect of Chemical Coupling Agents," Journal of Applied Physics, vol. 94, pp- 4551, 2003.

[12] Philips X'pert Pro Diffractometer Manual, 2002.

[13] G. Sivalingam, K. Nagaveni, G. Madras and M. S. Hegde, Ind. Eng. Chem. Resource, vol. 42, pp- 687, 2003.

[14] S. Asai, M. Funaki, H. Sawa and K. Kato, "Fabrication of an Insulated Metal Substrate (IMS), Having an Insulating Layer with a High Dielectric Constant," IEEE Trans. Comp. Hybrids Mfg. Technology, vol.16, pp- 499, 1993.

[15] J. Kulijanin, M. Vučković, M.I. Čomor, N. Bibić, V. Djoković and J. M. Nedeljković, "Influence of CdS-filler on the Thermal Properties of Polystyrene," European Polymer Journal, vol. 38, pp-1659, 2002.

CHAPTER IV

MICROWAVE CHARACTERIZATION OF PARTICLE

REINFORCED POLYMER COMPOSITE

4.1 INTRODUCTION

Complex permittivity is a crucial parameter in many radio frequency (r.f.) and microwave applications like high speed, wide band microwave circuits. It helps in determining important characteristics such as impedance, phase velocity and attenuation in signal transmission structures. As the operating frequencies of electronic devices continue to increase accurate data of the electromagnetic properties of these materials become mandatory for manufacturing high performance microwave, r.f. devices and circuits. Clausius and Mossotti [1] performed some of the earliest work on the dielectric properties of composite materials. Subsequently number of research works [2 -11] has been carried out for experimental determination of complex permittivity.

The effective electromagnetic properties of the particle filled composite materials, depend on the homogeneity of distribution of reinforced particles in the polymer matrix and its intrinsic microscopic properties. The angular frequency (ω) of the electromagnetic probing wave have to satisfy the relation $\omega \ll \frac{c}{a}(\epsilon\mu)^{\frac{1}{i}}$ where 'a' is the size of the filler particles [12-13]. Large size of filler particles as compared to probing wavelength leads to scattering in the wave transporting through such mixed media. As reported in chapter III, the sizes of filler particles are less than minimum probing wavelength.

In the present investigation, effect of properties of the inclusions like permittivity, loss and their amount in the polymer matrix on microwave characterization have been conducted. Dispersive behavior of these composite systems is also studied. The volume fraction (VF) of filler in the mixture is limited to 7%VF. When VF of particles in the mixture crosses this limit agglomeration of particles takes place in the composite systems as mentioned in chapter III, section 3.7. To determine the reliability of the results for complex permittivity measurements of both the composite systems three different methodology viz. cavity resonator method

[14 -15], waveguide method [16] and resonance method [17-18] are used. A theoretical aspect of permittivity using Bruggeman's effective medium theory is also presented.

4.2 EXPERIMENTAL TECHNIQUES FOR MEASUREMENT OF COMPLEX PERMITTIVITY

4.2.1 Cavity Resonator Technique

Cavity resonator method is a simple and quiet accurate method, widely used to determine the dielectric as well as the magnetic parameters in microwave frequency range. A TE_{103} reflection cavity of medium Q at 9.68 GHz is fabricated. Affirmation of measurement techniques is done on three different reference materials such as nylon, bakelite and teflon using cavity perturbation technique.

4.2.1.1 Design and fabrication of a TE_{103} resonator cavity at 9.68 GHz

A cavity resonates at frequencies where length of the cavity (l) is a multiple of $\lambda_g/2$, λ_g being the guide wavelength for propagation along length of the waveguide (say z-direction). A rectangular guide is shorted at z = l and excited by microwave signal at z = 0 to produce a standing wave pattern. The resonant condition is given by

$$l = p \frac{\lambda_g}{2}$$
4.1

The resonant wavelength λ_r of the TE_{mnp} mode is

$$\lambda_r = \frac{1}{\sqrt{\left(\frac{m}{2a}\right)^2 + \left(\frac{n}{2b}\right)^2 + \left(\frac{p}{2l}\right)^2}}$$
4.2

where m, n, p are the excited modes and a, b, l are the dimensions of the cavity. A finely machined rectangular X-band brass waveguide WR 90, which excites only TE_{10} mode is taken. The length of the cavity is calculated from equation 4.2 as 64 mm at 9.68 GHz. The cavity as shown in figure 4.1 is coupled to microwave signal through aperture coupling by a

critically coupled iris. The critically coupled iris shows the minimum reflected peak. The iris hole diameter for critical coupling in the cavity is found to be 4.4 mm. A tuning screw is placed subsequent to the iris coupling so as to adjust any shift in resonant frequency of the cavity due to mismatch. A frequency tuning range of ± 0.05 GHz, is observed during the investigation.
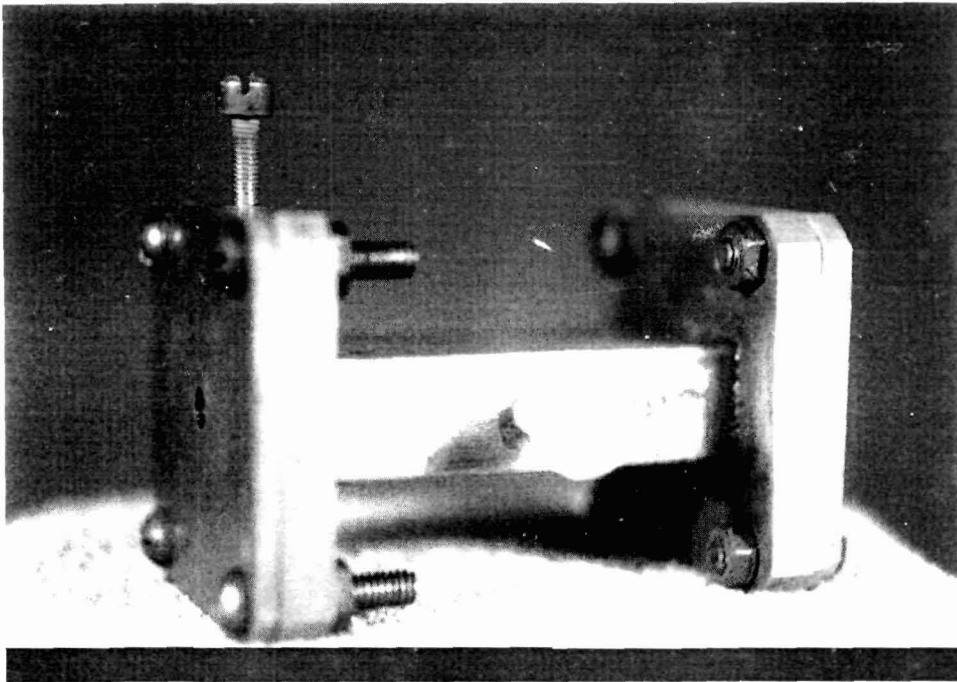
Figure 4.1: A TE$_{103}$ cavity resonator designed at 9.68 GHz

The loaded quality factor (Q$_L$) of the cavity is

$$Q_L = \frac{\text{Resonant frequency}}{\text{3dB band width}} = \frac{f_r}{(f_2 - f_1)} \qquad 4.3$$

where f$_1$ and f$_2$ are frequencies at which power is half of its maximum value at resonant frequency (f$_r$). The graph of the frequency response of the cavity is shown in figure 4.2. The quality factor of the cavity from equation 4.3 is found to be 3226.

55

4.2.1.2 Estimation of complex permittivity of the composite with TE_{103} cavity resonator

The material under test is assumed to have a permittivity $\varepsilon = [\varepsilon_r' - j\varepsilon_r'']\varepsilon_0 = \varepsilon_r^*\varepsilon_0$ where ε_0 is the permittivity of vacuum and ε_r^* is complex permittivity relative to ε_0. Sample is inserted at point of maximum electric field and minimum magnetic field. The resonant frequency of empty cavity and Q factor alters due to change in the overall capacitance and conductance of the cavity without perturbing the inductance. If f_1 and f_0 are the resonant frequencies with and without the samples, the dielectric constant ε' and dielectric loss ε'' are given by [15]

$$\varepsilon' = 1 + \frac{f_0^2 - f_1^2}{f_1^2} \frac{V_c}{4V_s} \qquad\qquad 4.4$$

$$\varepsilon'' = \frac{V_c}{4V_s}\left[\frac{f_0^2}{f_1^2}\left(\frac{1}{Q_1} - \frac{1}{Q_0}\right)\right] \qquad\qquad 4.5$$

where V_S is the volume of the sample, V_C is the volume of the cavity, Q_1, Q_0 are the respective quality factors (Q) of the cavity with and without the sample. The shortcoming of this technique is that complex permittivity of the material can be determined only at the resonant frequency of the cavity. Making a tunable cavity with a plunger to determine ε' and ε'' at different resonant frequency reduces the Q of the cavity.

4.2.2 Waveguide or Double Minima Method [16]

Waveguide method is used for determination of complex permittivity of the material for a wide range of frequencies. The most general description for electromagnetic properties of a given homogeneous material is given by its dielectric constant and loss factor. The dielectric constant of a material is associated with its ability to store electric energy.
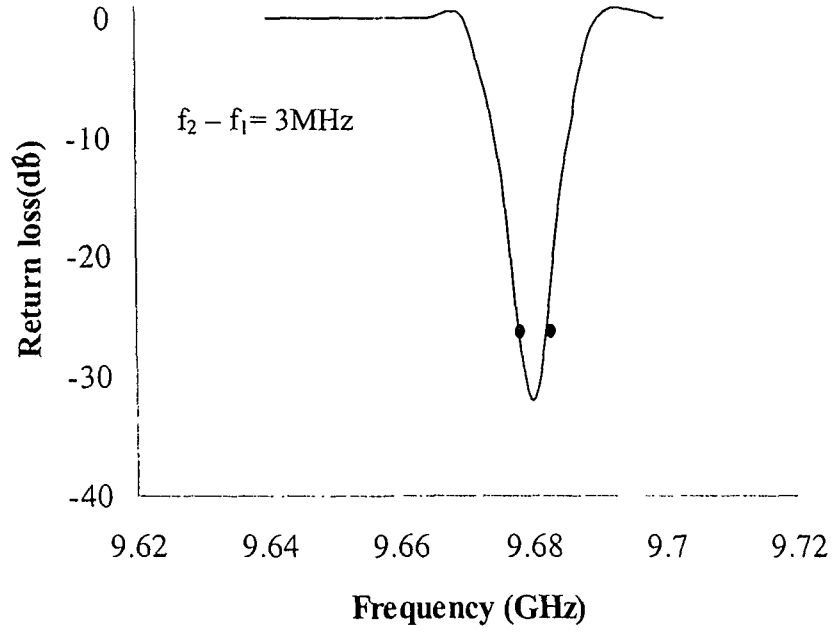
Figure 4.2: Frequency response of the TE$_{103}$ reflection type cavity resonator designed at 9.68GHz

According to Maxwell's law

$$\vec{\nabla} \times \vec{E} = -\frac{\partial \vec{B}}{\partial t}$$

4.6

$$\vec{\nabla} \times \vec{H} = -\frac{\partial \vec{D}}{\partial t} + \sigma \vec{E}$$

4.7

Since

$\vec{B} = \mu^* \vec{H}$, $\vec{D} = \varepsilon \vec{E}$ and σ is the conductivity of the material.

Equations 4.6 and 4.7 become

$$\vec{\nabla} \times \vec{E} = -j\omega\mu^* \vec{H}$$

and

$$\vec{\nabla} \times \vec{H} = j\omega\varepsilon\vec{E} + \sigma\vec{E}$$

$$\vec{\nabla} \times \vec{H} = j\omega\left(\varepsilon - j\frac{\sigma}{\omega}\right)\vec{E} = j\omega\varepsilon^* \vec{E}$$

57

where ε^* is the complex permittivity

$$\varepsilon^* = \varepsilon_o \left(\varepsilon' - j\varepsilon'' \right) \text{ where } \varepsilon'' = \frac{\sigma}{\omega\varepsilon_o}$$

Normalized complex permittivity is

$$\varepsilon_r = \frac{\overset{\bullet}{\varepsilon}}{\varepsilon_o} = \varepsilon' - j\varepsilon'' = \varepsilon' (1 - j\tan\delta)$$

where loss tangent ($\tan\delta$) is

$$\tan\delta = \frac{\varepsilon''}{\varepsilon'}$$

4.2.2.1 Methodology for measurement of complex permittivity of composites

The experimental setup for measurement of complex permittivity is shown in figure 4.3.
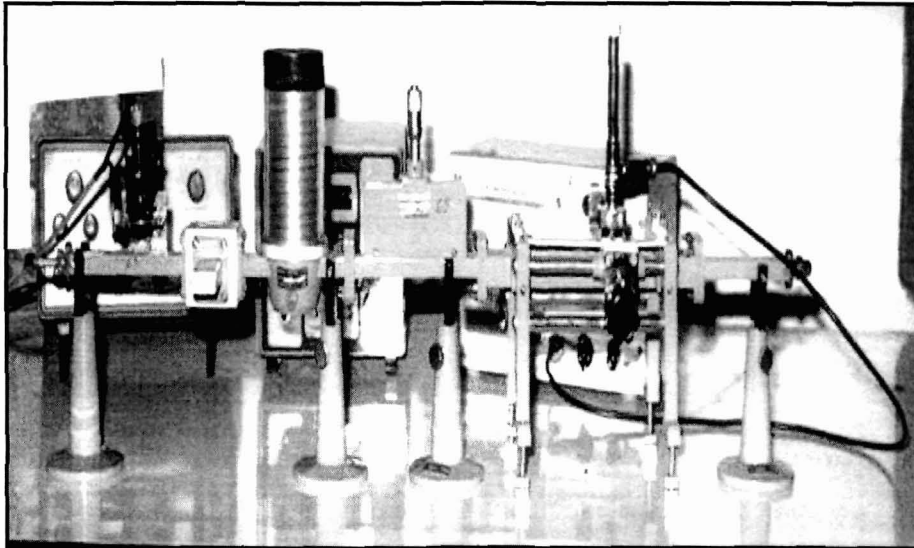
Figure 4.3: Experimental setup for complex permittivity measurement using waveguide technique

In this technique, voltage minima position (D_r) of empty short circuited waveguide is located with a probe as shown in figure 4.4a. When sample of length l_e is inserted in the

58

waveguide, the voltage minima position is shifted to a new position D as shown in figure 4.4b. The permittivity for loss less dielectric can be obtained from the transcendental equation [16]

$$K = \frac{\tan l_e (D_r - D - l_e)}{k_e l} = \frac{\tan k_e l_e}{k_e l_e} = \frac{\tan X}{X} \qquad\qquad 4.8$$

where $X = k_e l_e$ which is obtained from the solution of transcendental equation 4.8. A graph is plotted between X and $\frac{\tan X}{X}$. The value of K is determined from the graph and the corresponding X value is noted. The block diagram of complete experimental setup used for the measurement of complex permittivity of dielectric is shown in figure 4.5 .
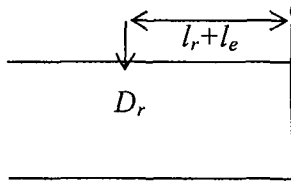
Figure 4.4a Empty waveguide
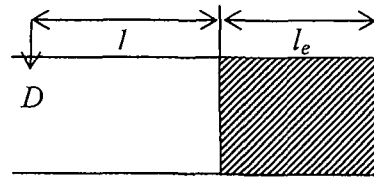
Figure 4.4b Filled waveguide
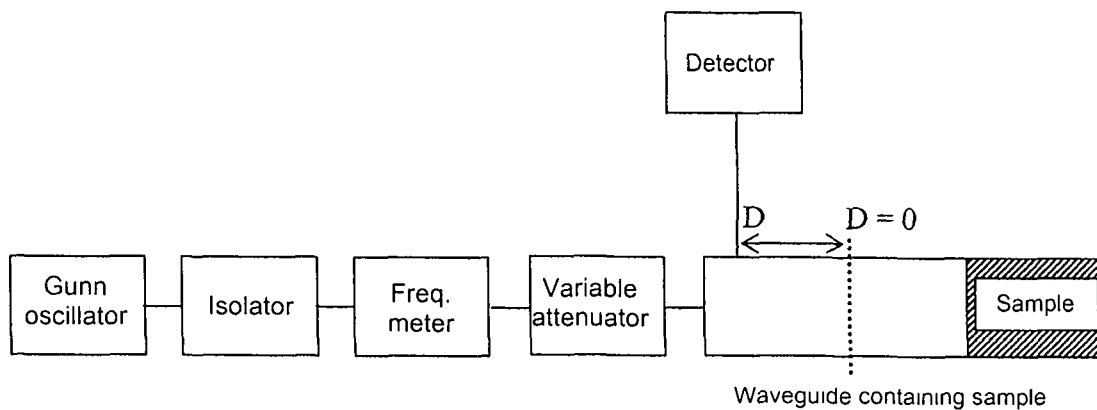
Figure 4.5: Block diagram of double minima method setup

Sample of different length e.g $l_{e,1}$ is taken and voltage minima position is noted. From the same transcendental plot, X is extracted and permittivity of both the samples are computed individually by using the following relationship

$$\varepsilon^{'} = \frac{\left(\frac{a}{\pi}\right)^2 \left(\frac{X}{l_e}\right)^2 + 1}{\left(\frac{2a}{\lambda_g}\right)^2} \qquad 4.9$$

where

a = width of waveguide and

λ_g = guide wavelength

For computing the complex permittivity of lossy dielectric, the reflection coefficient (Γ) of the sample is to be measured from the VSWR measurement where

$$VSWR = \frac{1+\Gamma}{1-\Gamma} \qquad 4.10$$

Complex impedance is computed by using the reflection coefficient thus obtained in complex transcendental equation

$$C = \frac{1}{j\beta l_e} \frac{1 - |\Gamma| e^{j\phi}}{1 + |\Gamma| e^{j\phi}} = \frac{\tan X \angle \theta}{X \angle \theta} \qquad 4.11$$

The admittance Y_ε is calculated as

$$Y_\varepsilon = \left(\frac{X}{\beta l_e}\right)^2 \angle 2(\theta - 90^0) = G_\varepsilon + jS_\varepsilon \qquad 4.12$$

Relative permittivity ($\varepsilon_r^{'}$) and the loss factor (ε_r^{*}) is related to the G_ε and S_ε as

$$\varepsilon^{'} = \frac{G_\varepsilon + \left(\lambda_g / 2a\right)^2}{1 + \left(\lambda_g / 2a\right)^2} \qquad 4.13$$

$$\varepsilon^{''} = \frac{-S_\varepsilon}{1 + \left(\lambda_g / 2a\right)^2} \qquad 4.14$$

The experimental computation of complex transcendental equation is not only complicated but time consuming also.

4.2.3 Resonance Method

In the resonance method the complex permittivity of a material is determined from the propagation constant measurement of a microstrip line [17]. This method is also known as dispersion method as the frequency dependence of dielectric constant is monitored.

4.2.3.1 Methodology for measurement of complex permittivity of composite

In this method the resonator is made up of a microstrip line shorted at both ends by conductor plates as shown in figure 4.6. The guide wavelength λ_g is measured as

$$\lambda_g = \frac{\text{physical length of the resonator}}{\text{No. of standing waves between the conductor plate}} \qquad 4.15$$

The ratio of free space wavelength (λ_0) and the guided wavelength (λ_g) is equals to ratio of propagation constant (β) of the microstrip line to the free space propagation constant (β_0).
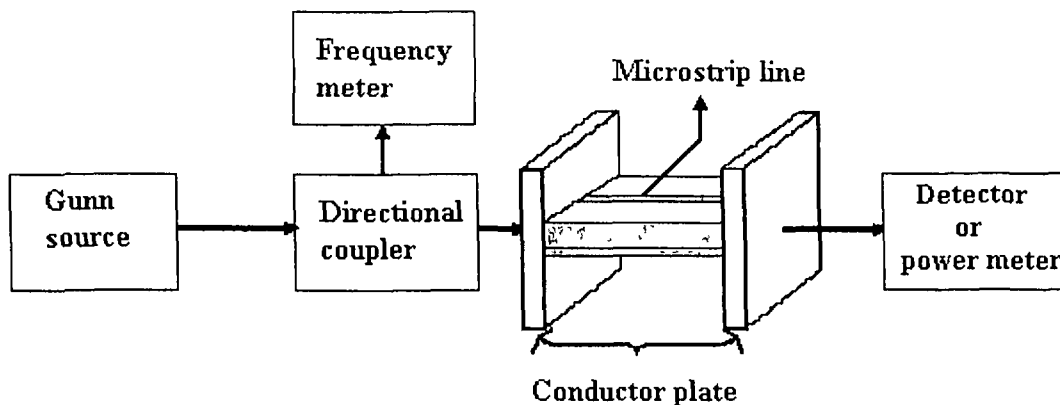
Figure 4.6: Block diagram of the experimental arrangement for resonance method

The complex permittivity (ε^*) of a microstrip line of strip width (w) and substrate height (h) can be calculated from the empirical relation given in reference [18] as

$$\frac{\beta}{\beta_o} = \frac{\sqrt{\varepsilon^*} - \frac{\beta_{TEM}}{\beta_o}}{1 + 4F^{-1.5}} + \frac{\beta_{TEM}}{\beta_o}$$

4.16

$$F = \frac{4h\sqrt{\varepsilon^* - 1}}{\lambda_o} + \left[0.5 + \left\{ 1 + \log_{10}\left(1 + \frac{w}{h}\right) \right\}^2 \right]$$

4.17

where β_{TEM} is the propagation constant at frequencies less than 0.1 GHz that can be determined by measuring the capacitance of a capacitor filled with the sample (C) and that with air (C_a).

$$\beta_{TEM} = \beta_o \sqrt{\frac{C_a}{C}}$$

4.18

4.3 THEORETICAL ASPECT OF PERMITTIVITY- EFFECTIVE MEDIUM THEORY

The importance of the dielectric properties of composites had been recognized long ago through the establishment of a number of phenomenological mixing laws to express the permittivity of heterogeneous mixture in terms of the permittivities and volume fraction of the constituent. Maxwell and Faraday originally discussed formulas for the permittivity of heterostructures [19]. When an electric field $\bar{E}$ is applied to material - cations and anions in the dielectric are displaced in response to the field [20]. This displacement produces an induced dipole moments and the aggregate of induced or permanent dipoles produces a net polarization in the material. The polarization is related to the displacement field by $\bar{D} = \varepsilon \bar{E} + \bar{P}$, where P is the polarization field density. Low loss materials usually have low permanent dipole moment, but possess appreciable induced dipole moment. The ratio of average displacement field vector and the applied electric field is defined as the complex effective dielectric constant ($\varepsilon = [\varepsilon_r' - j\varepsilon_r'']\varepsilon_0$) and it carries information about the average polarization in the heterogeneous medium [12-13]. The real part of permittivity is associated with the ability of the material to store electric field energy and the imaginary part reflects the ability of the material to dissipate electric energy of the composite system. The total energy

expressed as $\bar{E}^2\varepsilon = \left(\dfrac{1}{\Omega}\right)\displaystyle\int_\Omega \hat{\varepsilon}|\nabla V|^2 d\Omega$ where $\hat{\varepsilon}$ is the local electric permittivity value,

$\bar{E} = \dfrac{1}{\Omega}\displaystyle\int_\Omega E d\Omega$ denotes the average field which depends on the applied field potentials, E is

the local electric field in the medium and Ω is the volume of the medium.

The complex effective permittivity also depends on the permittivity of each constituent in the composite matrix, their volume fraction and eventually on the spatial arrangement in the mixture. The polarization of filler materials in an external field depends on its distribution in polymer and on intrinsic dielectric characteristics. With the increase in filler percentage the local potential increases in response to the same external applied electric field. This increase in potential increases the capacitance of the material. Higher value of capacitance results in higher effective permittivity of the composite.

When an inhomogeneous composite consist of two constituents, a dielectric filler having permittivity ε_1 surrounded by another material, polymer matrix with permittivity ε_2 as shown in figure 4.7, is acted by a macroscopic field $\bar{E}$, then the average displacement vector $\bar{D}$ is linearly proportional to the field as

$\bar{D} \alpha \bar{E}$

$\bar{D} = \varepsilon \bar{E}$ \hfill 4.19

where the proportionality coefficient (ε) defines the effective permittivity and is expressed as

$\varepsilon = \varepsilon_2 + n\alpha\dfrac{\bar{E_l}}{\bar{E}}$ \hfill 4.20

n is the number of filler per unit volume, α is the polarizability of each filler particle and $\bar{E}$ is the local electric field given by [21]

$\bar{E_l} = \bar{E} + \dfrac{1}{\varepsilon_2}\bar{L}n\alpha\,\bar{E_l}$ \hfill 4.21
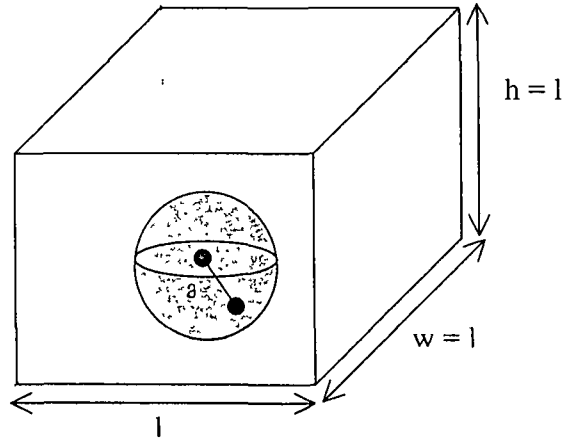
Figure 4.7: Pictorial representation of a spherical filler in cubic matrix

where $\overline{\overline{L}}$ is a depolarization dyadic or source dyadic that depends on the shape of the filler particle and is the key ingredients in homogenization analyses as they characterize the electromagnetic field inside filler (i.e. component phase particles) embedded within the homogenous background and is expressed as [22]

$$\overline{\overline{L}}_x = \frac{abc}{2} \int_0^\infty \frac{du}{(u + a^2)\sqrt{(u + a^2)(u + b^2)(u + c^2)}}$$ 4.22

where a, b, c is the dimension of the filler along the x, y, z axes respectively. Depolarization factor L_y, L_z is obtained by changing the position of a, b, c.

The polarizability α_i of the filler particle in the quasi-static limit is deduced from the solution of the internal field of the dielectric as [23]

$$\alpha_i = v_0(\varepsilon_1 - \varepsilon_2)\frac{\varepsilon_2}{\varepsilon_2 + (\varepsilon_1 - \varepsilon_2)L_i}$$ 4.23

where v_0 is the volume of a filler particle.

Structure and spherical symmetry of the reinforced particle, makes the composite medium isotropic. Therefore when the filler particles are spherical in nature, i.e $a = b = c$. The depolarization dyadic then takes the form

$$\overline{\overline{L}} = \frac{a^3}{3} \int_0^\infty \frac{du}{(u + a^2)^{5/2}} \qquad\qquad 4.24$$

The depolarization dyadic $\overline{\overline{L}}$ is then reduced to depolarization factor (L) characterizing all diagonal terms.

Integrating equation 4.24 within the limit specified the depolarization dyadic for spherical symmetry is calculated as

$$L = \overline{\overline{L}} = 1/3 \qquad\qquad 4.25$$

The polarizability α of spherical filler particle is computed from equation 4.23 as

$$\alpha = 4\pi a^3 \varepsilon_2 \frac{\varepsilon_1 - \varepsilon_2}{\varepsilon_1 + \varepsilon_2} \qquad\qquad 4.26$$

Local electric field of equation 4.21, for spherical particle can be written as

$$E_1 = \frac{\overline{E}}{1 - \dfrac{L n \alpha}{\varepsilon_2}} \qquad\qquad 4.27$$

Putting the value of local field of equation 4.27 in equation 4.20, the final expression is

$$\varepsilon = \varepsilon_2 + \frac{n\alpha}{1 - \dfrac{L n \alpha}{\varepsilon_2}} \qquad\qquad 4.28$$

Replacing the value of L and α from equations 4.25 and 4.26, equation 4.27 takes the form

$$\varepsilon = \varepsilon_2 \left[\frac{\varepsilon_1 + 2\varepsilon_2 + 2\dfrac{4}{3}\pi a^3 n(\varepsilon_1 - \varepsilon_2)}{\varepsilon_1 + 2\varepsilon_2 - \dfrac{4}{3}\pi a^3 n(\varepsilon_1 - \varepsilon_2)} \right] \qquad\qquad 4.29$$

Finally, the effective permittivity (ε) after mathematical manipulation is

$$\varepsilon = \varepsilon_2 \frac{\varepsilon_1 + 2\varepsilon_2 + 2f(\varepsilon_1 - \varepsilon_2)}{\varepsilon_1 + 2\varepsilon_2 - f(\varepsilon_1 - \varepsilon_2)} \qquad\qquad 4.30$$

Where $f = n v_0 = \dfrac{4}{3}\pi a^3 \dfrac{1}{l^3}$ is the volume fraction of filler particle and v_0 is the volume of a spherical particle in the composite.

65

When l = 2, volume fraction $f = \dfrac{\pi a^3}{6}$

After mathematical manipulation of equation 4.23

$$\frac{\varepsilon - \varepsilon_2}{\varepsilon + 2\varepsilon_2} = f\frac{\varepsilon_1 - \varepsilon_2}{\varepsilon_1 + 2\varepsilon_2}$$ 4.31

This formula is known as the Bruggeman's formula [24] of effective medium theory. The applicability of this formula rests firmly on the

i.   Quasi-static assumption

ii. Filler do not interact with each other

iii. The filler is embedded in an effective medium

iv. The filler particle is distributed randomly without interstices

v.   The volume average polarization in the composite material is equal to zero

In spite of the above mentioned approximations, Bruggeman's formula is used to analyze the electromagnetic properties of composite material with low volume fraction (up to 10% range) because of its simplicity in formulation and clear physical meaning.

4.4 SWEEP FREQUENCY MEASUREMENTS

The frequency dependence of the wave velocity in a transmission line is called dispersion property and it is an important parameter when the line is used in a wide frequency range.

The frequency dependence of dielectric constant gives rise to 'material dispersion' in which the wave velocity is frequency dependent. At microwave frequencies according to classical dispersion theory of dielectric [25], the dielectric constant is unchanged and the dielectric loss increases with frequency. Therefore the product of quality factor and frequency describes loss property of the dielectric.

For time domain measurement of complex permittivity in the 8.4 to 12 GHz range sweep frequency measurement set up is used. Using the resonance and waveguide

methods dispersive permittivity of the two composite systems are measured. In waveguide method, measurement of dispersive permittivity is computed from equation 4.9 at experimental frequency points. For resonance method the measurement, dispersive permittivity is measured from the measurement of uncalibrated scattering parameter (S -parameter) S_{11} and S_{12} over the frequency range. From these scattering parameters the complex propagation constant ($\gamma = a + j\ \beta$) of the same sample but of different lengths are calculated. The relative permittivity (ε') and loss factor (ε'') are calculated from the complex propagation constant as

$$\varepsilon' = \frac{\beta^2 + \left(\frac{\pi}{a}\right)^2}{\omega^2 \mu \varepsilon_0} \qquad\qquad 4.32$$

$$\varepsilon'' = \frac{2a\varepsilon'}{k}\sqrt{1 - \left(\frac{\lambda}{2a}\right)^2} \qquad\qquad 4.33$$

where 'a' is the physical length of the microstrip line, 'λ' is the wavelength, 'a' is the attenuation factor and 'β' is the propagation constant of the transverse electromagnetic mode.

The complex permittivity depends on the frequency but it stays almost constant over a small range of frequency spectrum [26-28]. The complex permittivity (ε) of a material is a function of angular frequency i.e. $\varepsilon(\omega) = \varepsilon_0[\varepsilon_r'(\omega) - j\varepsilon_r''(\omega)]$ where ε_r' is the time dependent relative permittivity, ε_r'' is the corresponding loss factor and ω is the radian frequency. The frequency dependence of the inductance and capacitance of the reinforced particle is negligible. Resonance dispersion law widely applied for the qualitative characterization of the dielectric properties of the composites [29] and is given by

$$\varepsilon(f) = \varepsilon_d + \frac{A}{1 - i\left(\frac{f}{f_{rel}}\right) - \left(\frac{f}{f_{res}}\right)^2} \qquad\qquad 4.34$$

where 'A' is the scale factor depends on the percentage of filler and f_{rel} and f_{res} are the relaxation and resonance frequencies defining the shape of dispersion curve.

4.5 RESULTS AND DISCUSSION

Generally, the dielectric response of a particulate filled polymer composites relies on characteristic of each phase in the composites [30-31]. From the interfacial polarization between two different dielectrics in the composite, under the influence of field, results in additional dielectric losses [32]. To substantiate permittivity of the new composite material at microwave frequencies, dielectric measurements are carried out at 5.5 GHz and 9.68 GHz using three techniques-cavity resonator, waveguide and resonance techniques.

4.5.1 Complex Permittivity Measurement Result for 1%VF of PS-alumina and PS-titania at 5.5 GHz

Complex permittivity of PS, 1%VF PS-alumina and 1%VF PS-titania composites are measured using network analyzer HP 8451C with all the three techniques mentioned above. The results obtained are tabulated in table 4.1.

Table 4.1: Complex permittivity of the composite with 1%VF of filler at C-band

Sample	%VF of filler	Cavity resonator method		Wave guide method		Resonance method	
		ε'	ε''	ε'	ε''	ε'	ε''
PS	0	2.5	0.0002	2.54	0.0002	2.54	0.0003
PS-alumina	1	2.55	0.0030	2.58	0.0036	2.58	0.0036
PS-titania	1	2.6	0.0040	2.62	0.0046	2.62	0.0045

4.5.2 Complex Permittivity Measurement Result for PS-alumina Composite at 9.68 GHz

It is observed from figure 4.8 that real part of complex permittivity of the PS-alumina composite system, measured with all the three techniques, increases from 2.5 to 2.785 at

9.68 GHz as the filler percentage increases from 0%VF to 7%VF. A deviation of permittivity values of PS-alumina composite using cavity resonator method is observed in comparison to other methods at higher volume fractions. As given in equation 4.4, ε' depends on the volume of the sample which is taken as physical volume of the composite placed in the cavity. Alumina particles have densities much higher than the polystyrene matrix (table 3.1, chapter III). As %VF of alumina increases in the composite, the embedded high density alumina also increases which may effectively change the volume of the sample, hence the deviation in permittivity values. Cavity resonator method may not be the best method to measure ε' for high density filler in the composite.
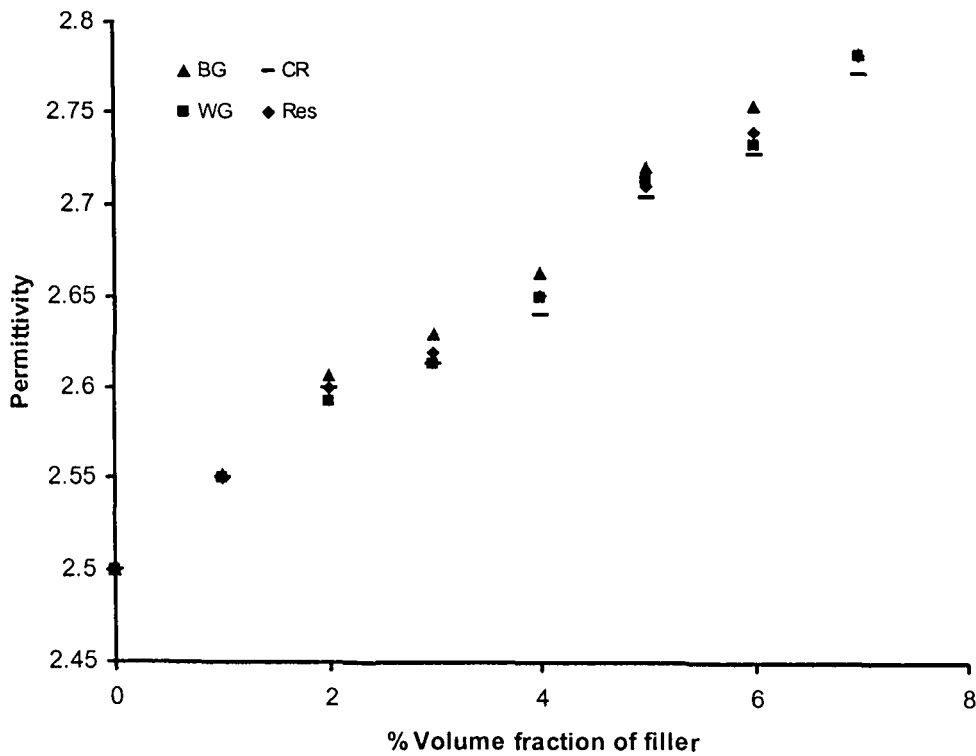
Figure 4.8: Permittivity of PS- alumina composite versus %VF of filler at 9.68GHz
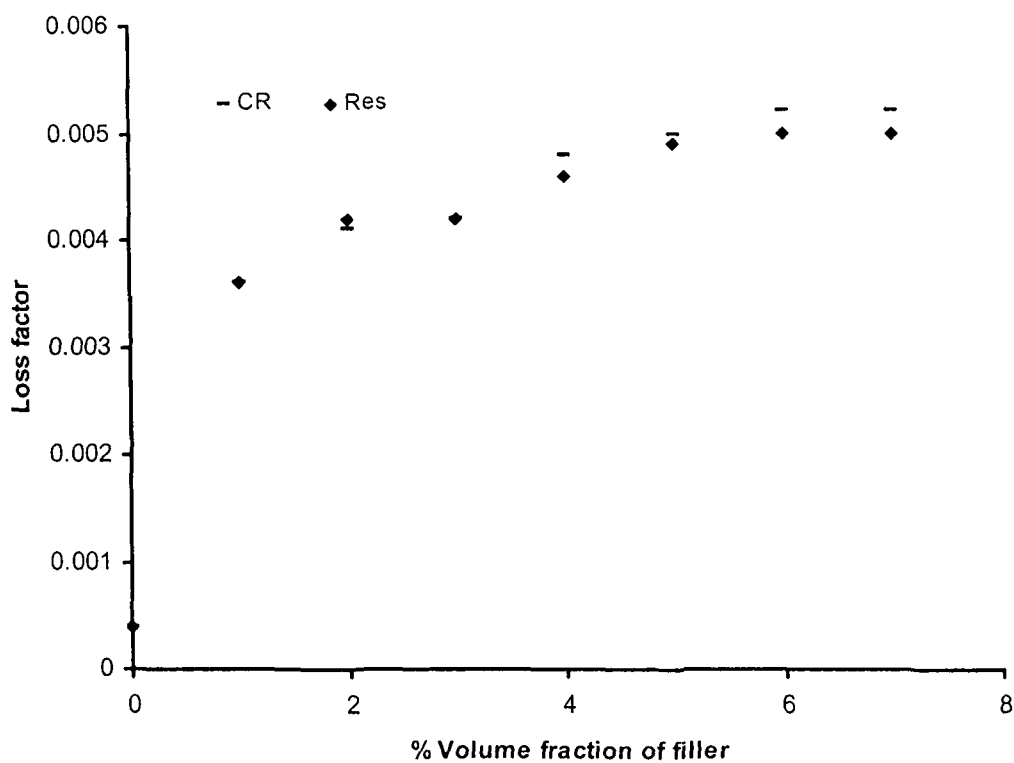
Figure 4.9: Loss factor of PS-alumina composite versus %VF of filler at 9.68GHz

With the increase in volume fraction of filler in PS-alumina composite, the loss factor (tanδ) shows an increasing trend (figure 4.9).

4.5.3 Complex Permittivity Measurement Result for PS-titania Composite at 9.68 GHz

The PS-titania composite system in figure 4.10 also shows an increase of permittivity from 2.5 to 3.338 for the same change in %VF of the filler. High dielectric constant of titania in comparison to alumina increases the effective permittivity of PS-titania composite as compared to PS-alumina for same volume fraction of filler. In PS-titania composite, the loss factor varies in the range 0.0035-0.005 for different volume fraction, as shown in figure 4.11. Although titania has higher tanδ as compared to alumina (table 3.1), PS-titania composite system shows a loss comparable to PS-alumina system. The decrease in particle size of titania (1 micron) as compared to the alumina (3 micron) in the matrix reduces the loss value.
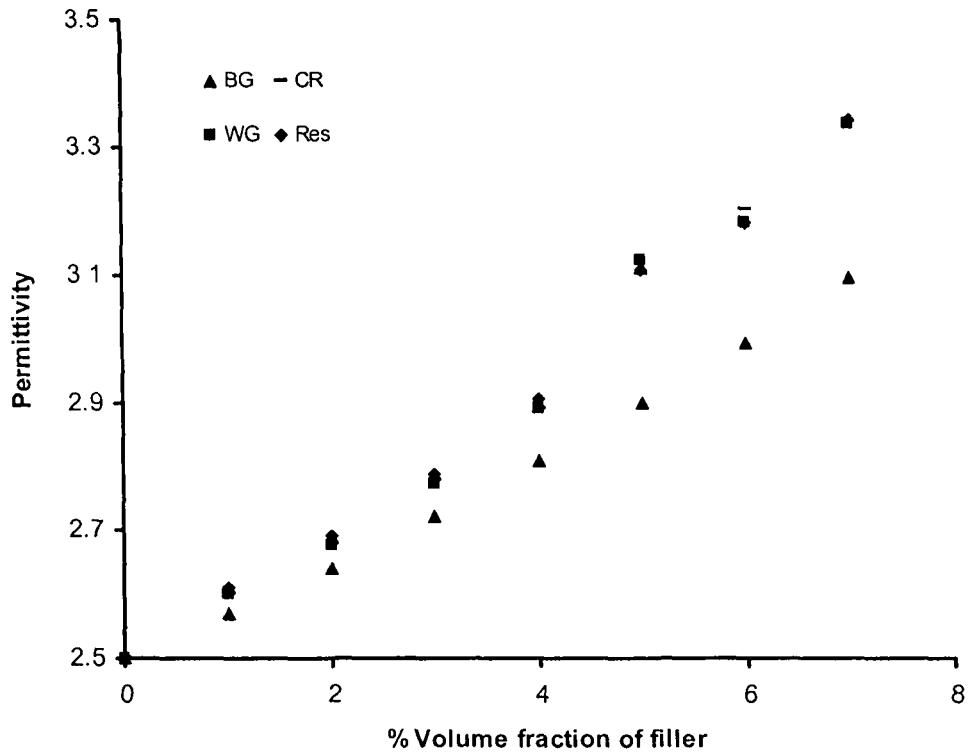
Figure 4.10: Permittivity of PS-titania composite versus %VF of filler at 9.68 GHz
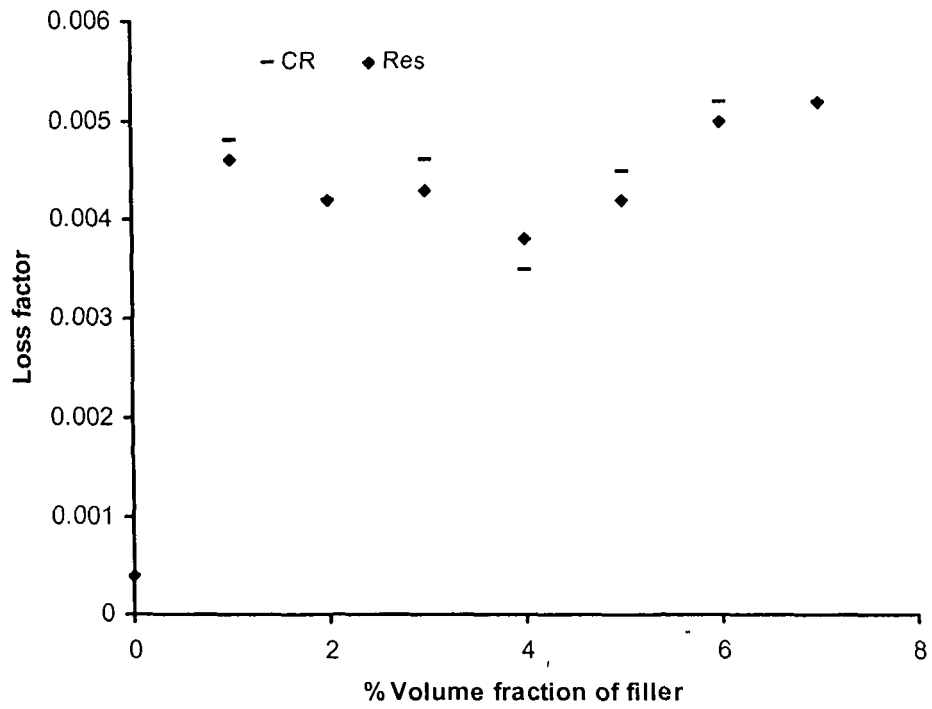
Figure 4.11: Loss factor of PS-titania composite versus %VF of filler at 9.68 GHz

4.5.4 Theoretical Results

The effective permittivity of the composite depends on the shape and size of the distribution of filler. The plot (figure 4.8) for PS-alumina composite shows a comparison of the experimental results with the results computed with the Bruggman's effective medium theory described in section 4.3. The experimental result is comparable with the analytical result. Small deviation from the theoretical value calculated by Bruggman's law is because of the presence of surfactant in the composite which gives better physical interaction of polymer and filler phase. The surfactant reduces the interphase region between the low dielectric polymer and high dielectric filler thus changing the effective dielectric constant of the composite [33].

The experimental results on PS-titania composite as shown figure 4.10, indicates deviation of effective permittivity from the Bruggman's effective medium approach. From the SEM photograph (figures 3.7 and 3.8) it can be observed that alumina particles are larger in size as compared to titania particles. It also shows that alumina particles are more regular in shape and distribution is more uniform than the titania particles. The filler quantity is kept very less (7%VF) than the percolation limit. So inter-particle interaction can be neglected and this is also approximated in generating the Bruggman's theory. High dielectric constant and small particle size of inclusions give rise to strong localized electric fields which may lead to higher displacement and hence showing the deviation. To accurately predict the dielectric variation of the composite with very high dielectric inclusion as filler, Bruggeman's theory has to be modified.

The effect of increase in number of particle with the real part of permittivity is tabulated in table 4.2. A steady increase in percentage permittivity is observed with increase in number of reinforced particles.

Table 4.2: Number of particle versus percentage increase in permittivity

%VF of filler	PS-alumina composite		PS-titania composite	
	Number of particles	% increase of permittivity	Number of particles	% increase of permittivity
1	28	1.96	40	4.2
2	46	3.84	62	7.132
3	65	4.58	90	10.32
4	85	5.3	120	13.94
5	106	7.74	152	19.5
6	128	8.75	169	21.35
7	151	10.1	190	25.1

4.5.5 Dispersive Complex Permittivity Measurement from 8.4 GHz to 12 GHz

Effective permittivity value of composites shows dispersive behavior. A frequency sweep from 8.4 to 12 GHz increases the real part permittivity of PS-alumina composite by 0.31- 0.39% and that of PS-titania composite by 0.60 to 0.69% as the volume fraction of filler in the composite increases from 1 to 7%. The dielectric spectra of 1% and 3%VF of PS-alumina and PS-titania, measured using resonance and waveguide method is shown in figures 4.12 to 4.15.

The variation of dispersive complex permittivity with different volume fraction measured with resonance method is shown in figures 4.15 and 4.16. The loss factor plot for polystyrene filled with 6%VF of alumina and titania are shown in figures 4.17 and 4.18 respectively. The loss ranges from 0.004 to 0.016 in PS-alumina composite and 0.0035 to 0.008 in PS-titania composite.
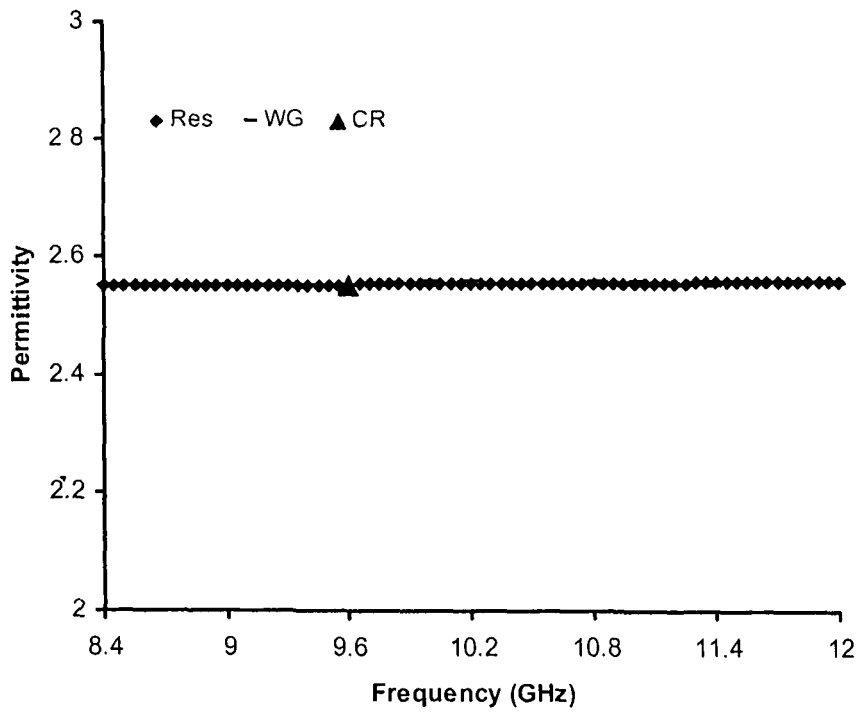
Figure 4.12: Dispersive permittivity of PS -1%VF alumina filler
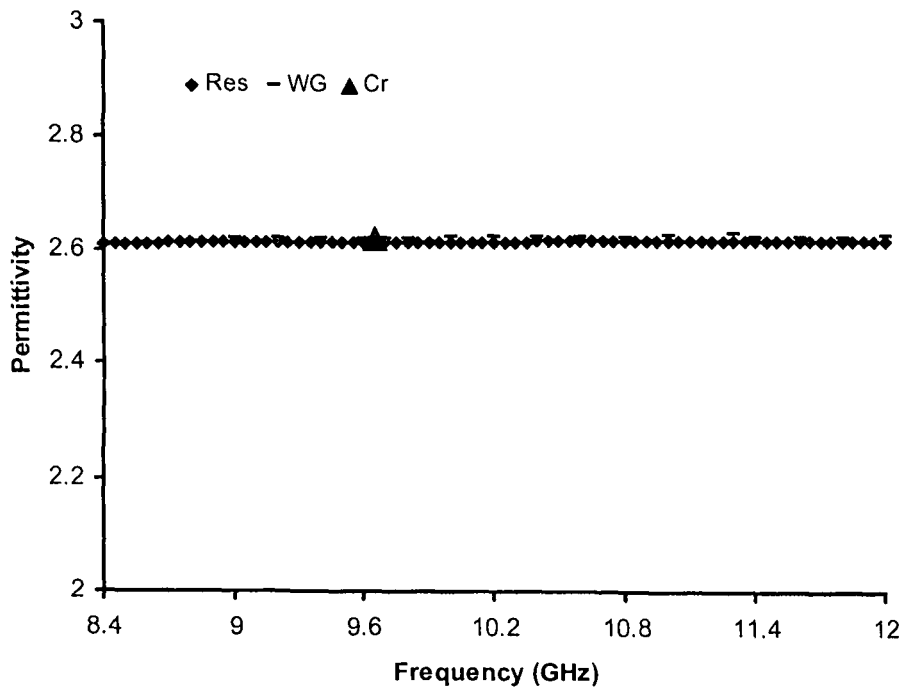
Figure 4.13: Dispersive permittivity of PS - 3%VF alumina filler
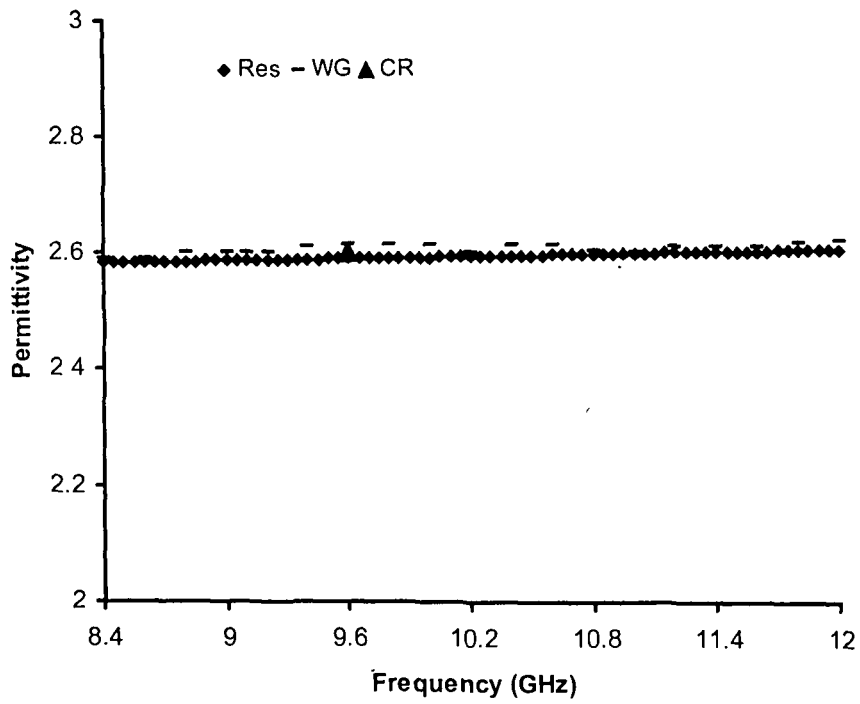
Figure 4.14: Dispersive permittivity of PS - 1%VF titania filler
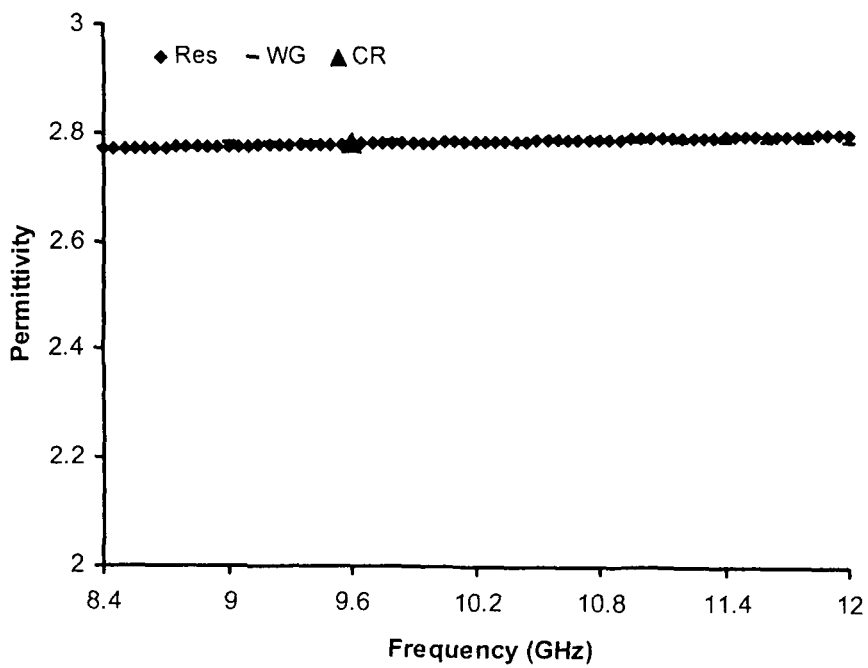
Figure 4.15: Dispersive permittivity of PS - 3%VF titania filler
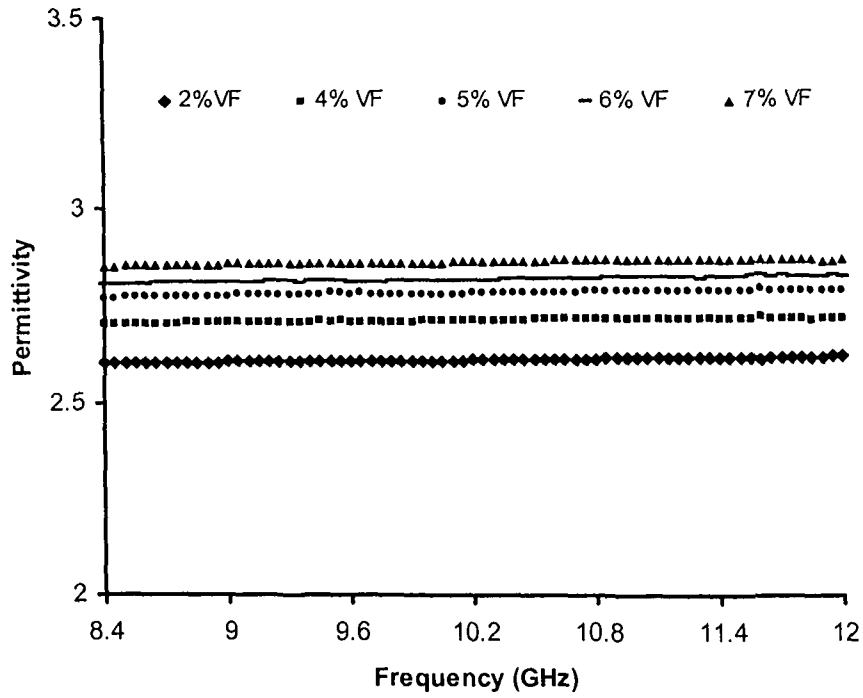
Figure 4.16: Dispersive permittivity of PS-alumina composite at a) 2%VF
b) 4%VF c) 5%VF d) 6%VF e) 7%VF of reinforced particles
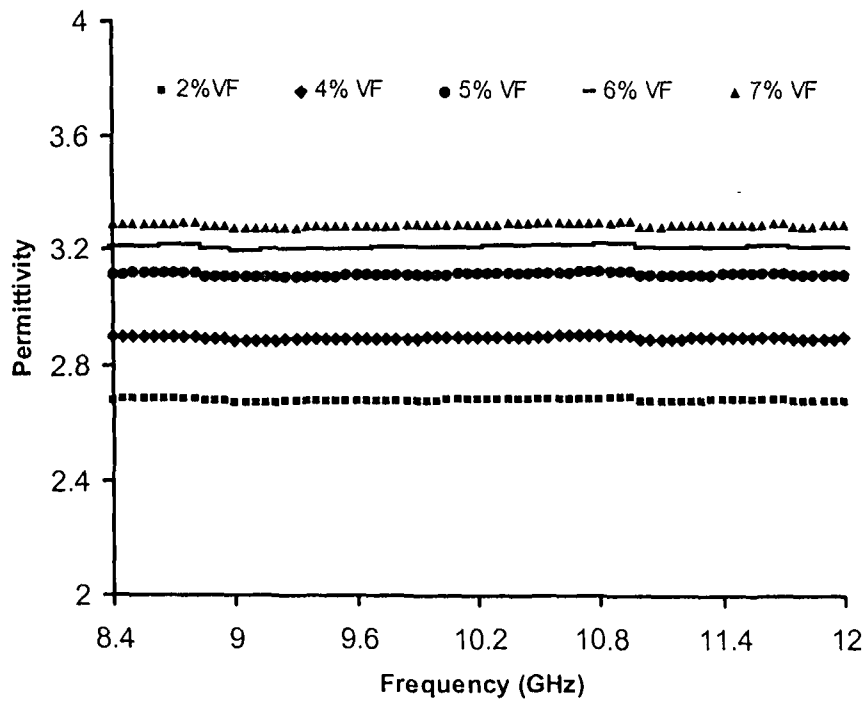
Figure 4.17: Dispersive permittivity of PS-titania composite at a) 2%VF
b) 4%VF c) 5%VF d) 6%VF e) 7%VF of reinforced particles
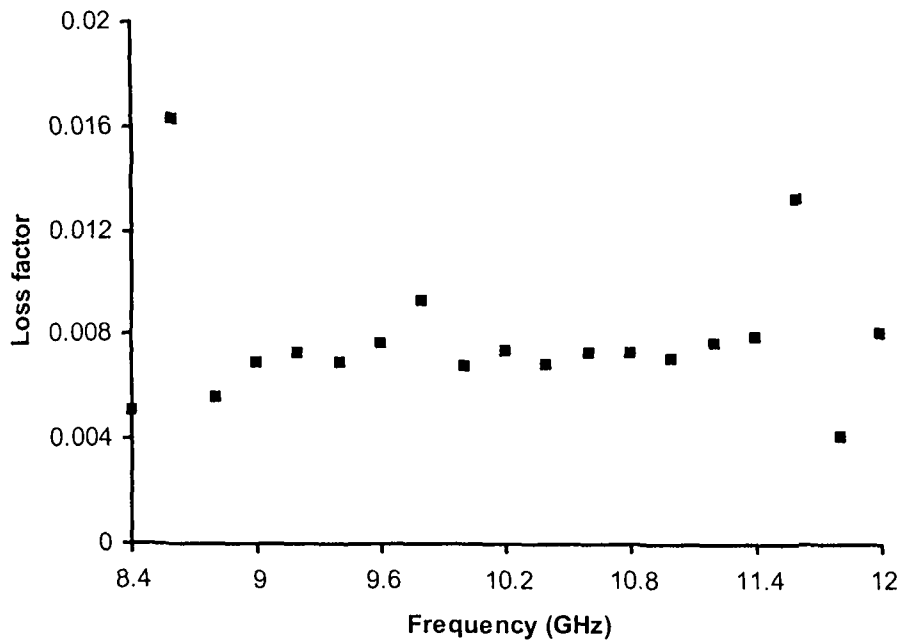
Figure 4.18: Loss factor versus frequency for PS-6%VF alumina
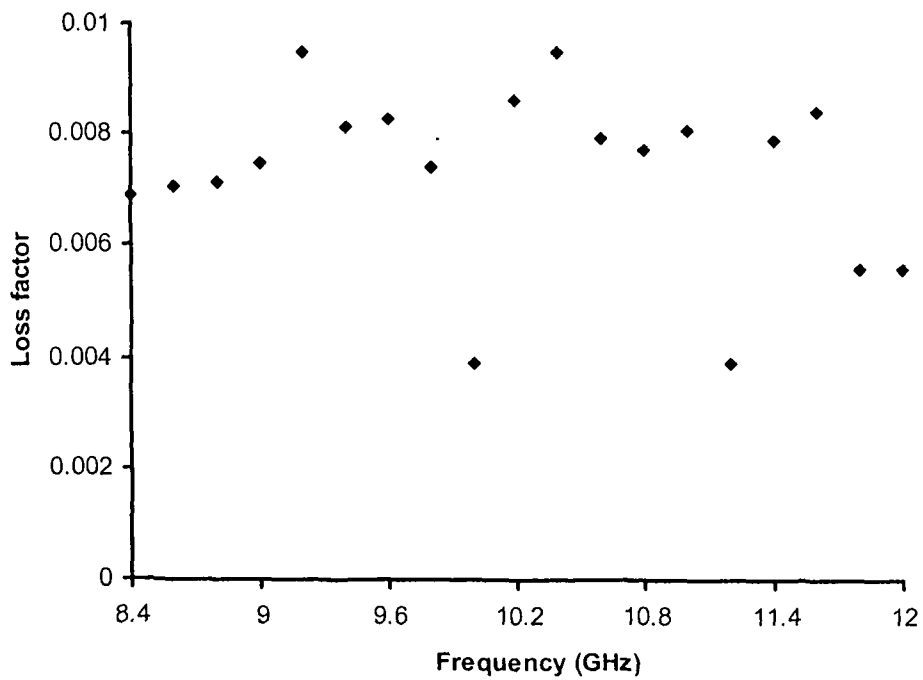
Figure 4.19: Loss factor versus frequency for PS-6%VF titania

4.6 CONCLUSION

A study of frequency behavior of the permittivity of the composite material containing homogeneous distribution of alumina and titania particles in the polystyrene matrix over a frequency range of 8.4-12.0 GHz is conducted. Resonance method for measuring complex permittivity is found simple as compared to other techniques. Real part of permittivity of composite is also calculated using Bruggeman's effective medium theory. High dielectric inclusion shows a marked deviation from the Bruggman's theory. The result obtained with all the three techniques employed to determine complex permittivities are comparable. Losses measured with cavity resonator and resonance method give good agreement in case of measurement for both the composites.

References:

[1] A. Issacs, J. Dainith and E. Martin, "A Dictionary of Science," Oxford University Press, Market House Books Limited, 1999.

[2] R. Landauer, In J. C. Garland and D. B. Tanner, "Electrical Transport and Optical Properties of Inhomogeneous Media," AIP Conf. Proc, vol. 40, pp- 2, 1978.

[3] A. K. Jonscher, "The Universal Dielectric Response and Its Physical Significance," IEEE Trans on Electrical Insulation, vol. 27, pp- 407, 1992.

[4] B. Sareni, L. Krahenbuhl, A. Beroual and C. Brosseau, "Effective Dielectric Constant of Periodic Composite Materials," Journal of Applied Physics, vol. 80, pp-1688, 1996.

[5] A. Priou, "Dielectric Properties of Heterogeneous Materials," Progress in Electromagnetics Research, New York, Elsevier, 1992.

[6] D. S. McLachlan, "The Complex Permittivity of Emulsions: An Effective Media-Percolation Equation," Solid State Communications, vol. 72, pp- 831, 1989.

[7] E. K Sichel, "Carbon Black-Polymer Composites," Edited by Marcel Dekker, New York, 1982.

[8] J. B. Donnet, R. C. Bansal and M. J. Wang, "Carbon Black, Science and Technology," Edited by Marcel Dekker, New York, 1983.

[9] F. Boulic, C. Brosseau, Y. Le Mest, J. Loa"ecx and F. Carmona, "Absorbency Properties and Electron Paramagnetic Resonance Characterization of Polymeric Carbon Black Composites," Journal of Physics. D: Applied Physics. vol. 31, pp- 1904, 1998.

[10] C. Brosseau, P. Queffelec and P. Talbot, "Microwave Characterization of Filled Polymer," Journal of Applied Physics, vol. 89, pp- 4532, 2001.

[11] H. M. Musal Jr., H. T. Hahn and G. G. Bush, "Validation of Mixture Equation for Dielectric-Magnetic Composite," Journal of Applied Physics, vol. 63, pp- 3768, 1988.

[12] B. Sareni, L. Krahenbuhl, A. Beroual and C. Brosseau, "Complex Effective Permittivity of a Lossy Composite Material," Journal of Applied Physics, vol. 80, pp- 4560, 1996.

[13] B. Sareni, L. Krahenbuhl, A. Beroual and C. Brosseau, "Effective Dielectric Constant of Random Composite Materials," Journal of Applied Physics, vol. 81, pp- 2375, 1997.

[14] M. Hajian, K. T. Mathew and L. P. Ligthart, "Measurement of Complex Permittivity with Waveguide Resonator using Perturbation Technique," Microwave and Optical Technology Letters, vol. 21, pp- 269, 1999.

[15] V. R. K. Murthy , S. Sunderam and B. Viswanathan, " Microwave Materials," Narosa Publishing House ,1990.

[16] S. Max and F. Jerome, "Handbook of Microwave Measurements," John Willey and Sons, New York, vol. 2, 1963.

[17] E. Yamashita, K. Atsuki and T. Hirahata, "Microstrip Dispersion in a Wide Frequency Range," IEEE Trans Microwave Theory and Techniques, vol. 29, pp- 610, 1981.

[18] E. Yamashita, K. Atsuki and T. Ueda, "An Approximate Dispersion Formula of Microstrip Lines for Computer Aided Design of Microwave Integrated Circuits," IEEE Trans Microwave Theory and Techniques, vol. 27, pp- 1036, 1979.

[19] J.C. Maxwell, "A Treatise on Electricity and Magnetics," 2nd Edition, Oxford: Clarendon Press, 1881.

[20] J. B. Jarvis, R. G. Geyer, J. H. Grosvenor, Jr., M. D. Genezic, C. A. Jones, B. Riddle and C. M. Weil, "Dielectric Characterization of Low Loss Materials Measurement Techniques," IEEE Trans on Dielectrics and Electrical Insulation, vol. 5, pp- 571, 1998.

[21] A. D. Yaghjian, "Maxwellian and Cavity Electromagnetic Fields within Continuous Sources," American Journal of Physics, vol. 53, pp- 859, 1985.

[22] B. B. Das Gupta and R. Fuchs, "Polarizability of a Small Sphere Including Non Local Effects," Physical Review B, vol. 24, pp- 554, 1981.

[23] B. K. P. Scaife, "Principles of Dielectrics," Oxford, Clarendon Press, 1998.

[24] D. A. G. Bruggeman, "The Calculation of Various Physical Constants of Heterogeneous Substances. I. The Dielectric Constants and Conductivities of Mixtures Composed of Isotropic Substances," Annalen der Physik (Berlin, Germany) vol. 24, pp- 636,1935.

[25] W. G. Spitzer, R. C. Miller, D. A. Kleinman and L. E. Howarth, "Far Infrared Dielectric Dispersion in $BaTiO_3$, $SrTiO_3$ and TiO_2," Physical Review, vol. 126, pp- 1710, 1962.

[26] W. J. Chudobiak, O. P. Jain and V. Makios, "Dispersion in Microstrip", IEEE Trans Microwave Theory and Techniques, vol. 19, pp- 783, 1971.

[27] B. Riddle and J. B. Jarvis, "Complex Permittivity Measurement of Common Plastic Over Variable Temperature," IEEE Trans Microwave Theory and Techniques, vol. 51, pp- 727, 2003.

[28] A. N. Lagarkov, S. M. Matytsin, K. N. Rozanov and A. K. Sarychev, "Dielectric Permittivity of Fiber-filled Composites: Comparison of Theory and Experiment," Physica A, vol. 241, pp- 58, 1997.

[29] W. M. Merrill, R. E. Diaz and N. G. Alexopoulos, "A Recasting of the Effective Parameters of Composite Mixtures into the Language of Artificial Dielectrics," Physica A, vol. 241, pp- 334, 1997.

[30] W. G. Spitzer, R. C. Miller, D. A. Kleinman and L. E. Howarth, "Far Infrared Dielectric Dispersion in $BaTiO_3$, $SrTiO_3$ and TiO_2," Physical Review, vol. 126, pp- 1710,1962.

[31] M. G. Todd and F. G. Shi, "Molecular Basis of the Interphase Dielectric Properties of Microelectronic and Opto-electronic Packaging Materials," IEEE Trans on Components and Packaging Technologies, vol. 26, pp- 667, 2003.

[32] Z. Yutao, C. Cheng, J. Weifang, X. Hengkun and L. Yaonan, "Relationship between Dielectric Loss and Interphase Structure of Filled-types Polymer Composite," State Key Lab of Electrical Insulation for Power Equipments, pp- 77.

[33] M. G. Todd and F. G. Shi, "Characterization of the Interphase Dielectric Constant of Polymer Composite Materials: Effect of Chemical Coupling Agents," Journal of Applied Physics, vol. 94, pp- 4551, 2003.

CHAPTER V

NUMERICAL MODELING FOR DETERMINATION OF

PROPAGATION CONSTANT IN COMPOSITE SUBSTRATE

5.1 INTRODUCTION

The widespread use of microwave integrated circuits (MIC's) in recent years has caused rapid progress in its theory and technology. The analysis of microstrip line with Fourier transform domain was first introduced by Yamashita and Mittra [1] for computation of the characteristic impedance and the phase velocity of a microstrip line, based on a quasi TEM approximation. For high frequencies, however, a rigorous treatment or a full-wave analysis is needed to account for the dispersive properties of the propagation characteristic of the microstrip lines [2-14]. The accuracy of the final results using this method depends on how accurately the current distributions on the microstrip line have been evaluated.

Various methods based on full wave theory have been proposed to obtain both longitudinal and transverse current distribution [15-19]. Any numerical methods for characterization need to be as efficient and economical as possible in both CPU time and temporary storage requirement. The storage requirement, CPU time, generality, preprocessing time of different numerical process for analysis of current distribution in a microstrip line is tabulated in table 5.1.

The spectral domain technique (SDT) is one of the most powerful analytical methods and is used for the analysis of fields in the composites. Galerkin's method is used to yield homogenous systems of equations to determine the propagation constant and the amplitude of current distribution, from which the characteristic impedance is derived [6,12].

In the present investigation, SDT is used to solve the electric field configuration of a microstrip line designed on a particle reinforced polymer composite substrate. The formulation of an exact theory for such microstrip structure is difficult because the cross-section is not uniform. Furthermore, microstrip is an open structure where the energy is not confined to a finite region. Due to boundary conditions involving transverse in homogeneity in the dielectric and the strip interface no pure transverse electric (TE) or transverse magnetic (TM) modes may exist. Thus a hybrid mode solution that can be expressed in

terms of a complete set of simpler solutions having z-dependence of exp(-ikz) is sought. To analyze the electric and magnetic field configuration on particulate composite substrate, SDT is modified for composite (SDTMC). Particle reinforced polymer composite substrate polystyrene/alumina and polystyrene/titania are basically high dielectric filler particles embedded homogeneously in the polymer matrix. Therefore a uniform single layer with effective dielectric constant of the composite or a regular polymer-filler multilayer structure can not analyze the field pattern completely.

Table 5.1: Comparison of Various Numerical Methods

Methods	Storage requirement	CPU time	Generality	Preprocessing
Finite Difference	Large	Large	Very Good	Nil
Finite element	Large	Moderate, Large	Very Good	Small
Boundary element	Moderate	Moderate	Very Good	Small
Transmission line matrix	Moderate, Large	Moderate, Large	Very Good	Small
Integral equation	Small, Moderate	Small, Moderate	Good	Moderate
Mode matching	Moderate	Small, Moderate	Good	Moderate
Transverse resonance	Small, Moderate	Small, Moderate	Marginal	Moderate
Method of lines	Moderate	Small	Good	Large
Spectral domain	Small	Small	Marginal	Large

Hence, SDT is modified to rigorously analyze the circuit behavior. The entire composite substrate is approximated as consisting of number of polymer-filler units. The resultant electric and magnetic field distribution of the circuit designed on the composite will be combined effect of such fields. The average distribution of such units is determined from microstructure studies conducted in chapter III. SDTMC has been successfully applied in the analysis of a microstrip line in the next chapter.

5.2 FORMULATION OF THE PROBLEM

Microstrip line is the simplest transmission line in microwave integrated circuits with a ground plane at the bottom and a metal strip etched on and top of the substrate. Spectral domain solution as reported in [20] can analyze propagation constant on the microstrip line on a substrate in single as well as in multilayer structure where permittivity of the substrate layer/layers has same value. However in the present investigation the substrate material does not posses the characteristic of a single layer or a multilayer substrate.
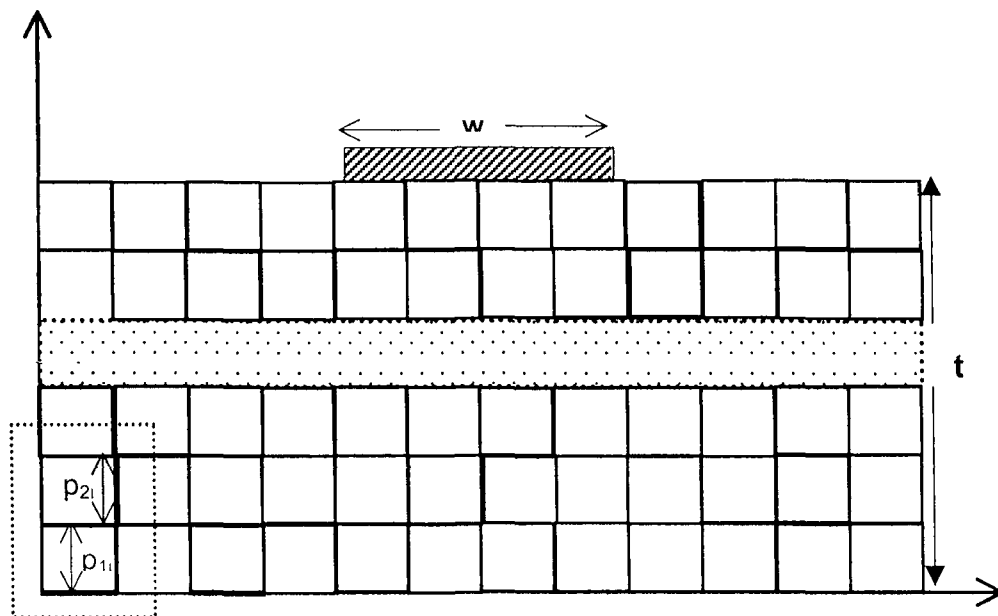
Figure 5.1: Cross- section of an open microstrip line on homogeneously distributed polymer filler composite.
(fill box – filler particle, white box- polymer, shaded portion- conducting strip)
(The blocks inside the dashed box represents one polymer filler unit)

5.2.1 Approximation for Development of Spectral Domain Technique for Composite

To develop SDT for the composite substrate some approximations are considered. As mentioned in the previous section the substrate is divided into numbers of polymer filler units as shown in figure 5 1. One polymer-filler unit is that which contains a polystyrene layer and a alumina /titania particle layer. The height of the polymer layer (P_1), is average distance between two consecutive filler particles, which is determined from the scanning electron micrographs (SEM). The filler particle is approximated to be spherical, the filler layer height (P_2) is taken as that of the average diameter of the reinforced particle. The width of each polymer- filler unit is taken as the diameter of the filler particle. The cell containing the filler particle has been approximated as square, completely filled with the filler particle. The number of such cells is average number of reinforced particles (N) on the composite substrate and is determined from the SEM and optical micrographs studies conducted in chapter III.

Initially, electric and magnetic field is generated for one polymer-filler unit using the spectral domain technique for multilayer structure [20-26] The resultant field components are then multiplied by number of particle in the area under the conductor strip. Structure modeled with the above approximations is shown in figure 5.1.The filler particles are distributed uniformly in the polymer matrix as shown in figure 5.2.
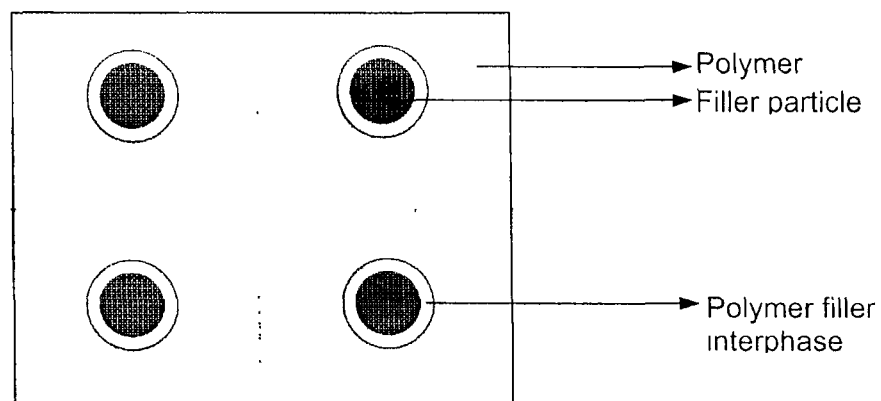
Figure 5.2: Interphase region between filler particle and polymer in a polymer–ceramic composite

Although the inter-phase layer dielectric constant also plays important role in the dielectric behavior of the composite [27] but in the present formulation interphase dielectric constant is ignored as surfactant is added to reduce this layer.

5.2.2 Electric and Magnetic Field Equations in the Fourier Domain

In SDT and in several other techniques of solving planar structure the objective is to reduce the solution of the problem to a complete set of coupled integral equations [28]. These equations relate the tangential components of electric field at the interfaces where strips of conductor are laid, to the current distributions of the strips. The expressions for the electric and magnetic field in dielectric medium are

$$\tilde{E}_{zi} = (k_i^2 - \beta^2)\tilde{\phi}(\alpha_n, y)e^{-j\beta z}$$

5.1

$$\tilde{H}_{zi} = (k_i^2 - \beta^2)\tilde{\psi}_i(\alpha_n, y)e^{-j\beta z}$$

5.2

$$\tilde{E}_{ti} = -j\beta\left[\tilde{\nabla}_t\phi_i(\alpha_n y) - \frac{\omega\mu_i}{\beta}(k \times \tilde{\nabla}_t)\psi_i(\alpha_n y)\right]e^{-j\beta z}$$

5.3

$$\tilde{H}_{ti} = -j\beta\left[\tilde{\nabla}_t\psi_i(\alpha_n y) - \frac{\omega\mu_i}{\beta}(k \times \tilde{\nabla}_t)\phi_i(\alpha_n y)\right]e^{-j\beta z}$$

5.4

where

$$\tilde{\nabla}_t = -j\alpha_n\hat{i} + \frac{\partial}{\partial y}\hat{j}$$

5.5

and i, j are the x and y directed unit vectors.

$$k_i^2 = \omega^2\mu_i\varepsilon_i$$

5.6

$$\gamma_i^2 = \alpha^2 + \beta^2 - k_i^2$$

5.7

Now,

$$\tilde{E}_{t,i} = -\left[\left(-j\alpha_n\hat{x} + \frac{\partial}{\partial y}\hat{y}\right)\tilde{\phi}_i + \frac{\omega\mu_i}{\beta}\left\{k \times \left(-j\alpha_n\hat{x} + \hat{y}\frac{\partial}{\partial y}\right)\tilde{\psi}_i\right\}\right]e^{-j\beta z}$$

$$= -\left[\left\{-j\alpha_n\phi_i\hat{x} + \hat{y}\frac{\partial\phi_i}{\partial y}\right\} + \frac{\omega\mu_i}{\beta}\left\{-\hat{y}j\psi_i - \hat{x}\frac{\partial\psi_i}{\partial y}\right\}\right]e^{-j\beta z}$$

$$= \left[j\alpha_n\phi_i\hat{x} - \hat{y}\frac{\partial\phi_i}{\partial y} - \hat{y}\frac{\omega\mu_i}{\beta} - \hat{y}\frac{\omega\mu_i}{\beta}j\alpha_n\psi_i - \hat{x}\frac{\omega\mu_i}{\beta}\frac{\partial\psi_i}{\partial y}\right]e^{-j\beta z}$$

$$\tilde{E}_{x,i} = j\alpha_n\phi_i - \frac{\omega\mu_i}{\beta}\frac{\partial\psi_i}{\partial y} \qquad\qquad 5.8$$

$$\tilde{H}_{t,i} = -(-j\alpha_n\hat{x} - \hat{y}\frac{\partial}{\partial y})\psi_i - \frac{\omega\epsilon_i}{\beta}\left\{k\times\left(-j\alpha\hat{x} + \hat{y}\frac{\partial}{\partial y}\right)\phi_i\right\}$$

$$= j\alpha_n\hat{x}\psi_i - \hat{y}\frac{\partial}{\partial y}\psi_i - \frac{\omega\epsilon_i}{\beta}\left\{-\hat{y}j\phi_i\left(-j\alpha\hat{x} + \hat{y}\frac{\partial}{\partial y}\right)\phi_i\right\}$$

$$\tilde{H}_{t,i} = j\alpha_n\psi_i\hat{x} + \frac{\omega\epsilon_i}{\beta}\hat{x}\frac{\partial\phi_i}{\partial y} + \hat{y}\frac{\omega\epsilon_i}{\beta}j\phi_i - \hat{y}\frac{\partial\psi_i}{\partial y}$$

$$\tilde{H}_x = j\alpha_n\psi_i + \frac{\omega\epsilon_i}{\beta}\frac{\partial\phi_i}{\partial y} \qquad\qquad 5.9$$

Let there be 'i' number of layers with heights h_1, h_2, ...h_t and $v_i = h_i$

$$\phi_i = A_i\sinh(\gamma_i v_i) + B_i\cosh(\gamma_i v_i) \qquad\qquad 5.10$$

$$\psi_i = C_i\sinh(\gamma_i t) + D_i\cosh(\gamma_i t) \qquad\qquad 5.11$$

Applying boundary conditions at the interface between two layers,

$$\tilde{E}_{z,i} = \tilde{E}_{z,i+1} \qquad\qquad 5.12$$

$$\tilde{E}_x = \tilde{E}_{x,i+1} \qquad\qquad 5.13$$

$$\tilde{H}_{z,i} = \tilde{H}_{z,i+1} \qquad\qquad 5.14$$

$$\tilde{H}_x = \tilde{H}_{x,i+1} \qquad\qquad 5.15$$

Putting values of equations 5.10 and 5.11 in 5.1-5.4, the resultant electric and magnetic fields becomes,

$$(k_i^2 - \beta^2)A_{i,n}s_v + (k_i^2 - \beta^2)B_{i,n}c_v = (k_{i+1}^2 - \beta^2)A_{i+1}s_u + (k_{i+1}^2 - \beta^2)B_{i+1}c_v \qquad 5.16$$

$$-j\alpha_n A_i s_v - j\alpha_n B_i c_v + \frac{\omega\mu_i\gamma_i}{\beta}C_{i,n}c_v + \frac{\omega\mu_i\gamma_i}{\beta}D_1 s_v = -j\alpha_n A_{i+1}s_u - j\alpha_n B_{i+1}c_u$$

$$+ \frac{\omega\mu_{i+1}\gamma_{i+1}}{\beta}C_{i+1}c_u + \frac{\omega\mu_{i+1}\gamma_{i+1}}{\beta}D_{i+1}s_u$$

$$[\gamma_i v_i] = \begin{bmatrix} (k_i^2 - \beta^2)\sinh(\gamma_i v_i) & (k_i^2 - \beta^2)\cosh(\gamma_i v_i) & 0 & 0 \\ 0 & 0 & (k_i^2 - \beta^2)\sinh(\gamma_i v_i) & (k_i^2 - \beta^2)\cosh(\gamma_i v_i) \\ -j\alpha_n\sinh(\gamma_i v_i) & -j\alpha_n\cosh(\gamma_i v_i) & -\frac{\omega\mu_i\gamma_{i,n}}{\beta}\cosh(\gamma_i v_i) & \frac{\omega\mu_i\gamma_{i,n}}{\beta}\sinh(\gamma_i v_i) \\ \frac{\omega\epsilon_i\gamma_{i,n}}{\beta}\cosh(\gamma_i v_i) & \frac{\omega\epsilon_i\gamma_{i,n}}{\beta}\sinh(\gamma_i v_i) & -j\alpha_n\sinh(\gamma_i v_i) & -j\alpha_n\cosh(\gamma_i v_i) \end{bmatrix} \quad 5.17$$

where

$$k_i^2 = \omega^2\mu_i\epsilon,$$

$$i = p$$

$$\epsilon_i = \epsilon_p$$

v_i = height of polymer layer, p_1

Now,

$$a_{13} = a_{14} = a_{21} = a_{22} = 0$$

$$a_{11} = a_{23} = (k_p^2 - \beta^2)\sinh(\gamma_p p_1)$$

$$a_{12} = a_{24} = (k_p^2 - \beta^2)\cosh(\gamma_p p_1)$$

$$a_{31} = a_{43} = -j\alpha_n\sinh(\gamma_i v_i)$$

$$a_{32} = a_{44} = -j\alpha_n\cosh(\gamma_i v_i)$$

$$a_{33} = -\frac{\omega\mu_i\gamma_{i,n}}{\beta}\cosh(\gamma_i v_i)$$

$$a_{34} = \frac{\omega\mu_i\gamma_{i,n}}{\beta}\sinh(\gamma_i v)$$

$$a_{41} = \frac{\omega\epsilon_i\gamma_{i,n}}{\beta}\cosh(\gamma_i v_i)$$

$$a_{42} = \frac{\omega \epsilon_i \gamma_{i,n}}{\beta} \sinh(\gamma_i v_i)$$

$$
[\gamma_{p_2} p_2] = [P] = \begin{bmatrix}
(k_p^2 - \beta^2)\sinh(\gamma_{p_2} p_2) & (k_p^2 - \beta^2)\cosh(\gamma_{p_2} p_2) & 0 & 0 \\
0 & 0 & (k_p^2 - \beta^2)\sinh(\gamma_{p_2} p_2) & (k_p^2 - \beta^2)\cosh(\gamma_{p_2} p_2) \\
-j\alpha_n \sinh(\gamma_{p_2} p_2) & -j\alpha_n \cosh(\gamma_{p_2} p_2) & -\frac{\omega\mu_p\gamma_{p_2}}{\beta}\cosh(\gamma_{p_2} p_2) & \frac{\omega\mu_p\gamma_{p_2}}{\beta}\cosh(\gamma_{p_2} p_2) \\
\frac{\omega\varepsilon_p\gamma_{p_2}}{\beta}\cosh(\gamma_{p_2} p_2) & \frac{\omega\varepsilon_p\gamma_{p_2}}{\beta}\sinh(\gamma_{p_2} p_2) & -j\alpha_n \sinh(\gamma_{p_2} p_2) & -j\alpha_n \cosh(\gamma_{p_2} p_2)
\end{bmatrix}
$$

$$5.18$$

$$p_{13} = p_{14} = p_{21} = p_{22}$$

$$p_{11} = p_{23} = (k_p^2 - \beta^2)\sinh(\gamma_{p_2} p_2)$$

$$p_{12} = p_{24} = (k_p^2 - \beta^2)\cosh(\gamma_{p_2} p_2)$$

$$p_{31} = p_{43} = -j\alpha_n \sinh(\gamma_{p_2} p_2)$$

$$p_{32} = p_{44} = -j\alpha_n \cosh(\gamma_{p_2} p_2)$$

$$\det[\gamma_{p_2} p_2] = (p_{12}p_{31} - p_{11}p_{32})(p_{23}p_{44} - p_{24}p_{43}) + (p_{11}p_{42} - p_{12}p_{41})(p_{23}p_{34} - p_{24}p_{33}) \quad 5.19$$

$$p_{11}^c = -p_{23}p_{32}p_{44} + p_{23}p_{34}p_{42} + p_{24}p_{32}p_{43} - p_{24}p_{33}p_{42}$$

$$p_{12}^c = p_{23}(p_{31}p_{44} - p_{34}p_{41}) - p_{24}(p_{31}p_{43} - p_{33}p_{41})$$

$$p_{13}^c = p_{24}(p_{31}p_{42} - p_{32}p_{41})$$

$$p_{14}^c = -p_{23}(p_{31}p_{42} - p_{41}p_{32})$$

$$p_{21}^c = -p_{12}(p_{33}p_{44} - p_{34}p_{43})$$

$$p_{22}^c = p_{11}(p_{33}p_{44} - p_{34}p_{43})$$

$$p_{23}^c = p_{12}(p_{31}p_{44} - p_{34}p_{41}) - p_{11}(p_{32}p_{44} - p_{34}p_{42})$$

$$p_{24}^c = p_{11}(p_{32}p_{43} - p_{33}p_{42}) - p_{12}(p_{31}p_{43} - p_{33}p_{41})$$

$$p_{31}^c = p_{12}(p_{23}p_{44} - p_{24}p_{43})$$

$$p_{32}^c = -p_{11}(p_{23}p_{44} - p_{24}p_{43})$$

$$p_{33}^c = p_{24}p_{12}p_{41} - p_{11}p_{24}p_{42}$$

$$p_{34}^c = p_{11}p_{23}p_{42} - p_{12}p_{23}p_{34}$$

$$p_{41}^c = p_{12}p_{24}p_{33} - p_{12}p_{23}p_{34}$$

$$p_{42}^c = p_{11}p_{23}p_{34} - p_{11}p_{24}p_{33}$$

$$p_{43}^c = p_{11}p_{24}p_{32} - p_{12}p_{24}p_{31}$$

$$p_{44}^c = p_{12}p_{23}p_{31} - p_{11}p_{23}p_{32}$$

$$[P]^{-1} = \left[\gamma_{p_2} P_2 \right]^{-1} = \det = \frac{1}{\det \left[\gamma_{p_2} P_2 \right]} \begin{bmatrix} p_{11}^c & p_{12}^c & p_{13}^c & p_{14}^c \\ p_{21}^c & p_{22}^c & p_{23}^c & p_{24}^c \\ p_{31}^c & p_{32}^c & p_{33}^c & p_{34}^c \\ p_{41}^c & p_{42}^c & p_{43}^c & p_{44}^c \end{bmatrix}$$

$$[P]^{-1} = \begin{bmatrix} A_{11} & A_{12} & A_{13} & A_{14} \\ A_{21} & A_{22} & A_{23} & A_{24} \\ A_{31} & A_{32} & A_{33} & A_{34} \\ A_{41} & A_{42} & A_{43} & A_{44} \end{bmatrix} \qquad\qquad 5\,20$$

$$A_{ij} = \frac{p_{ji}^c}{\det} \qquad \text{where } i = 1,2,3,4$$
$$j = 1,2,3,4$$

$$[\gamma_{P_1} P_1][\gamma_{P_2} P_2]^{-1} = \begin{bmatrix} a_{11} & a_{12} & a_{13} & a_{14} \\ a_{21} & a_{22} & a_{23} & a_{24} \\ a_{31} & a_{32} & a_{33} & a_{34} \\ a_{41} & a_{42} & a_{43} & a_{44} \end{bmatrix} \begin{bmatrix} A_{11} & A_{12} & A_{13} & A_{14} \\ A_{21} & A_{22} & A_{23} & A_{24} \\ A_{31} & A_{32} & A_{33} & A_{34} \\ A_{41} & A_{42} & A_{43} & A_{44} \end{bmatrix} \qquad 5.21$$

$$= \begin{bmatrix} L_{11} & L_{12} & L_{13} & L_{14} \\ L_{21} & L_{22} & L_{23} & L_{24} \\ L_{31} & L_{32} & L_{33} & L_{34} \\ L_{41} & L_{42} & L_{43} & L_{44} \end{bmatrix}$$

where
$$L_{11} = a_{11}A_{11} + a_{12}A_{21}$$

$$L_{12} = a_{11}A_{12} + a_{12}A_{22}$$

91

$$L_{13} = a_{11}A_{13} + a_{12}A_{23}$$

$$L_{14} = a_{11}A_{14} + a_{12}A_{24}$$

$$L_{21} = a_{23}A_{31} + a_{24}A_{41}$$

$$L_{22} = a_{23}A_{32} + a_{24}A_{42}$$

$$L_{23} = a_{23}A_{33} + a_{24}A_{43}$$

$$L_{24} = a_{23}A_{34} + a_{24}A_{44}$$

$$L_{31} = a_{23}A_{31} + a_{24}A_{41} + a_{33}A_{31} + a_{34}A_{41}$$

$$L_{32} = a_{31}A_{12} + a_{32}A_{22} + a_{33}A_{32} + a_{34}A_{42}$$

$$L_{33} = a_{31}A_{13} + a_{32}A_{23} + a_{33}A_{33} + a_{34}A_{43}$$

$$L_{34} = a_{31}A_{14} + a_{32}A_{24} + a_{33}A_{34} + a_{34}A_{44}$$

$$L_{41} = a_{41}A_{11} + a_{42}A_{21} + a_{43}A_{31} + a_{44}A_{41}$$

$$L_{42} = a_{41}A_{12} + a_{42}A_{22} + a_{43}A_{32} + a_{44}A_{42}$$

$$L_{43} = a_{41}A_{13} + a_{42}A_{23} + a_{43}A_{33} + a_{44}A_{43}$$

$$L_{44} = a_{41}A_{14} + a_{42}A_{24} + a_{43}A_{34} + a_{44}A_{44}$$

The coefficients are related as

$$\begin{bmatrix} A_{P_2} \\ B_{P_2} \\ C_{P_2} \\ D_{P_2} \end{bmatrix} = [L] \begin{bmatrix} A_{P_1} \\ B_{P_2} \\ C_{P_2} \\ D_{P_2} \end{bmatrix} \qquad \text{5.22}$$

$$\begin{bmatrix} A_{P_N} \\ B_{P_N} \\ C_{P_N} \\ D_{P_N} \end{bmatrix} = [L] \begin{bmatrix} A_{P_1} \\ B_{P_2} \\ C_{P_2} \\ D_{P_2} \end{bmatrix} \qquad \text{5.23}$$

It gives,

$$A_{P_n} = n[L_{11}A_{P_1} + L_{12}B_{P_1} + L_{13}C_{P_1} + L_{14}D_{P_1}$$

92

$$B_{P_n} = n[L_{21}A_{P_1} + L_{22}B_{P_1} + L_{23}C_{P_1} + L_{24}D_{P_1}$$

$$C_{P_n} = n[L_{31}A_{P_1} + L_{32}B_{P_1} + L_{33}C_{P_1} + L_{34}D_{P_1}$$

$$D_{P_n} = n[L_{41}A_{P_1} + L_{42}B_{P_1} + L_{43}C_{P_1} + L_{44}D_{P_1}$$

Let the substrate height is 't' and the bottom layer is polymer. The resultant electric and magnetic scalar potential function on the top surface is expressed as,

$$\phi_{i,n} = A_{P_n} \sinh(\gamma_p t) + B_{P_n} \cosh(\gamma_{P_n} t) \qquad i<t \qquad 5.24$$

$$\psi_{i,n} = C_{P_n} \sinh(\gamma_p t) + D_{P_n} \cosh(\gamma_{P_n} t) \qquad 5.25$$

Substituting the values of coefficients

$$\phi_{in} = A_{P_1}(nL_{11}S + nL_{21}C) + B_{P_1}(nL_{12}S + nL_{22}C) + C_{P_1}(nL_{13}S + nL_{23}C) + D_{P_1}(nL_{14}S + nL_{24}C)$$

$$\psi_{in} = A_{P_1}(nL_{31}S + nL_{41}C) + B_{P_1}(nL_{32}S + nL_{42}C) + C_{P_1}(nL_{33}S + nL_{43}C) + D_{P_1}(nL_{34}S + nL_{44}C)$$

Where

$$S = \sinh(\gamma_p t)$$

$$C = \cinh(\gamma_p t)$$

The Fourier transform of the z and x-component of electric and magnetic field takes the following form

$$\tilde{E}_z = A_{P_1}(nK_{11}L_{11}S + nK_{11}L_{21}C) + B_{P_1}(nK_{11}L_{12}S + nK_{11}L_{22}C) +$$
$$C_{P_1}(nK_{11}L_{13}S + nK_{11}L_{23}C) + D_{P_1}(nK_{11}L_{14}S + nK_{11}L_{24}C) \qquad 5.26$$

$$\tilde{H}_z = A_{P_1}(nK_{11}L_{31}S + nK_{11}L_{41}C) + B_{P_1}(nK_{11}L_{32}S + nK_{11}L_{42}C) +$$
$$C_{P_1}(nK_{11}L_{33}S + nK_{11}L_{43}C) + D_{P_1}(nK_{11}L_{34}S + nK_{11}L_{44}C) \qquad 5.27$$

$$\tilde{E}_x = A_{P_1}\left[j\alpha_n n(L_{11}S + L_{21}C) - \frac{\omega\gamma_p n}{\beta}(L_{31}C + L_{41}S)\right] + B_{P_1}\left[j\alpha_n n(L_{12}S + L_{22}C) - \frac{\omega\gamma_p n}{\beta}(L_{32}C + nL_{42}S)\right]$$
$$+ C_{P_1}\left[j\alpha_n n(L_{13}S + L_{23}C) - \frac{\omega\gamma_p n}{\beta}(L_{33}C + L_{43}S)\right] + D_{P_1}\left[j\alpha_n n(L_{14}S + L_{24}C) - \frac{\omega\gamma_p n}{\beta}(L_{34}C + nL_{44}S)\right]$$
$$5.28$$

$$\tilde{H}_x = A_{P_i}\left[j\alpha_n n(L_{31}S + L_{41}C) + \frac{\omega\varepsilon_P\gamma_P n}{\beta}(L_{31}C + L_{41}S)\right] + B_{P_i}\left[j\alpha_n n(L_{32}S + L_{42}C) + \frac{\omega\varepsilon_P\gamma_P n}{\beta}(L_{32}C + L_{42}S)\right]$$

$$+ C_{P_i}\left[j\alpha_n n(L_{33}S + L_{43}C) + \frac{\omega\varepsilon_P\gamma_P n}{\beta}(L_{33}C + L_{43}S)\right] + D_{P_i}\left[j\alpha_n n(L_{34}S + L_{44}C) + \frac{\omega\varepsilon_P\gamma_P n}{\beta}(L_{34}C + L_{44}S)\right]$$

5.29

Where,

$$\tilde{E}_z = [x_{11}A_{P_i} + x_{12}B_{P_i} + x_{13}C_{P_i} + x_{14}D_{P_i}]$$

$$\tilde{H}_z = [x_{21}A_{P_i} + x_{22}B_{P_i} + x_{23}C_{P_i} + x_{24}D_{P_i}]$$

$$\tilde{E}_x = [x_{31}A_{P_i} + x_{32}B_{P_i} + x_{33}C_{P_i} + x_{34}D_{P_i}]$$

$$\tilde{H}_x = [x_{41}A_{P_i} + x_{42}B_{P_i} + x_{43}C_{P_i} + x_{44}D_{P_i}]$$

$$x_{11} = nK_{11}[L_{11}S + L_{21}C]$$

$$x_{12} = nK_{11}[L_{12}S + L_{22}C]$$

$$x_{13} = nK_{11}[L_{13}S + L_{23}C]$$

$$x_{14} = nK_{11}[L_{14}S + L_{24}C]$$

$$x_{21} = nK_{11}[L_{31}S + L_{41}C]$$

$$x_{22} = nK_{11}[L_{32}S + L_{42}C]$$

$$x_{23} = nK_{11}[L_{33}S + L_{43}C]$$

$$x_{24} = nK_{11}[L_{34}S + L_{44}C]$$

$$x_{31} = j\alpha_n n(L_{11}S + L_{21}C) - \frac{\omega\gamma_P n}{\beta}(L_{31}C + L_{41}S)$$

$$x_{32} = j\alpha_n n(L_{12}S + L_{22}C) - \frac{\omega\gamma_P n}{\beta}(L_{32}C + L_{42}S)$$

$$x_{33} = j\alpha_n n(L_{13}S + L_{23}C) - \frac{\omega\gamma_P n}{\beta}(L_{33}C + L_{43}S)$$

$$x_{34} = j\alpha_n n(L_{14}S + L_{24}C) - \frac{\omega\gamma_P n}{\beta}(L_{34}C + L_{44}S)$$

$$X_{41} = j\alpha_n n(L_{31}S + L_{41}C) + \frac{\omega\varepsilon_p\gamma_p n}{\beta}(L_{31}C + L_{41}S)$$

$$X_{42} = j\alpha_n n(L_{32}S + L_{42}C) + \frac{\omega\varepsilon_p\gamma_p n}{\beta}(L_{32}C + L_{42}S)$$

$$X_{43} = j\alpha_n n(L_{33}S + L_{43}C) + \frac{\omega\varepsilon_p\gamma_p n}{\beta}(L_{33}C + L_{43}S)$$

$$X_{44} = j\alpha_n n(L_{34}S + L_{44}C) + \frac{\omega\varepsilon_p\gamma_p n}{\beta}(L_{34}C + L_{44}S)$$

$$\begin{bmatrix} \tilde{E}_{zn} \\ \tilde{H}_{zn} \\ \tilde{E}_{xn} \\ \tilde{H}_{xn} \end{bmatrix} = \begin{bmatrix} X_{11} & X_{12} & X_{13} & X_{14} \\ X_{21} & X_{22} & X_{23} & X_{24} \\ X_{31} & X_{32} & X_{33} & X_{34} \\ X_{41} & X_{42} & X_{43} & X_{44} \end{bmatrix} \begin{bmatrix} A_{p_1} \\ B_{p_1} \\ C_{p_1} \\ D_{p_1} \end{bmatrix}$$

5.30

Now applying boundary condition at air dielectric interface

$$\tilde{E}_{za} - \tilde{E}_{zn} = 0$$

5.31

$$\tilde{H}_{za} - \tilde{H}_{zn} = -\tilde{J}_x$$

5.32

$$\tilde{E}_{xa} - \tilde{E}_{xn} = 0$$

5.33

$$\tilde{H}_{xa} - \tilde{H}_{xn} = \tilde{J}_z$$

5.34

In addition to above boundary conditions, the boundary conditions to be satisfied on the strip is,

$$E_{za}(x,t) = 0 \qquad |x| < \frac{w}{2}$$

5.35

$$\left(\frac{d}{dy}\right)H_{z2}(x,t) = 0 \qquad |x| < \frac{w}{2}$$

5.36

The electric and magnetic scalar potential in air medium takes the form

$$\phi_{i,n} = B_a \exp[-\gamma_a(y-t)]$$

5.37

$$\psi_{i,n} = D_a \exp[-\gamma_a(y-t)]$$

5.38

The electric and magnetic field in the air medium is represented as,

95

$$
\begin{bmatrix} \tilde{E}_{za} \\ \tilde{H}_{za} \\ \tilde{E}_{xa} \\ \tilde{H}_{xa} \end{bmatrix} = \begin{bmatrix} 0 & k_a^2 - \beta^2 & 0 & 0 \\ 0 & 0 & 0 & k_a^2 - \beta^2 \\ 0 & -j\alpha_n \exp[-\gamma_a(y-t)] & 0 & -\dfrac{\omega\gamma_a \exp[-\gamma_a(y-t)]}{\beta} \\ 0 & \dfrac{\omega\epsilon_a\gamma_a \exp[-\gamma_a(y-t)]}{\beta} & 0 & j\alpha_n \exp[-\gamma_a(y-t)] \end{bmatrix} \begin{bmatrix} 0 \\ B_a \\ 0 \\ D_a \end{bmatrix}
$$
5.39

$$
\begin{bmatrix} \tilde{E}_{za} \\ \tilde{H}_{za} \\ \tilde{E}_{xa} \\ \tilde{H}_{xa} \end{bmatrix} = \begin{bmatrix} y_{11} & y_{12} & y_{13} & y_{14} \\ y_{21} & y_{22} & y_{23} & y_{24} \\ y_{31} & y_{32} & y_{33} & y_{34} \\ y_{41} & y_{42} & y_{43} & y_{44} \end{bmatrix} \begin{bmatrix} 0 \\ B_a \\ 0 \\ Da \end{bmatrix}
$$
5.40

$$
\begin{bmatrix} \tilde{E}_{za} \\ \tilde{H}_{za} \\ \tilde{E}_{xa} \\ \tilde{H}_{xa} \end{bmatrix} = [y] \begin{bmatrix} 0 \\ B_a \\ 0 \\ Da \end{bmatrix}
$$
5.41

where

$$y_{11} = y_{13} = y_{14} = y_{21} = y_{22} = y_{23} = 0$$

$$y_{31} = y_{33} = y_{41} = y_{43} = 0$$

$$y_{11} = y_{24} = (k_a^2 - \beta^2)$$

$$y_{32} = -y_{44} = -j\alpha_n \exp[-\gamma_a(y-t)]$$

$$y_{42} = \frac{\omega\varepsilon_a\gamma_a \exp[-\gamma_a(y-t)]}{\beta}$$

$$y_{34} = \frac{\omega\gamma_a \exp[-\gamma_a(y-t)]}{\beta}$$

Putting this value in boundary equations

$$
[X] \begin{bmatrix} A_{p_1} \\ B_{p_1} \\ C_{p_1} \\ D_{p_1} \end{bmatrix} - [Y] \begin{bmatrix} 0 \\ B_a \\ 0 \\ D_a \end{bmatrix} = \begin{bmatrix} 0 \\ -\tilde{J}_x \\ 0 \\ \tilde{J}_z \end{bmatrix}
$$
5.42

On the ground plane,

$$B_{p_1} = C_{p_1} = 0 \quad \text{(magnetic walls)}$$
5.43

Then

$$[X]\begin{bmatrix} A_{p_1} \\ 0 \\ 0 \\ D_{p_1} \end{bmatrix} - [Y]\begin{bmatrix} 0 \\ B_a \\ 0 \\ D_a \end{bmatrix} = \begin{bmatrix} 0 \\ -\tilde{J}_x \\ 0 \\ \tilde{J}_z \end{bmatrix}$$

5.44

With mathematical manipulation,

$$x_{11}A_{p_1} + x_{14}D_{p_1} - y_{12}B_a = 0$$

$$x_{21}A_{p_1} + x_{24}D_{p_1} - y_{24}D_a = -\tilde{J}_x$$

$$x_{31}A_{p_1} + x_{34}D_{p_1} - y_{32}B_a - y_{34}D_a = 0$$

$$x_{41}A_{p_1} + x_{44}D_{p_1} - y_{42}B_a - y_{44}D_a = \tilde{J}_z$$

$$\begin{bmatrix} x_{11} & x_{14} & -y_{12} & 0 \\ x_{21} & x_{24} & 0 & -y_{24} \\ x_{31} & x_{34} & -y_{32} & -y_{34} \\ x_{41} & x_{44} & -y_{42} & -y_{44} \end{bmatrix} \begin{bmatrix} A_{p_1} \\ D_{p_1} \\ B_a \\ D_a \end{bmatrix} = \begin{bmatrix} 0 \\ -\tilde{J}_x \\ 0 \\ \tilde{J}_z \end{bmatrix}$$

5.45

$$[M]\begin{bmatrix} A_{p_1} \\ D_{p_1} \\ B_a \\ D_a \end{bmatrix} = \begin{bmatrix} 0 \\ -\tilde{J}_x \\ 0 \\ \tilde{J}_z \end{bmatrix}$$

$$\begin{bmatrix} A_{p_1} \\ D_{p_1} \\ B_a \\ D_a \end{bmatrix} = [M]^{-1}\begin{bmatrix} 0 \\ -\tilde{J}_x \\ 0 \\ \tilde{J}_z \end{bmatrix}$$

5.46

$$[M] = \begin{bmatrix} x_{11} & x_{14} & -y_{12} & 0 \\ x_{21} & x_{24} & 0 & -y_{24} \\ x_{31} & x_{34} & -y_{32} & -y_{34} \\ x_{41} & x_{44} & -y_{42} & -y_{44} \end{bmatrix}$$

5.47

$$\det M = |M|$$

$$\Delta = x_{11}\begin{vmatrix} x_{24} & 0 & -y_{24} \\ x_{34} & -y_{32} & -y_{34} \\ x_{44} & -y_{24} & -y_{44} \end{vmatrix} - x_{14}\begin{vmatrix} x_{21} & 0 & -y_{24} \\ x_{31} & -y_{32} & -y_{34} \\ x_{41} & -y_{43} & -y_{44} \end{vmatrix} - y_{12}\begin{vmatrix} x_{21} & x_{24} & -y_{24} \\ x_{31} & x_{34} & -y_{34} \\ x_{41} & x_{44} & -y_{44} \end{vmatrix}$$

$$\Delta = Q_1 - Q_2$$

5.48

Where,

$$Q_1 = x_{11}x_{24}y_{32}y_{44} + x_{11}x_{34}y_{24}y_{42} + x_{14}x_{21}y_{34}y_{42} + x_{14}x_{41}y_{24}y_{32} + x_{21}x_{34}y_{12}y_{44} +$$
$$x_{21}x_{34}y_{12}y_{34} + x_{24}x_{41}y_{12}y_{24}$$

$$Q_2 = x_{11}x_{24}y_{32}y_{42} + x_{11}x_{44}y_{24}y_{32} + x_{14}x_{21}y_{32}y_{44} + x_{31}x_{14}y_{42}y_{24} + x_{21}x_{44}y_{12}y_{34} +$$
$$x_{24}x_{31}y_{12}y_{44} + x_{34}x_{41}y_{12}y_{24}$$

$$x_{11}^c = Z_{11} = \begin{vmatrix} x_{24} & 0 & -y_{24} \\ x_{34} & -y_{32} & -y_{34} \\ x_{44} & -y_{42} & -y_{44} \end{vmatrix} = (x_{24}y_{32}y_{44} + x_{34}y_{24}y_{42}) - (x_{24}y_{34}y_{42} - x_{44}y_{24}y_{32})$$

$$x_{14}^c = -\begin{vmatrix} x_{21} & 0 & -y_{24} \\ x_{31} & -y_{32} & -y_{34} \\ x_{41} & -y_{42} & -y_{44} \end{vmatrix} = y_{24}(x_{41}y_{32} - x_{31}y_{42}) - x_{21}(y_{32}y_{44} - y_{34}y_{42})$$

$$(-y)_{12}^c = \begin{vmatrix} x_{21} & x_{24} & -y_{24} \\ x_{31} & x_{34} & -y_{34} \\ x_{41} & x_{44} & -y_{44} \end{vmatrix} = x_{21}(x_{44}y_{34} - x_{34}y_{44}) - x_{24}(x_{41}y_{34} - x_{31}y_{44}) - y_{24}(x_{31}x_{44} - x_{34}x_{41})$$

$$(0)^c = Z_{14} = -\begin{vmatrix} x_{21} & x_{24} & 0 \\ x_{31} & x_{34} & -y_{32} \\ x_{41} & x_{44} & -y_{42} \end{vmatrix} = x_{24}(x_{31}x_{44} - x_{34}x_{41}) - x_{21}(x_{44}y_{32} - x_{34}y_{42})$$

$$x_{21}^c = Z_{21} = -\begin{vmatrix} x_{14} & -y_{12} & 0 \\ x_{34} & -y_{32} & -y_{32} \\ x_{44} & -y_{42} & -y_{44} \end{vmatrix} = -x_{14}(y_{32}y_{44} - y_{34}y_{42}) - y_{21}(x_{44}y_{34} - x_{34}y_{44})$$

$$x_{24}^c = Z_{22} = \begin{vmatrix} x_{11} & -y_{12} & 0 \\ x_{31} & -y_{32} & -y_{32} \\ x_{41} & -y_{42} & -y_{44} \end{vmatrix} = x_{11}(y_{32}y_{44} - y_{34}y_{42}) - y_{12}(x_{31}y_{44} + x_{41}y_{34})$$

Cofactor of matrix $|M|$

$$x_{11}^c = Z_{11} = \begin{vmatrix} x_{24} & 0 & -y_{24} \\ x_{34} & -y_{32} & -y_{34} \\ x_{44} & -y_{42} & -y_{44} \end{vmatrix} = (x_{24}y_{32}y_{44} + x_{34}y_{24}y_{42}) - (x_{24}y_{34}y_{42} - x_{44}y_{24}y_{32})$$

$$x_{14}^c = -\begin{vmatrix} x_{21} & 0 & -y_{24} \\ x_{31} & -y_{32} & -y_{34} \\ x_{41} & -y_{42} & -y_{44} \end{vmatrix} = y_{24}(x_{41}y_{32} - x_{31}y_{42}) - x_{21}(y_{32}y_{44} - y_{34}y_{42})$$

$$(-y)_{12}^c = \begin{vmatrix} x_{21} & x_{24} & -y_{24} \\ x_{31} & x_{34} & -y_{34} \\ x_{41} & x_{44} & -y_{44} \end{vmatrix} = x_{21}(x_{44}y_{34} - x_{34}y_{44}) - x_{24}(x_{41}y_{34} - x_{31}y_{44}) - y_{24}(x_{31}x_{44} - x_{34}x_{41})$$

$$(0)^C = Z_{14} = -\begin{vmatrix} x_{21} & x_{24} & 0 \\ x_{31} & x_{34} & -y_{32} \\ x_{41} & x_{44} & -y_{42} \end{vmatrix} = x_{24}(x_{31}x_{44} - x_{34}x_{41}) - x_{21}(x_{44}y_{32} - x_{34}y_{42})$$

$$x_{21}^c = Z_{21} = -\begin{vmatrix} x_{14} & -y_{12} & 0 \\ x_{34} & -y_{32} & -y_{32} \\ x_{44} & -y_{42} & -y_{44} \end{vmatrix} = -x_{14}(y_{32}y_{44} - y_{34}y_{42}) - y_{21}(x_{44}y_{34} - x_{34}y_{44})$$

$$x_{24}^c = Z_{22} = \begin{vmatrix} x_{11} & -y_{12} & 0 \\ x_{31} & -y_{32} & -y_{32} \\ x_{41} & -y_{42} & -y_{44} \end{vmatrix} = x_{11}(y_{32}y_{44} - y_{34}y_{42}) - y_{12}(x_{31}y_{44} + x_{41}y_{34})$$

$$o^c = Z_{23} = -\begin{vmatrix} x_{11} & x_{14} & 0 \\ x_{31} & x_{34} & -y_{32} \\ x_{41} & x_{44} & -y_{44} \end{vmatrix} = x_{14}(x_{41}y_{34} - x_{31}y_{44}) - x_{11}(x_{44}y_{34} - x_{34}y_{44})$$

$$(-y_{24})^c = Z_{24} = \begin{vmatrix} x_{11} & x_{14} & -y_{12} \\ x_{31} & x_{34} & -y_{32} \\ x_{41} & x_{44} & -y_{44} \end{vmatrix} = x_{11}(x_{44}y_{32} - x_{34}y_{42}) - x_{14}(x_{41}y_{32} - x_{31}y_{42}) - y_{12}(x_{31}x_{44} - x_{41}x_{34})$$

$$(x_{31})^c = Z_{31} = \begin{vmatrix} x_{14} & -y_{12} & 0 \\ x_{24} & 0 & -y_{24} \\ x_{44} & -y_{42} & -y_{44} \end{vmatrix} = y_{12}(x_{44}y_{24} - x_{24}y_{44}) - x_{11}y_{42}y_{24}$$

$$(x_{34})^c = Z_{32} = -\begin{vmatrix} x_{11} & -y_{12} & 0 \\ x_{21} & 0 & -y_{24} \\ x_{41} & -y_{42} & -y_{44} \end{vmatrix} = -y_{12}(x_{41}y_{24} - x_{21}y_{43}) + x_{11}y_{42}y_{24}$$

$$(-y_{32})^c = Z_{33} = \begin{vmatrix} x_{11} & x_{14} & 0 \\ x_{21} & x_{24} & -y_{24} \\ x_{41} & x_{44} & -y_{44} \end{vmatrix} = x_{11}(y_{24}x_{44} - x_{24}y_{44}) - x_{14}(x_{21}x_{44} - x_{24}x_{41})$$

$$(-y_{34})^c = Z_{34} = -\begin{vmatrix} x_{11} & x_{14} & -y_{12} \\ x_{21} & x_{24} & 0 \\ x_{41} & x_{44} & -y_{42} \end{vmatrix} = x_{11}x_{24}y_{42} - x_{14}x_{21}y_{42} + y_{12}(x_{21}x_{44} - x_{24}x_{41})$$

$$(x_{41})^c = Z_{41} = -\begin{vmatrix} x_{14} & -y_{12} & 0 \\ x_{24} & 0 & -y_{24} \\ x_{34} & -y_{32} & -y_{34} \end{vmatrix} = x_{14}y_{24}y_{32} - y_{12}(x_{34}y_{24} - x_{24}y_{34})$$

99

$$(x_{44})^c = Z_{42} = \begin{vmatrix} x_{11} & -y_{12} & 0 \\ x_{21} & 0 & -y_{24} \\ x_{31} & -y_{32} & -y_{34} \end{vmatrix} = y_{12}(x_{31}y_{24} - x_{21}y_{34}) - x_{11}y_{24}y_{32}$$

$$(-y_{42})^c = Z_{43} = -\begin{vmatrix} x_{11} & x_{14} & 0 \\ x_{21} & x_{24} & -y_{24} \\ x_{31} & x_{34} & -y_{34} \end{vmatrix} = -x_{11}(x_{34}y_{24} - x_{24}y_{34}) - x_{14}(y_{24}x_{31} - x_{21}y_{34})$$

$$(-y_{43})^c = Z_{44} = \begin{vmatrix} x_{11} & x_{14} & -y_{12} \\ x_{21} & x_{24} & 0 \\ x_{31} & x_{34} & -y_{32} \end{vmatrix} = x_{14}x_{21}y_{32} - x_{11}x_{24}y_{32} - y_{12}(x_{21}x_{34} - x_{24}x_{31})$$

$$[M]^c = \begin{bmatrix} Z_{11} & Z_{12} & Z_{13} & Z_{14} \\ Z_{21} & Z_{22} & Z_{23} & Z_{24} \\ Z_{31} & Z_{32} & Z_{33} & Z_{34} \\ Z_{41} & Z_{42} & Z_{43} & Z_{44} \end{bmatrix}$$

$$[M]^{CT} = \begin{bmatrix} Z_{11} & Z_{21} & Z_{31} & Z_{41} \\ Z_{12} & Z_{22} & Z_{32} & Z_{42} \\ Z_{13} & Z_{23} & Z_{33} & Z_{43} \\ Z_{14} & Z_{24} & Z_{34} & Z_{44} \end{bmatrix}$$

$$[M]^{-1} = \frac{1}{\Delta} \begin{bmatrix} Z_{11} & Z_{21} & Z_{31} & Z_{41} \\ Z_{12} & Z_{22} & Z_{32} & Z_{42} \\ Z_{13} & Z_{23} & Z_{33} & Z_{43} \\ Z_{14} & Z_{24} & Z_{34} & Z_{44} \end{bmatrix} \qquad 5.49$$

$$\begin{bmatrix} A_{P_1} \\ B_{P_1} \\ C_{P_1} \\ D_{P_1} \end{bmatrix} = \frac{1}{\Delta} \begin{bmatrix} Z_{11} & Z_{21} & Z_{31} & Z_{41} \\ Z_{12} & Z_{22} & Z_{32} & Z_{42} \\ Z_{13} & Z_{23} & Z_{33} & Z_{43} \\ Z_{14} & Z_{24} & Z_{34} & Z_{44} \end{bmatrix} \begin{bmatrix} 0 \\ -\tilde{J}_x \\ 0 \\ \tilde{J}_z \end{bmatrix} \qquad 5.50$$

$$\begin{bmatrix} A_{P_1} \\ B_{P_1} \\ C_{P_1} \\ D_{P_1} \end{bmatrix} = \begin{bmatrix} n_{11} & n_{21} & n_{31} & n_{41} \\ n_{12} & n_{22} & n_{32} & n_{42} \\ n_{13} & n_{23} & n_{33} & n_{43} \\ n_{14} & n_{24} & n_{34} & n_{44} \end{bmatrix} \begin{bmatrix} 0 \\ -\tilde{J}_x \\ 0 \\ \tilde{J}_z \end{bmatrix} \qquad 5.51$$

$$n_{ij} = \frac{Z_{ij}}{\Delta} \qquad i = 1 \text{ to } 4, \; j = 1 \text{ to } 4 \qquad 5.52$$

$$\begin{bmatrix} A_{P_1} \\ B_{P_1} \\ C_{P_1} \\ D_{P_1} \end{bmatrix} = \begin{bmatrix} -n_{21}\tilde{J}_x + n_{41}\tilde{J}_z \\ -n_{22}\tilde{J}_x + n_{42}\tilde{J}_z \\ -n_{23}\tilde{J}_x + n_{43}\tilde{J}_z \\ -n_{24}\tilde{J}_x + n_{44}\tilde{J}_z \end{bmatrix}$$

5.53

where

$$A_{P_1} = -n_{21}\tilde{J}_x + n_{41}\tilde{J}_z$$

5.54

$$B_{P_1} = -n_{22}\tilde{J}_x + n_{42}\tilde{J}_z$$

5.55

$$C_{P_1} = -n_{23}\tilde{J}_x + n_{43}\tilde{J}_z$$

5.56

$$D_{P_1} = -n_{24}\tilde{J}_x + n_{44}\tilde{J}_z$$

5.57

Now writing the electric and magnetic field equation

$$\tilde{E}_z = A_{P_1} X_{11} + D_{P_1} X_{14}$$

5.58

$$\tilde{E}_x = A_{P_1} X_{31} + D_{P_1} X_{34}$$

5.59

Putting the values of A_{P_1}, B_{P_1}, C_{P_1}, D_{P_1} in electric field equation and writing it in matrix form,

$$\begin{bmatrix} \tilde{E}_z \\ \tilde{E}_x \end{bmatrix} = \begin{bmatrix} -(n_{21}X_{11} + n_{22}X_{34}) & (n_{41}X_{11} + n_{42}X_{34}) \\ -(n_{21}X_{31} + n_{22}X_{34}) & (n_{41}X_{31} + n_{42}X_{34}) \end{bmatrix} \begin{bmatrix} \tilde{J}_x \\ \tilde{J}_z \end{bmatrix}$$

$$\begin{bmatrix} \tilde{E}_z \\ \tilde{E}_x \end{bmatrix} = \begin{bmatrix} G_{11} & G_{12} \\ G_{21} & G_{22} \end{bmatrix} \begin{bmatrix} \tilde{J}_x \\ \tilde{J}_z \end{bmatrix}$$

5.60

where,

$$G_{11} = -(n_{21}X_{11} + n_{22}X_{34})$$

5.61

$$G_{12} = n_{41}X_{11} + n_{42}X_{34})$$

5.62

$$G_{21} = -(n_{21}X_{x1} + n_{22}X_{34})$$

5.63

$$G_{22} = n_{41}X_{31} + n_{42}X_{34})$$

5.64

101

5.3 METHOD OF SOLUTION

In this section an efficient method for solving the coupled equations is presented. The method is essentially Galerkin's procedure applied to a Fourier transform domain. In this method the boundary condition on the strip is given by [16] are now applied in Fourier transform domain (FTD).

As a first step let us consider,

$$E_{za}(x,t) = j\frac{k_a^2 - \beta^2}{\beta}u(x) \qquad |x| > \frac{w}{2} \qquad\qquad 5.65$$

$$\frac{d}{dy}H_{za}(x,t) = j\frac{k_a^2 - \beta^2}{\beta}v(x) \qquad |x| > \frac{w}{2} \qquad\qquad 5.66$$

where, u and v are unknown potentials.

Fourier transforms of E_{za} (equations 5.35 and 5.36) and $\frac{d}{dy}H_{za}$ equations (5.65 and 5.66) for $|x| < \infty$ is taken. Using expressions given by field equations 5.1- 5.4, on the left hand sides of the transformed equations, following coupled equations for the two current components, corresponding to 5.61 to 5.64 are obtained.

$$G_{11}(\alpha,\beta)\tilde{J}_x(\alpha) + G_{12}(\alpha,\beta)\tilde{J}_z(\alpha) = \tilde{U}_1(\alpha) + \tilde{U}_2(\alpha) \qquad\qquad 5.67$$

$$G_{21}(\alpha,\beta)\tilde{J}_x(\alpha) + G_{22}(\alpha,\beta)\tilde{J}_z(\alpha) = \tilde{V}_1(\alpha) + \tilde{V}_2(\alpha) \qquad\qquad 5.68$$

where

$$\tilde{U}_1(\alpha) = \int_{-\infty}^{-\frac{w}{2}} u(x)e^{j\alpha x}dx \qquad\qquad 5.69$$

$$\tilde{U}_2(\alpha) = \int_{\frac{w}{2}}^{\infty} u(x)e^{j\alpha x}dx \qquad\qquad 5.70$$

$$\tilde{V}_1(\alpha) = \int_{-\infty}^{-\frac{w}{2}} v(x)e^{j\alpha x}dx \qquad\qquad 5.71$$

102

$$\tilde{V}_2(\alpha) = \int_{\frac{W}{2}}^{\infty} v(x)e^{j\alpha x} dx \qquad 5.72$$

Equations 5.67 and 5.68 contain six unknowns $\tilde{U}_1$, $\tilde{U}_2$, $\tilde{V}_1$, $\tilde{V}_2$, $\tilde{J}_x$ and $\tilde{J}_z$. On applying Parseval's identity to these equations following expression is obtained,

$$\int_{-\infty}^{\infty} \tilde{J}_{zm}(\alpha)\left[\tilde{U}_1(\alpha) + \tilde{U}_2(\alpha)\right]d\alpha = \frac{1}{2\pi}\int_{-\infty}^{\infty} J_{zm}(x)\left[\frac{\beta}{j\left(k_a^2 - \beta^2\right)}E_{za}(x,t)\right]dx = 0 \qquad 5.73$$

Equation 5.73 becomes zero as the current density $J_{zm}(x)$, the inverse transform of $\tilde{J}_{zm}(\alpha)$ and $E_{za}(x,t)$ are non-zero in the complementary region of x. Thus four unknown quantities $\tilde{U}_1$, $\tilde{U}_2$, $\tilde{V}_1$, $\tilde{V}_2$ are eliminated.

To solve the transformed coupled equations 5.67 and 5.68, the unknown current components $\tilde{J}_x$ and $\tilde{J}_z$ are considered in terms of known basis functions $\tilde{J}_{xn}$ and $\tilde{J}_{zn}$ as follows

$$\tilde{J}_x(\alpha) = \sum_{n=1}^{M} c_n \tilde{J}_{xn}(\alpha) \qquad 5.74$$

$$\tilde{J}_z(\alpha) = \sum_{n=1}^{N} d_n \tilde{J}_{zn}(\alpha) \qquad 5.75$$

The basis functions are chosen in such a way that their inverse Fourier transforms are non zero only on the strip $|X| < \frac{W}{2}$

Equations 5.74 and 5.75 are substituted into equations 5.58 and 5.59 and inner products with the basis functions $\tilde{J}_{zm}$ and $\tilde{J}_{xm}$ for different values of m are taken. The final matrix equations take the form

$$\sum_{n=1}^{M} K_{mn}^{11}(\alpha)c_n + \sum_{n=1}^{N} K_{mn}^{12}d_n = 0 \qquad m = 1,2\ldots\ldots N \qquad 5.76$$

$$\sum_{n=1}^{M} K_{mn}^{21}(\alpha)c_n + \sum_{n=1}^{N} K_{mn}^{22}d_n = 0 \qquad m = 1,2\ldots\ldots M \qquad 5.77$$

$$K_{mn}^{11} = \int_{-\infty}^{\infty} \tilde{J}_{zm}(\alpha)G_{11}(\alpha,\beta)\tilde{J}_{xn}(\alpha)d\alpha \qquad 5.78$$

$$K_{mn}^{12} = \int_{-\infty}^{\infty} \tilde{J}_{zm}(\alpha)G_{12}(\alpha,\beta)\tilde{J}_{zn}(\alpha)d\alpha \qquad 5.79$$

$$K_{mn}^{21} = \int_{-\infty}^{\infty} \tilde{J}_{xm}(\alpha)G_{21}(\alpha,\beta)\tilde{J}_{zn}(\alpha)d\alpha \qquad 5.80$$

$$K_{mn}^{22} = \int_{-\infty}^{\infty} \tilde{J}_{xm}(\alpha)G_{22}(\alpha,\beta)\tilde{J}_{zn}(\alpha)d\alpha \qquad 5.81$$

Simultaneous equations 5.76 and 5.77 are solved for the propagation constant β by setting the determinant of this set of equations equal to zero. The propagation constant β is calculated for each frequency ω to obtain the dispersion relation for the microstrip line structure. Here the results depend on the choice of the basis function and the values of M and N selected. The accuracy of results can be increased by selecting higher values of M and N.

5.4 NUMERICAL PROCEDURE

For the dominant mode excited in the microstrip line, J_z is even-symmetric with respect to the y axis and J_x is odd-symmetric. The choice of the basis function $\tilde{J}_{x1}$ $\tilde{J}_{z1}$ $\tilde{J}_{x2}, \tilde{J}_{z2}$ are shown in figure 5.3 and 5.4. These four functions are used in evaluating the coefficients of final matrix equation. In zero order approximation (N=1, M=0), only the axial component $\tilde{J}_{z1}$, on the strip is retained. The first order approximation, (M=N=1) uses J_{x1} and J_{z1} and the second order approximation i.e. M=N=2, uses J_{x1}, J_{z1}, J_{x2}, J_{z2}.

Figure 5.3: Basis function for J_{x1} and J_{z1}

Figure 5.4: Basis function for J_{x2} and J_{z2}

For the dominant mode, the following forms for J_{z1} and J_{x1} are suitable,

$$J_{z1}(x) = \left\{ \frac{1}{w}\left[1 + \left| \frac{2x}{w} \right|^3 \right] \right. \qquad |x| \le \frac{w}{2}$$

$$= 0 \qquad \frac{w}{2} < x < L \qquad\qquad 5.82$$

$$J_{x1}(x) = \left\{ \frac{2}{w}\sin\frac{2\pi x}{w} \right. \qquad |x| \le \frac{w}{2}$$

$$= 0 \qquad \frac{w}{2} < x < L \qquad\qquad 5.83$$

The Fourier transform of above current distribution are given by

$$\tilde{J}_{z1} = \frac{2\sin\left(\alpha\frac{w}{2} \right)}{\alpha\frac{w}{2}} + \frac{3}{\left(\alpha\frac{w}{2} \right)^3}\left\{ \cos\left(k_n\frac{w}{2} \right) - \frac{2\sin\left(\alpha\frac{w}{2} \right)}{\alpha\frac{w}{2}} + \frac{2\left[1 - \cos\left(\alpha\frac{w}{2} \right) \right]}{\left(\alpha\frac{w}{2} \right)^2} \right\} \qquad 5.84$$

and

$$\tilde{J}_{x1} = \frac{2\pi\sin\left(\alpha\frac{w}{2} \right)}{\left(\alpha\frac{w}{2} \right)^2 - \pi^2} \qquad\qquad 5.85$$

105

5.5 ALGORITHM DEVELOPMENT FOR SOFTWARE

To analyze phase velocity (β) versus frequency for device under test with SDTMC, a program is developed in C- language. Flowchart of the software developed is shown in figure 5.5. The technique is developed as follows:

- ❖ Reading the data

- ❖ *Generation of Greens function*

- ❖ Compute the roots of the determinant

- ❖ Writing the results and messages

First input parameters like permittivities of polystyrene (EP) and filler (EF), polystyrene (P1) and filler (P2) height, number of particles (N), operating frequency (FREQ), Area (A), and length (L) of the microstrip circuit are fed into the program. In the program T is assigned the value of substrate height. The effective permittivity of the composite is represented by EC.

The program is executed to perform Fourier transform of the basis function. Two values β_{max} and β_{min} are associated with the process of finding the roots of the determinant of the final matrix. The spectral domain Greens function corresponding to these phase constant values are determined, which finally compute the elements of the final matrix.

For the excited mode, determinant associated with the propagation constant vanishes. The actual root of the equation is computed by using bisection method. The details of program listing are given as appendix II.

```
                    ┌─────────────┐
                    │    START    │
                    └──────┬──────┘
                           ▼
        ┌──────────────────────────────────────┐
        │        OPEN INPUT/OUTPUT FILES        │
        └──────────────────┬───────────────────┘
                           ▼
        ┌──────────────────────────────────────┐
        │   READ EP, EC, EF, P1, P2, T, N, FREQ,│
        │           AREA, STRUCTURE             │
        └──────────────────┬───────────────────┘
                           ▼
        ┌──────────────────────────────────────┐
        │    TRANSFORM BASIS FUNTION INTO       │
        │           FOURIER DOMAIN              │
        └──────────────────┬───────────────────┘
                           ▼
        ┌──────────────────────────────────────┐
        │     INPUT THE OPERTAING FREQUENCY     │
        └──────────────────┬───────────────────┘
                           ▼
        ┌──────────────────────────────────────┐
        │        FOR BETA=0, BETA+0.001         │
        └──────────────────┬───────────────────┘
                           ▼
        ┌──────────────────────────────────────┐
        │   GENERATE ELEMENTS OF GREENS         │
        │   FUNCTION [G] FOR THE ENTIRE         │
        │            SUBSTRATE                  │
        └──────────────────┬───────────────────┘
                           ▼
        ┌──────────────────────────────────────┐
        │   GENERATE ELEMENTS OF FINAL          │
        │            MATRIX                     │
        └──────────────────┬───────────────────┘
                           ▼
        ┌──────────────────────────────────────┐
        │   COMPUTE DETERMINANT OF THE          │
        │          FINAL MATRIX                 │
        └──────────────────┬───────────────────┘
                           ▼
            NO          ◇ IS DET=0 ? ◇
                           │ YES
                           ▼
        ┌──────────────────────────────────────┐
        │         DISPLAY BETA VALUE            │
        └──────────────────┬───────────────────┘
                           ▼
        ┌──────────────────────────────────────┐
        │             CLOSE FILES               │
        └──────────────────┬───────────────────┘
                           ▼
        ┌──────────────────────────────────────┐
        │          END OF PROGRAM               │
        └──────────────────────────────────────┘
```
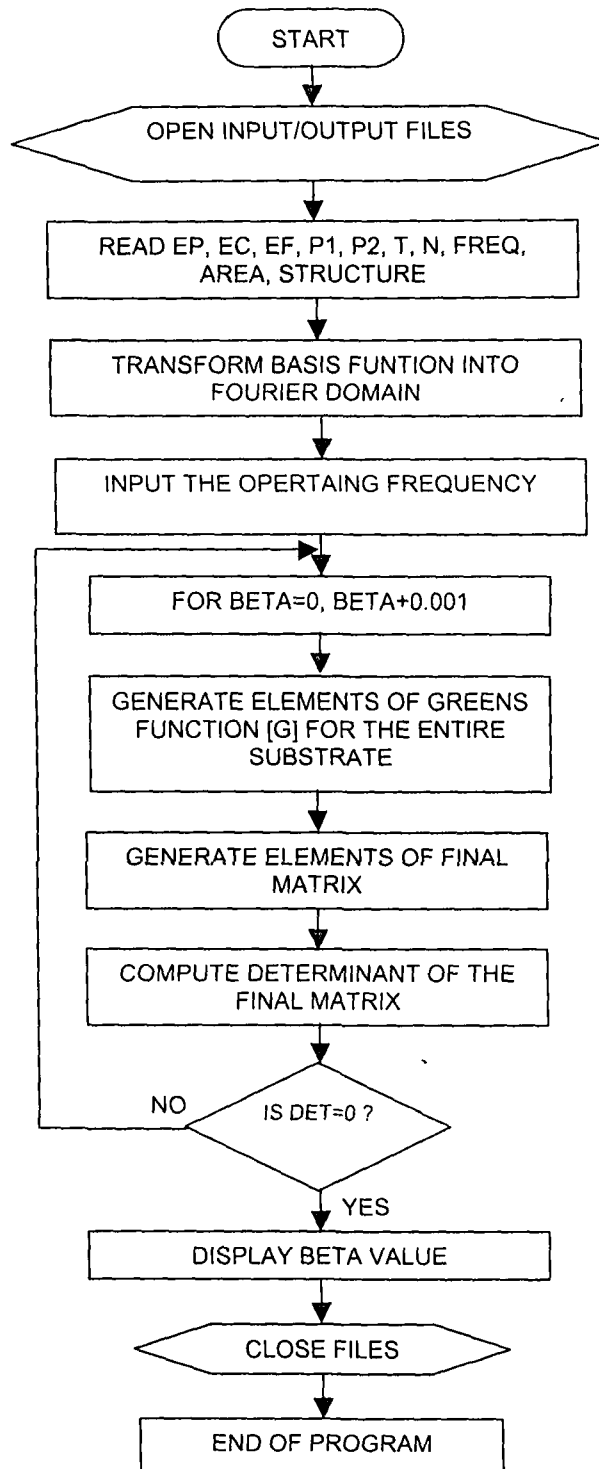
Figure 5.5: Flowchart for spectral domain technique modified for composite (SDTMC) substrate.

5.6 RESULTS AND DISCUSSION

The full wave analysis of the microstrip provides information about frequency dependence of the normalized guide wavelength (λ_m/λ_0) and the characteristic impedance [29] of the line on the two composite systems. Figure 5.6 (a-b) and 5.7(a-b) shows the variation of normalized guide wavelength with frequency for PS-alumina and PS-titania composite systems computed by SDTMC for zero order approximation.

It is observed from the plot 5.6a and 5.6b that normalized guide wavelength (λ_m/λ_0) decreases with increase in frequency indicating that propagation constant (β) increases with the increase in frequency. At higher frequencies more and more energy propagates inside and fields get concentrated below the strip.
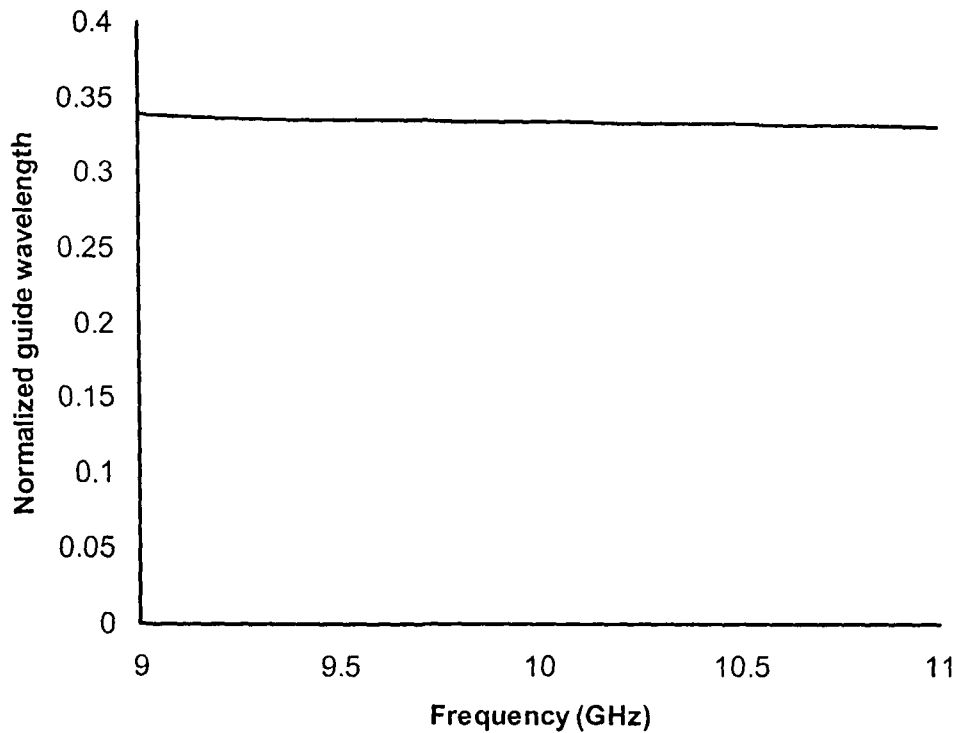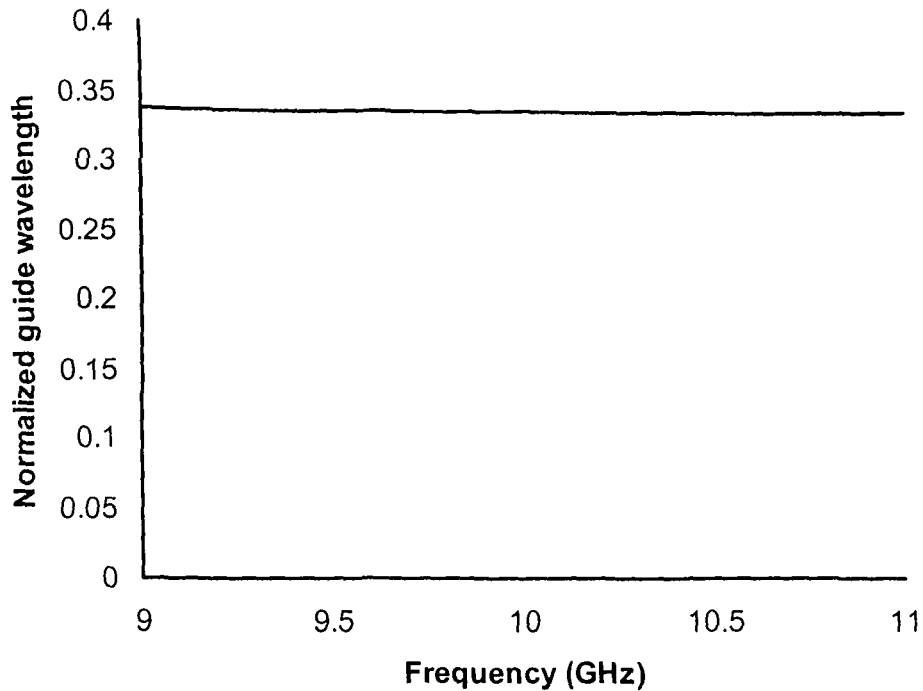

Figure 5.6a: Variation of microstrip guide wavelength with frequency for PS-1% VF alumina composite

Figure 5.6b: Variation of microstrip guide wavelength with frequency for PS-4%VF alumina composite

The basis function consider in the present investigation can analyze the phase velocity. The size of the particle and its distribution in the polymer matrix also plays an important role. A theoretical variation of propagation constant with variation of particle size is shown in table 5.2a. It is observed that propagation constant increases with the increase in particle size.

Table 5.2a: Variation of propagation constant with increase in particle size

Particle size (mm)	Propagation constant (mm^{-1}) PS-alumina (ϵ_r=2.55)	Propagation constant (mm^{-1}) PS-titania (ϵ_r=2.6)
1	0.64273	1.9340
0.1	0.64272	0.8990
0.01	0.64272	0.8920
0.001	0.64271	0.8915

Plots 5.7a and 5.7b of normalized guide wavelength for PS-titania composite

shows an increasing trend with frequency. The increase in normalized wavelength reduces

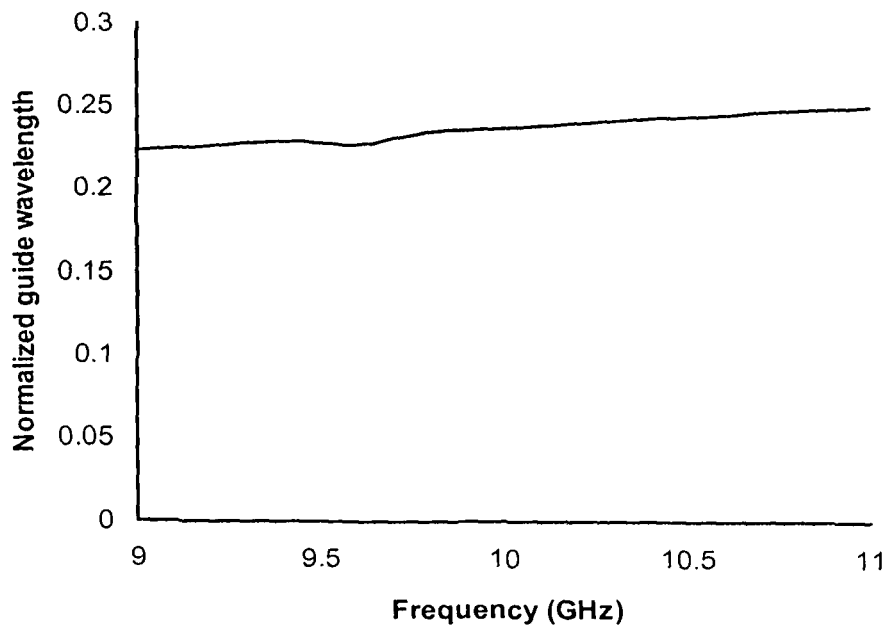the effective dielectric constant which is an unexpected behavior.

Figure 5.7a: Variation of microstrip guide wavelength with frequency for
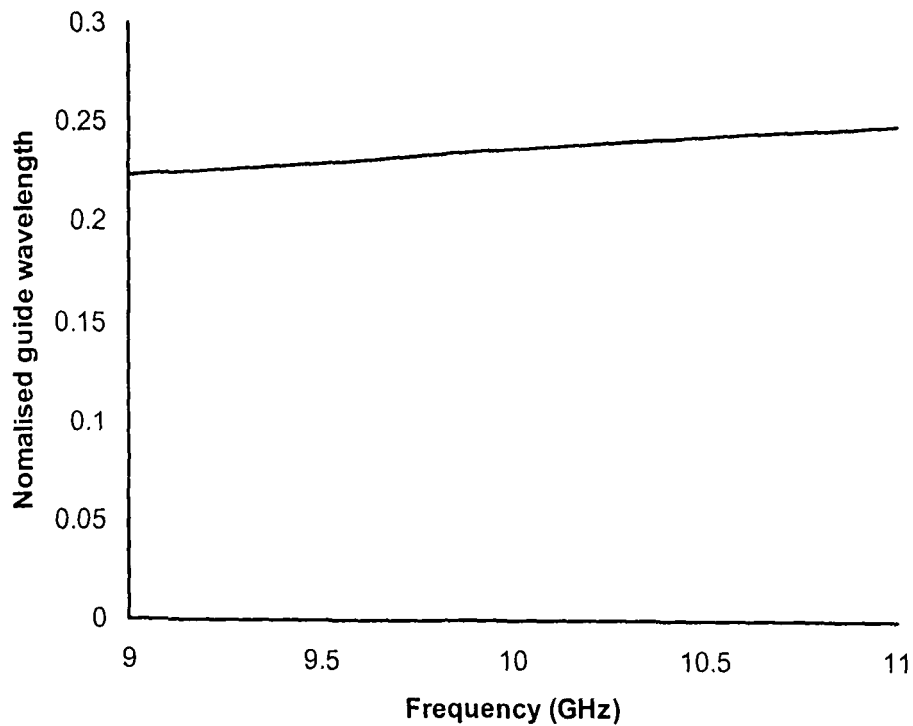PS-1%VF titania composite

Figure 5.7b: Variation of microstrip guide wavelength with frequency for
PS-4%VF titania composite

110

From the numerical results obtained for the propagation constant, an increase in its value is observed as inter-particle distance decreases. The reduction in inter-particle distance means more number of filler particles in the same area which enhances the effective permittivity and hence reduces the guide wavelength. Table 5.2b shows the dependence of propagation constant on the distribution of reinforced particle on the polystyrene matrix. The increase in number of filler particles will also lead to inter particle interaction which may change the microwave characterization values for the composite materials.

Table 5.2b: Variation of propagation constant with decrease in inter particle distance

Inter particle distance(mm)	Propagation constant (mm^{-1}) PS-alumina (ϵ_r=2.55)	Propagation constant (mm^{-1}) PS-titania (ϵ_r=2.6)
1	0.64244	0.8883
0.1	0.64272	0.8915
0.01	0.64273	0.89166
0.001	0.64273	0.89167

In order to systematically increase the solution accuracy, the number of basis function has to be increased where the basis function must belong to a complete set.

5.7 CONCLUSION

In the present investigation spectral domain technique for analysis of microstrip line structure on a single substrate is modified to study microstrip line on particle reinforced polymer composites, PS-alumina and PS-titania. This technique is successfully used to analyze propagation constant of the wave in microstrip line fabricated on the composite substrate which is discussed in the next chapter. An insight to variation of normalized wavelength with frequency and effect of size and distribution of reinforced particle on the phase velocity can be obtained.

References:

[1] E. Yamashita and R. Mittra, "Variational Method for the Analysis of Microstrip Lines," IEEE Trans Microwave Theory and Techniques, vol. 16, pp- 251, 1968.

[2] E. Yamashita, "Variational Method for the Analysis of Microstrip-like Transmission Lines," IEEE Trans Microwave Theory and Techniques, vol. 16, pp- 529, 1968.

[3] M. V. Schneider, "Microstrip Dispersion," Proc. IEEE, vol. 60, pp- 144, 1972.

[4] R. Mittra and T. Itoh, "Analysis of Microstrip Transmission Lines," Advances in Microwaves. vol.8, Academic Press, New York, 1974.

[5] R. P. Owens, "Predicted Frequency Dependence of Microstrip Characteristic Impedance Using the Planar-Waveguide Model," Electron Letter, vol. 12, pp- 269, 1976.

[6] B. Bianco, "Frequency Dependence of Microstrip Parameters," Alta Frequenza, vol. 43, pp- 413, 1974.

[7] H. A. Wheeler, "Transmission Line Properties of Parallel Strips Separated by a Dielectric Sheet," IEEE Trans Microwave Theory and Techniques, vol. 13, pp- 172, 1965.

[8] H. A. Wheeler, "Transmission Line Properties of a Strip on a Dielectric Sheet on a Plane," IEEE Trans Microwave Theory and Techniques, vol. 25, pp- 631, 1977.

[9] H. R. Kaupp, "Characteristics of Microstrip Transmission Lines," IEEE Trans, vol. EC- 6, pp-185,1967.

[10] E. J. Denlinger," A Frequency Dependent Solution for Microstrip Transmission Lines," IEEE Trans Microwave Theory and Techniques, vol. 19, pp- 30, 1971.

[11] T. Itoh and R. Mittra, "Spectral-Domain Approach for Calculating Dispersion Characteristics of Microstrip Lines," IEEE Trans Microwave Theory and Techniques, vol. 21, pp- 496, 1973.

[12] J. B. Knorr, and A. Tufekcioglu, "Spectral-Domain Calculation of Microstrip Characteristics Impedance," IEEE Trans Microwave Theory and Techniques, vol. 23, pp- 725, 1975.

[13] J. S. Hornsby and A. Gopinath, "Numerical Analysis of a Dielectric Loaded Waveguide with a Microstrip Line – Finite Difference Methods," IEEE Trans Microwave Theory and Techniques, vol. 17, pp- 684, 1969.

[14] D. G. Corr and J. B. Davies, "Computer Analysis of the Fundamental and Higher Order Modes in Single and Coupled Microstrip," IEEE Trans Microwave Theory and Techniques, vol. 20, pp- 669, 1972.

[15] W. Barth, "Calculation of the Eigenvalues of a Symmetric Tridiagonal Matrix by the Method of Bisection," Numerische Mathematik, vol. 9, pp- 336, 1967.

[16] G. I. Zysman and D. Varon, "Wave propagation in Microstrip Transmission Lines," IEEE G-MTT Int. Microwave Symposium Digest, pp- 2, 1969.

[17] R. Mittra and T. Itoh, "A New Technique for the Analysis of the Dispersion Characteristics of Microstrip Lines," IEEE Trans Microwave Theory and Techniques, vol. 19, pp- 47, 1971.

[18] T. Itoh and R. Mittra, "A Technique for Computing Dispersion Characteristics of Shielded Microstrip Lines," IEEE Trans Microwave Theory and Techniques, vol. 22, pp- 896, 1974.

[19] R. H. Jansen, "The Spectral Domain Approach for Microwave Integrated Circuits," IEEE Trans Microwave Theory and Techniques, vol. 33, pp-1043, 1985.

[20] D. Syahkal Mirshekar, "The Spectral Domain Method for Microwave Integrated Circuit," John Wiley and Sons INC, 1990.

[21] J. L. Tsalamengas, N. K. Uzunoglu and N. G. Alexopoulos, "Propagation Characteristics of A Microstrip Line Printed on A General Anisotropic Substrate," IEEE Trans Microwave Theory and Techniques, vol. 33, pp- 941, 1985.

[22] R. Marques and M. Horno, "On the Spectral Dyadic Green's Function for Stratified Linear Media- Application to Multilayer MIC Lines With Anisotropic Dielectrics," IEE Proceedings, vol. 134, pp- 241, 1987.

[23] A. Farrar and A.T. Adams, "Computation of Propagation Constants for the Fundamental and Higher Order Modes in Microstrip," Microwave Theory and Techniques, vol. 24, pp- 456, 1976.

[24] M. Hashimoto, "A Rigorous Solution for Dispersive Microstrip," Microwave Theory and Techniques, vol. 33, pp- 1131, 1985.

[25] M. K. Krage and G. I. Haddad, "Frequency Dependent Characteristics of Microstrip Transmission Lines," Microwave Theory and Techniques, vol. 20, pp- 678, 1972.

[26] D. Syahkal Mirshekar and J. B. Davies, "An Accurate, Unified Solution to Various Fin-Line Structures of Phase Constant, Characteristic Impedance and Attenuation," IEEE Trans Microwave Theory and Techniques, vol. 30, pp- 1854, 1982.

[27] M. G. Todd and F. G. Shi, "Characterization of the Interphase Dielectric Constant of Polymer Composite Materials: Effect of Chemical Coupling Agent," Journal of Applied Physics, vol. 94, pp- 4551, 2003.

[28] A. S. Omar and K. S̨hunemann, "Formulation of the Singular Integral Equation for General Planar Transmission Lines, " IEEE MTT-S Digest, pp 135, 1985.

[29] J. B. Knorr and A. Tufekcioglu, "Spectral Domain Calculation of Microstrip Characteristic Impedance," IEEE Trans Microwave Theory and Techniques, vol. 23, pp- 725, 1975.

CHAPTER VI

DESIGN AND FABRICATION OF MICROSTRIP LINE

6.1 INTRODUCTION

Satellite, airborne communication and EW system have requirement for small size, light weight and low cost microwave passive components. Miniaturizations of components have become inevitable in microwave technology. Although waveguide components are indispensable for high power handling, planar components due to its small size, light weight, good reliability and flexibility in laying out circuit have led to its evolution. Low cost for mass production is an additional advantage for fast growth of this technology.

Microstrip line is one of the most frequently used planar inhomogeneous transmission line on account of its simple construction and ease of mounting passive and active components and lumped devices to it. The substrate is often referred to as the "guiding structure" for microstrip circuit. The choice of the substrate is crucial in designing the microstrip circuits for various applications. Figure 6.1 shows the geometry of a microstrip line on the composite substrate.
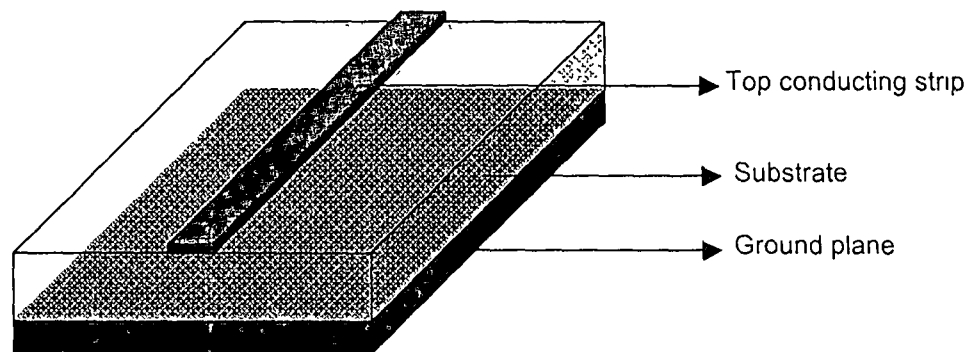
Figure 6.1: Geometry of a microstrip line

To make a sensible choice of the material for particular applications, largely depends on permittivity of the microwave material. In addition to this substrates anisotropy, dissipation factor, dielectric thickness, coefficient of thermal expansion, metallization thickness, surface finish and peel strength plays a significant role.

In this chapter the substrate relevance of polymer composite are studied. Microstrip line has been designed in C- and X-band on composite substrates with varying

volume fraction of filler. The fabrication technique employed has been discussed. The microwave propagation through the device is determined by measuring the scattering parameters. The results are analyzed using SDT technique modified for composite material described in Chapter V and compared with conventional SDT.

6.2 COMPOSITE MATERIAL FOR MICROWAVE INTEGRATED CIRCUIT

To consider composite materials as substrate in MIC's, it is important to find out the change in group and phase velocities of electromagnetic wave when traveling through such a mixed dielectric medium and solve electromagnetic equations to determine the field patterns.

As mentioned in chapter I section 1.2, advantage of using particulate composites is that their microwave properties can be varied with shape, size, distribution, quantity and properties of inclusions (filler) added to it [1-2]. Further to reduce loss due to scattering, the size of particulate is kept less than the probing wavelength, additional loss present is mostly due to attenuation [3]. In particulate composites, an additional dielectric loss due to the interfacial polarization between the two different dielectrics under field is also present [4]. To reduce this additional dielectric loss tetraethyl orthotitanate is added as surfactant which helps in reducing the interfacial 'molecular polarizability'. Moreover it increases adhesion between metal and polymer during the metallization process [5].

It is also important that the filler distribution in the polymer matrix be homogeneous so as electromagnetic wave transmission velocity throughout the media be same. The micro-structural studies conducted on PS-alumina and PS-titania systems, as reported in chapter III, show that both the conditions are satisfied.

The excitation of higher order modes in a microstrip is avoided by operating it below the cutoff frequency (f_c) of the first higher order mode which is represented as [6]

$$f_c = \frac{300}{\sqrt{\varepsilon_r}\,(2w + 0.8h)}$$

6.1

116

where f_c is in gigahertz, w, the width of the line and h, the height of substrate are in millimeters. In the present investigation for the 7% volume fraction is found to be 49.99 GHz.

At microwave frequencies, according to the classical dispersion theory of dielectrics, the dielectric constant is unchanged and dielectric loss increases with frequency. The product of quality factor (Q) and frequency (f) describes these basic properties of the dielectric material [7]. Therefore, dielectric loss of the material is also an important parameter in determining the length of electromagnetic wave in substrate and hence its frequency of operation.

The thickness of polymer composite substrate used for microstrip line fabrication should be such that it does not change its physical dimensions during the fabrication process. For a thick substrate, higher order modes are generated and there is an increase in microwave dielectric losses. Very thin composite substrates (< 0.3 mm) were critical to handle and did not retain its shape and surface smoothness during metallization. For polystyrene-alumina/titania samples optimum thickness of the substrate is found to be 0.6 mm. The sample's cross-sectional dimensions are taken as 16mm × 16mm.

6.3 DESIGN OF MICROSTRIP LINE

The mode propagating along the microstrip line is not purely TEM but quasi-TEM. Quasi- static approach for designing is simple but limited for low frequencies, where the strip width and substrate thickness is smaller than wavelength in the dielectric. A quasi-empirical method known as "microstrip dispersion model" is used in designing the circuits at high frequencies.

The dispersion model given by Edward and Owens [8] is used for designing the microstrip line. Prior to determining dispersive characteristic of permittivity of the composite substrate [9], the effective relative permittivity for the dielectric is found as

$$\varepsilon_{eff} = 1 + q(\varepsilon_r - 1) \qquad\qquad 6.2$$

117

where 'q' is the filling factor and

$$q = \frac{\varepsilon_{eff} - 1}{\varepsilon_r - 1}$$

6.3

while ε_{eff} for a given $\frac{w}{h}$ is calculated from the relation given by Wheeler [10]

$$\varepsilon_{eff} = \frac{(1 + \varepsilon_r)}{2} \left(\frac{A}{A - B} \right)^2$$

6.4

where

$$A = \ln\left(\frac{8h}{w} \right) + \frac{1}{32}\left(\frac{w}{h} \right)^2$$

6.5

$$B = \frac{1}{2}\left(\frac{\varepsilon_r - 1}{\varepsilon_r + 1} \right)\left[\ln \frac{\pi}{2} + \frac{1}{\varepsilon_r}\ln \frac{4}{\pi} \right]$$

6.6

and $\frac{w}{h}$ of microstrip line is found from the following relationship

$$\frac{w}{h} = \left[\frac{\exp H'}{8} - \frac{1}{4\exp H'} \right]^{-1}$$

6.7

where

$$H' = \frac{Z_0\sqrt{2(\varepsilon_r + 1)}}{119.9} + \frac{(\varepsilon_r - 1)}{2(\varepsilon_r + 1)}\left[\ln \frac{\pi}{2} + \frac{1}{\varepsilon_r}\ln \frac{4}{\pi} \right]$$

6.8

where

Z_0 = Characteristic impedance of the line

h = Height of the substrate

ε_r = Relative permittivity of the substrate

ε_{eff} = Effective relative permittivity

w = Width of the microstrip line

Considering the frequency dependent characteristic of ε the final equation for effective permittivity [8] is given by

118

$$\varepsilon_{eff}(f) = \varepsilon_r - \frac{\varepsilon_r - \varepsilon_{eff}}{1 + \left(\dfrac{h}{Z_0}\right)^{1.33} \left(0.43 f^2 - 0.009 f^3\right)} \qquad 6.9$$

where f is the operating frequency Z_0 is the characteristic impedance of the line and h is the thickness of the substrate.

The guide wavelength (λ_g) and the characteristic impedance (Z_0) in composite substrate is found by the following formulas

$$\lambda_g = \frac{\lambda_0}{\sqrt{\varepsilon_{eff}(f)}} \qquad 6.10$$

and

$$Z_g = \left(\frac{1}{\sqrt{\varepsilon_{eff}(f)}}\right) Z_0 \qquad 6.11$$

where λ_0 is the free space wavelength.

These equations are taken into account while designing a 50 Ω microstrip line at 5.5 GHz (C-band) and 10 GHz (X-band) on composite substrate.

The width of the line should not be less than the computed value from the design equation 6.7 as it is found to increase ripple and widen out 3 dB band width. The calculated design parameters of the microstrip line for both C- and X- band are given in the following sub sections.

6.3.1 Design Parameters for Microstrip Line at C- band

The design parameters of microstrip line on both the composite systems for 1%VF filler designed at 5.5 GHz are given in table 6.1. The physical length of the line was taken as 16 mm.

Table 6.1: Design parameters of microstrip line at 5.5 GHz

Samples	ε_r	h(mm)	w(mm)	q	λ_g (mm)
Polystyrene(PS)	2.5	0.6	1.714	0.746	37.358
PS+ 1%Alumina	2.55	0.6	1.691	0.744	37.055
PS +1%Titania	2.6	0.6	1.668	0.743	36.76

6.3.2 Design Parameters for Microstrip Line at X- band

The design parameters of microstrip line of both the composite with 1-7%VF of filler designed at 10 GHz are given in tables 6.2a and 6.2b respectively. The dimension of the line along the propagation direction is kept as 16 mm.

Table 6.2a: Design parameters of microstrip line on PS –alumina composite at 10 GHz

%VF	ε_r	h(mm)	w(mm)	q	λ_g (mm)
1	2.55	0.6	1.691	0.744	20.278
2	2.614	0.6	1.662	0.742	20.069
3	2.671	0.6	1.637	0.740	19.889
4	2.728	0.6	1.614	0.738	19.715
5	2.785	0.6	1.591	0.736	19.545
6	2.823	0.6	1.576	0.735	19.435
7	2.902	0.6	1.546	0.732	19.213

Table 6.2b: Design parameters of microstrip line on PS – titania composite at 10 GHz

%VF	ε_r	h(mm)	w(mm)	q	λ_g (mm)
1	2.6	0.6	1.668	0.743	20.114
2	2.68	0.6	1.634	0.740	19.861
3	2.78	0.6	1.593	0.736	19.560
4	2.89	0.6	1.550	0.733	19.247
5	3.10	0.6	1.476	0.730	18.693
6	3.210	0.6	1.440	0.723	18.424
7	3.31	0.6	1.409	0.720	18.191

120

6.4 FABRICATION OF MICROSTRIP LINE

The width of the microstrip line is determined from frequency of operation. Metallization of copper on polystyrene composite material is challenging. Copper metallization can be done by two processes-rolled and electrodeposition. For drawing the line on the composite material, electrodeposition technique was used. Electrodeposited copper is a material produced by a chemical building process in which the individual copper particles are electrically joined to form the desired sheet thickness [11].

To optimize the fabrication process a negative mask is placed on the substrate followed by copper deposition. Prior to this, the substrate is thoroughly cleaned with acetone to remove oil and grime from the surface. Subsequently, the substrate is dried at 30°C in a vacuum oven and masked with an adhesive tape. The artwork of microstrip line in accordance with the design formulae (6.7 and 6.8) is drawn on the masked substrate by specially designed sharp tool with precision of 0.002 mm attached to milling machine whose least count was 0.02 mm. The adhesive strip is peeled off and the first layer of copper of thickness 0.0499 microns is deposited using high vacuum technique (at 10^{-6} torr). A similar layer of copper of thickness 3.129 micron is deposited for the ground plane. The thickness of the copper layer on both sides is increased up to 4 to 6 microns (i.e. few times the skin depth) by electroplating. The masking tape is completely removed and substrate is cleaned again to remove traces of tape adhesive. To determine any discrepancies in the line pattern, the microstrip line is observed under a microscope of least count 0.01 mm. This process of transferring artwork on the substrate, avoids the underneath etching of copper which leads to change in dimension of the line and hence the frequency of operation. The circuit is placed on the launcher and scattering parameter S_{11} and S_{21} are measured.

6.5 TECHNIQUES FOR MICROWAVE MEASUREMENT

The microstrip line with the launcher is shown in figure 6.2. To either end of the line, 50 ohms SMA connectors are attached. It is assured that the connector feeding point is in contact with the copper strip. A teflon post is inserted on the walls of the launcher for complete isolation of the feed line from the ground plane.

C-band measurements are carried out using network analyzer HP 8451C in a sweeping range from 3 to 6 GHz. The C-band measurement set up is given in figure 6.3.
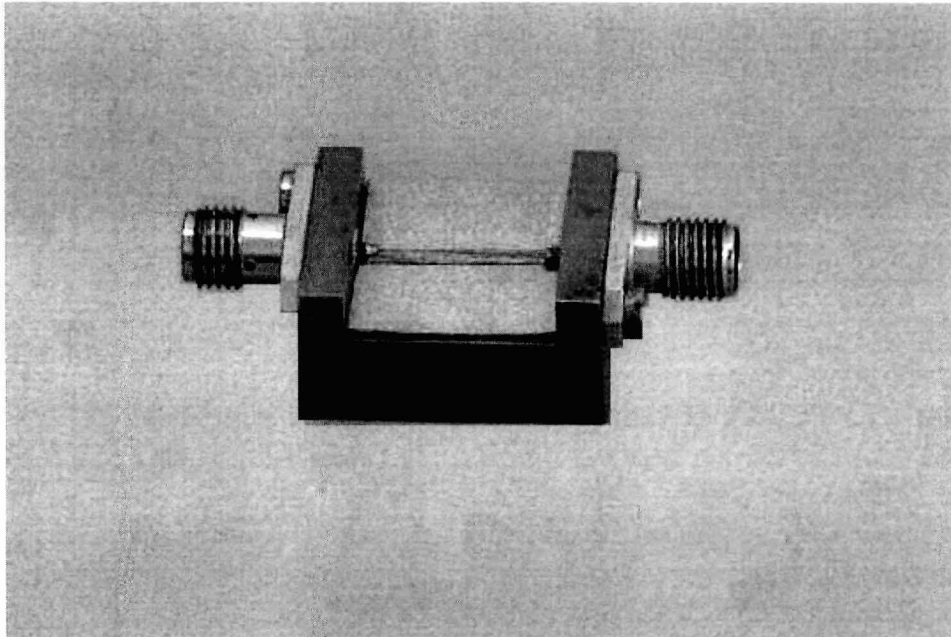

Figure 6.2 Photograph of the launcher with a mounted substrate

Figure 6.3: Experimental setup for measurement of scattering parameter at C-band

122

For X-band measurements the sweeping range is from 8.4 to 12 GHz carried out with the automated system developed in laboratory as described in chapter II. Prior to measurement the cables and connectors are shorted, and reference power level for the frequency range is stored in a data file in case of X-band measurements and into the memory of the network analyzer in case of C-band measurements.

6.5.1 Insertion Loss Measurement

For X band measurement:

P_{in} = Incident power

P_{ref} = Power with shorting all cables and connectors

Final incident power (P_{fin}) at port 1,1 is

$$P_{fin} = P_{in} - P_{ref}$$ 6.12

P_{dut} = Power measured at port 1,1 with device under test (DUT) connected

The magnitude of scattering parameter S_{11} is calculated as

$$S_{11} = \left(\frac{P_{dut}}{P_{fin}} \right)$$ 6.13

Scattering parameter S_{12} is found as follows:

Power transmitted to port 2,2 (P_{trans}) with DUT is measured. Then port 2,2 is shorted and power (P_L) at port 1, 1 is measured. Figure 6.4 shows the block diagram of a two port network [12] where a_1, b_1 are incident and scattered waves at the input port and a_2, b_2 are the incident and scattered signal at the output port. For a two port transmission line, magnitude of reverse transmission coefficient (S_{12}) is equal to the forward transmission coefficient (S_{21}).

$S_{12} = S_{21}$ is calculated as

$$S_{12} = \left(\frac{P_L}{P_{trans}} \right)$$ 6.14

The magnitude of insertion loss (IL) of the device is calculated as

$$IL = 10\log\frac{1}{|S_{12}|}$$

6.15

Four sets of measurements are taken to verify the repeatability of the insertion loss curve. The studies are conducted on all the filler concentrations for PS-alumina and PS-titania composite systems. The results so obtained are recorded and analyzed.
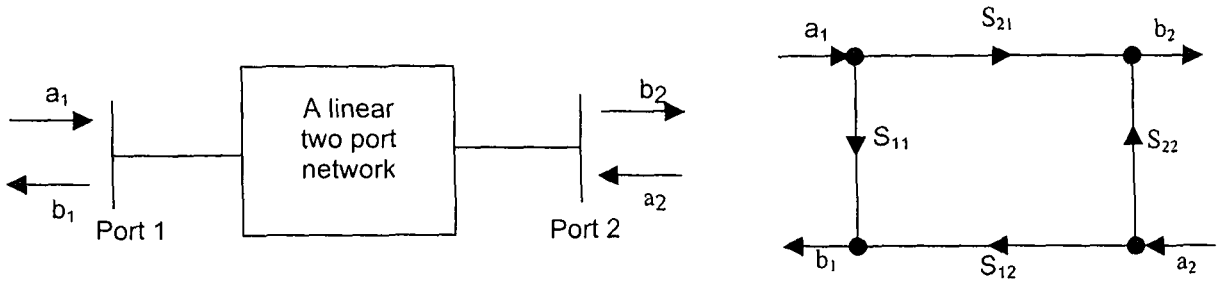
Figure 6.4: Block diagram of a two port network and signal flow graph representation

6.5.2 Determination of Attenuation Constant

Microwave power is swept in the C- and X-band frequency range. An insertion loss (IL) minima is observed indicating maximum microwave power transmission at the design frequency. The frequency of the notch, f_0 and 3 dB band width (Δf) from the IL plot, loaded Q factor is determined as

$$Q = \frac{f_0}{\Delta f}$$

6.16

The attenuation constant (α) is found by the following expression [12]

$$\alpha = \frac{27.3}{Q\lambda_g} \text{ dB/mm}$$

6.17

where the wavelength is in millimeter.

124

6.5.3 Propagation Constant Measurement

The electric and magnetic field patterns on a microstrip line are a function of attenuation and phase velocity of the electromagnetic wave inside the substrate. The sum of attenuation constant (α) and phase velocity (β) is expressed as propagation constant (γ),

$$\gamma = \alpha + j\beta \qquad\qquad 6.18$$

The phase velocity of the microwave signal is determined from guided wavelength. The guided wavelength (λ_g) is measured by twice the distance between two successive minima in the standing wave pattern. From this the phase velocity (β) is computed as

$$\beta = \frac{2\pi}{\lambda_g} \ (mm^{-1}) \qquad\qquad 6.19$$

6.6 RESULTS AND DISCUSION

Microstrip line is fabricated on all the filler concentration of both the composite systems and tested. The experimental results for insertion loss (IL) and attenuation constant in C- and X-band are given in the following sub sections.

6.6.1 C-Band Measurement

Characteristic of the microstrip line designed at 5.5 GHz for polystyrene and polystyrene filled with 1%VF of alumina/ titania are measured with HP 8451C.

6.6.1.1 Insertion loss of microstrip line

Insertion loss characteristics of the three samples are shown in figure 6.5 (a-c).
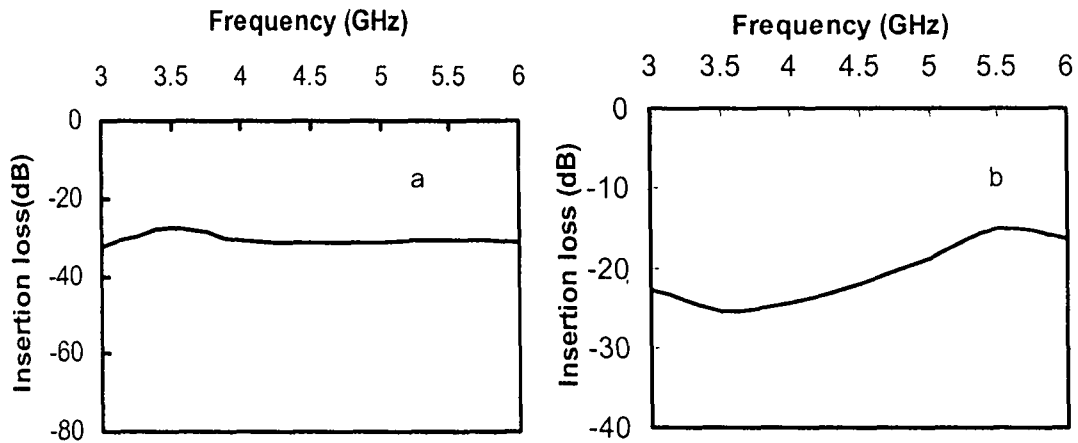
Figure 6.5: Insertion loss of microstrip line on a) PS b) PS-1% VF alumina substrate at 5.5 GHz
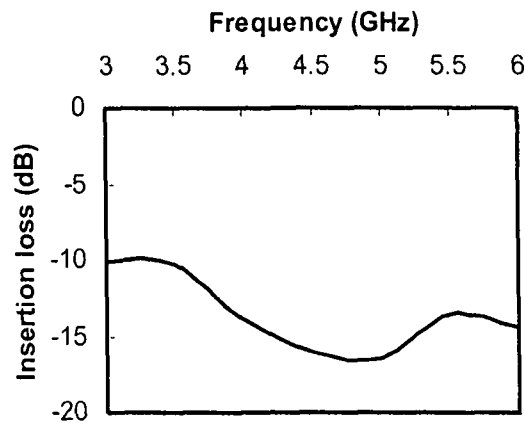
Figure 6.5c: Insertion loss of microstrip line on PS-1% titania at 5.5 GHz

The results obtained in C-band are not very encouraging. The new materials produced seem not to be a suitable material as substrate in C-band.

6.6.2 X-Band Measurement

The frequency is swept from 8.4 to 12.0 GHz and scattering parameters are measured. The results for IL characteristics, attenuation constants and propagation constants are described below.

126

6.6.2.1 Insertion loss of microstrip line

PS-alumina composite

The insertion loss of microstrip line on PS-alumina composite designed at 10 GHz is shown in figure 6.6 (a-g).

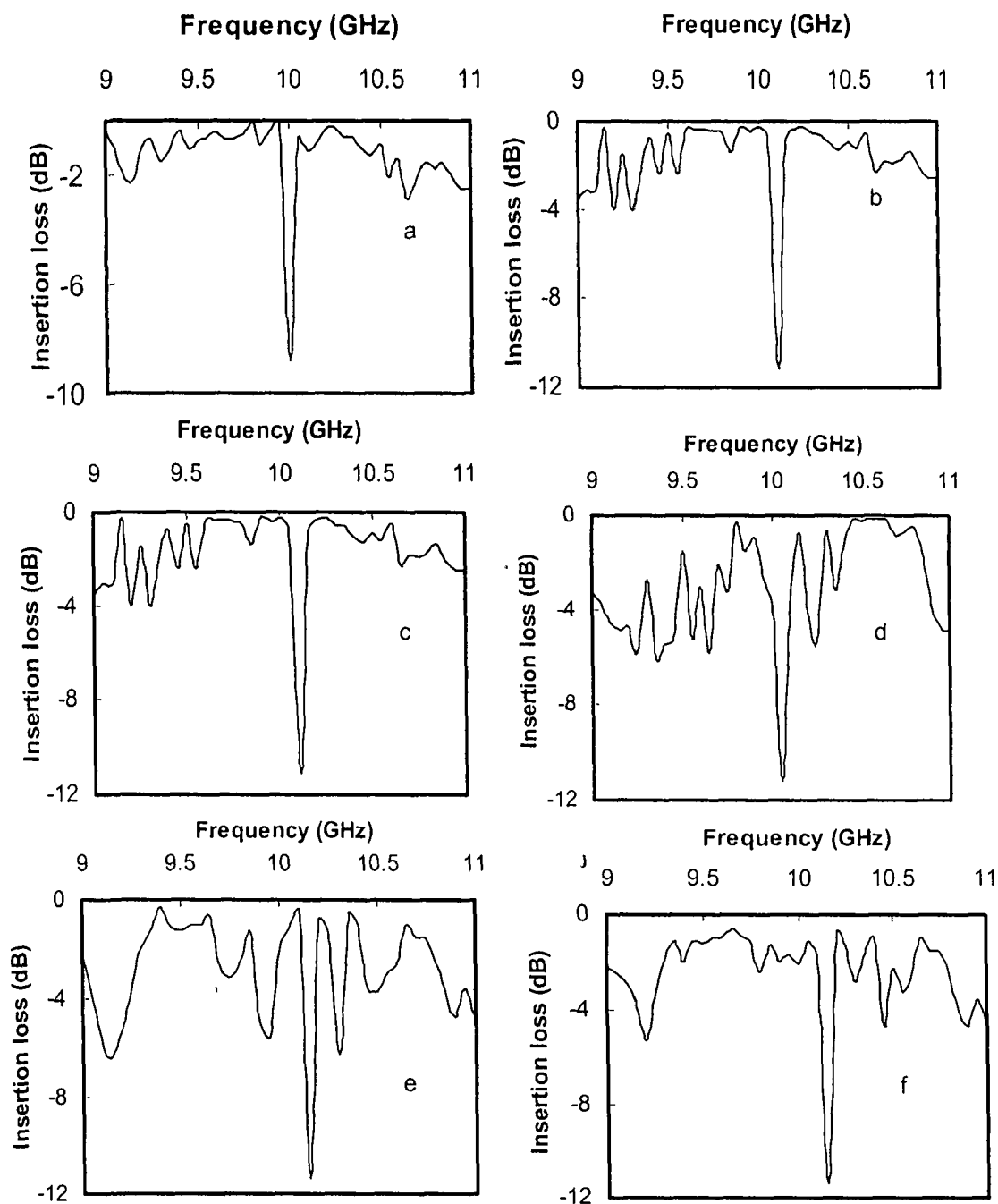Figure 6.6: Insertion loss of microstrip line on a) PS-1%VF b) PS-2%VF c) PS-3%VF d) PS-4%VF e) PS-5%VF and f) PS-6%VF alumina
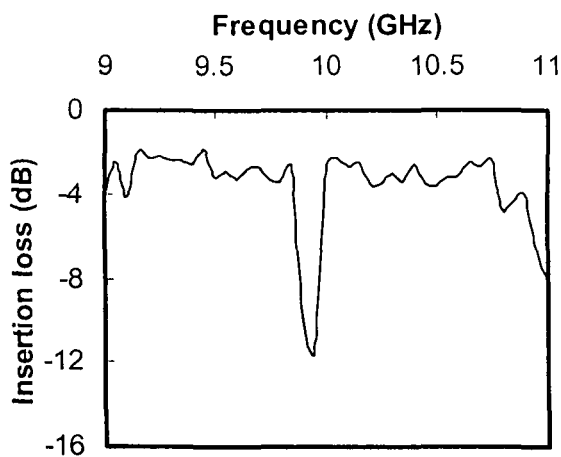
Figure 6.6g: Insertion loss of microstrip line on PS-7%VF

PS- titania composite

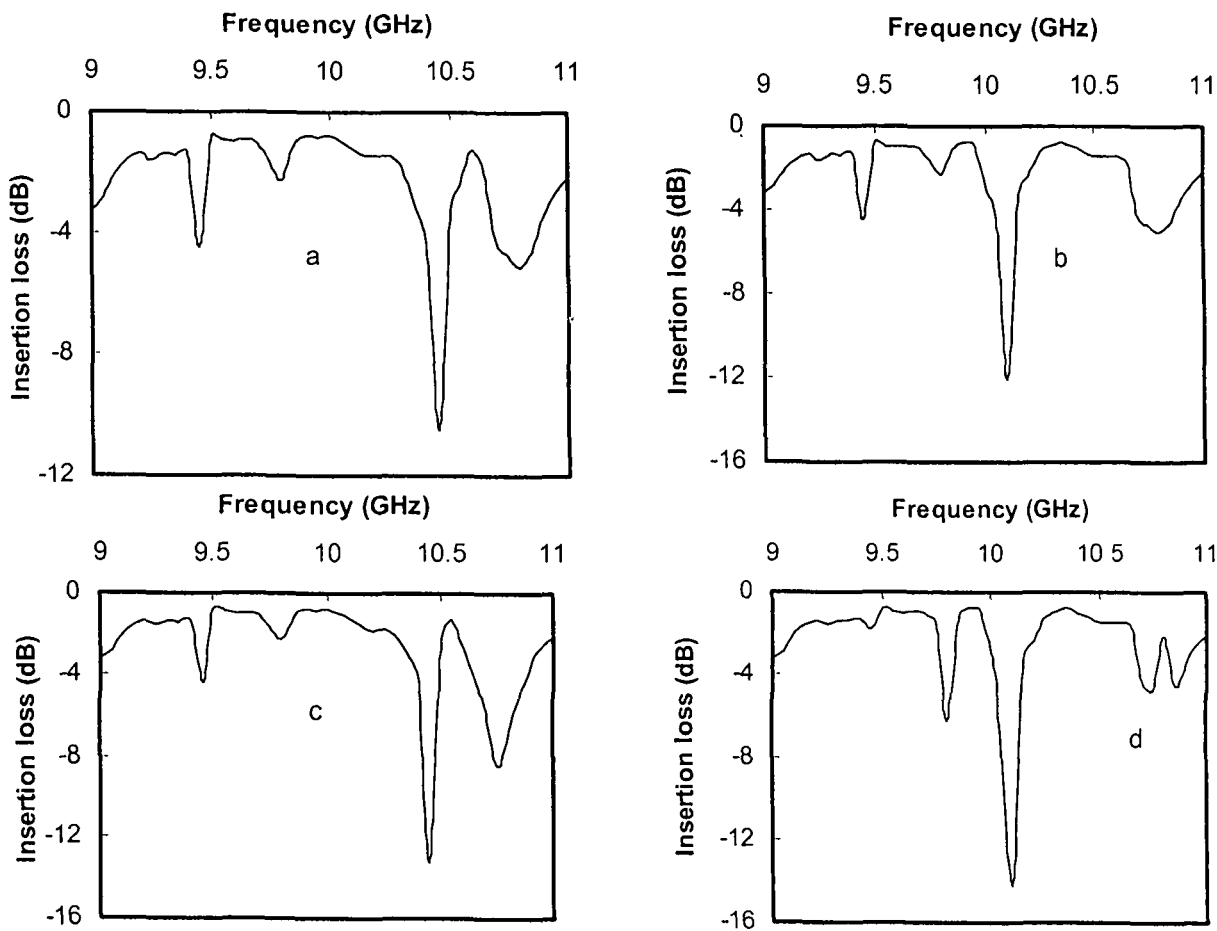Insertion loss of microstrip line on PS-titania composite designed at 10 GHz is shown in figure 6.7 (a-g).

Figure 6.7: Insertion loss of microstrip line on a) PS-1%VF b) PS-2%VF c) PS-3%VF d) PS-4%VF titania
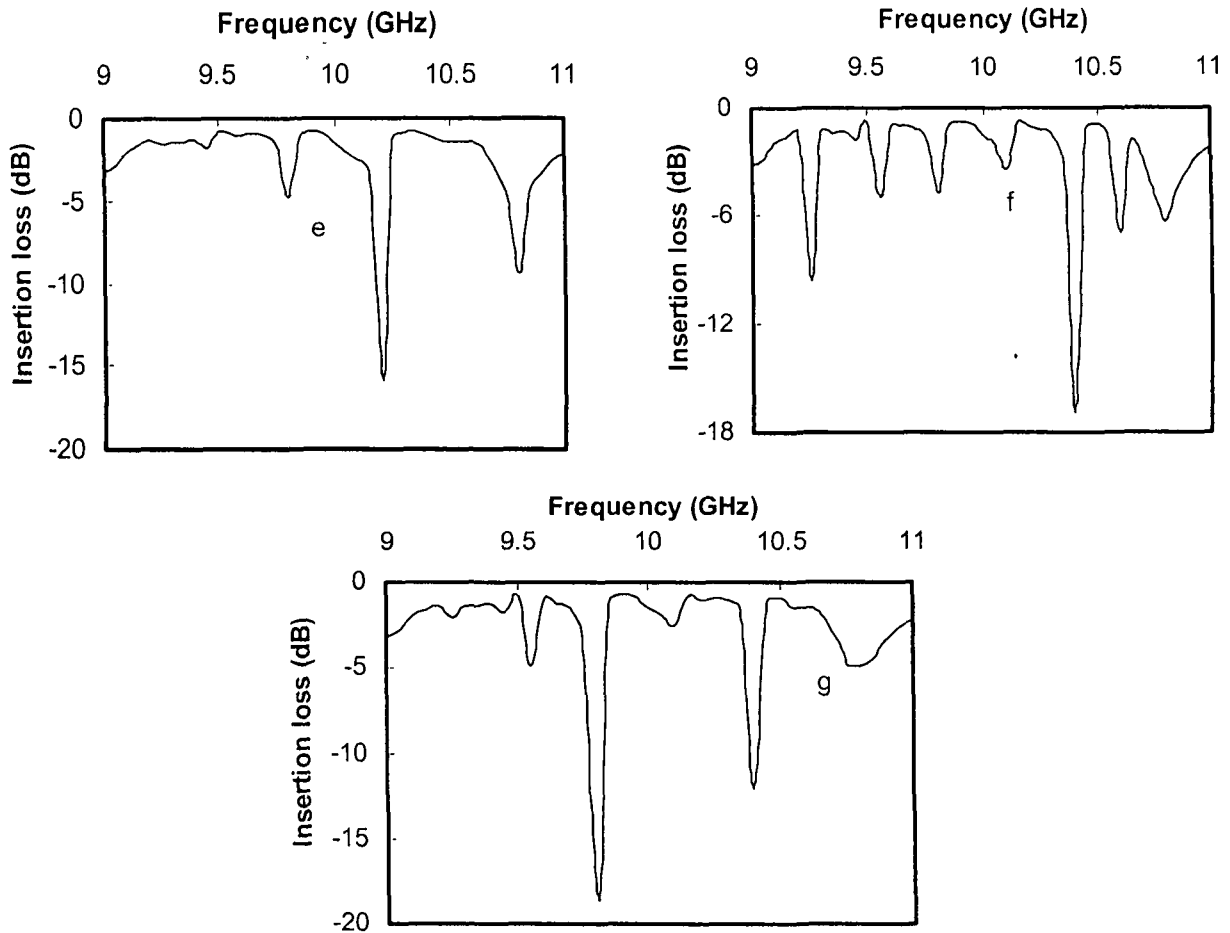
Figure 6.7: Insertion loss of microstrip line on e) PS-5%VF f) PS-6%VF and
g) 7%VF PS- titania composite

Insertion loss (IL) measurement on both the composite systems shows that it increases with the increase in filler percentage. In PS-alumina composite, it changes from -8.0 dB to -12.0 dB with increase in filler quantity from 1% -7% volume fractions. A change of IL value from -10.0 dB to -19.0 dB is observed in PS-titania composite. The increase in alumina/ titania reinforced particle in the polymer increases the permittivity of the PS-alumina and PS-titania composite. This increase in permittivity increases the effective dielectric constant. The effective dielectric constant also increases with increase in frequency and effective strip width decreases. The decrease in effective strip width increases the characteristic impedance.

6.6.2.2 Attenuation constant measurement

Table 6.3 shows the attenuation constant of microstrip line designed at 10 GHz on PS-alumina and PS-titania composite respectively. An increase in attenuation value with increase in filler percentage is observed. The increase in filler quantity increases the dielectric loss and dielectric conductivity.

Table 6.3: Attenuation constant of PS- alumina and PS-titania composite at 10 GHz

% Volume fraction	PS-alumina		PS-titania	
	ε_r	Attenuation (db/mm)	ε_r	Attenuation (db/mm)
1	2.55	0.0053	2.6	0.0045
2	2.614	0.0053	2.68	0.0081
3	2.671	0.0054	2.78	0.005
4	2.728	0.006	2.89	0.007
5	2.785	0.0078	3.10	0.0057
6	2.823	0.0055	3.210	0.0039
7	2.902	0.0114	3.31	0.005

6.6.2.3 Propagation constant measurements and analysis

Experimental propagation constant for the microstrip line on composite substrate is determined from equation 6.19, mentioned in section 6.5.3. Figure 6.8 shows variation of propagation constant with %VF for the PS-alumina and PS-titania composite.
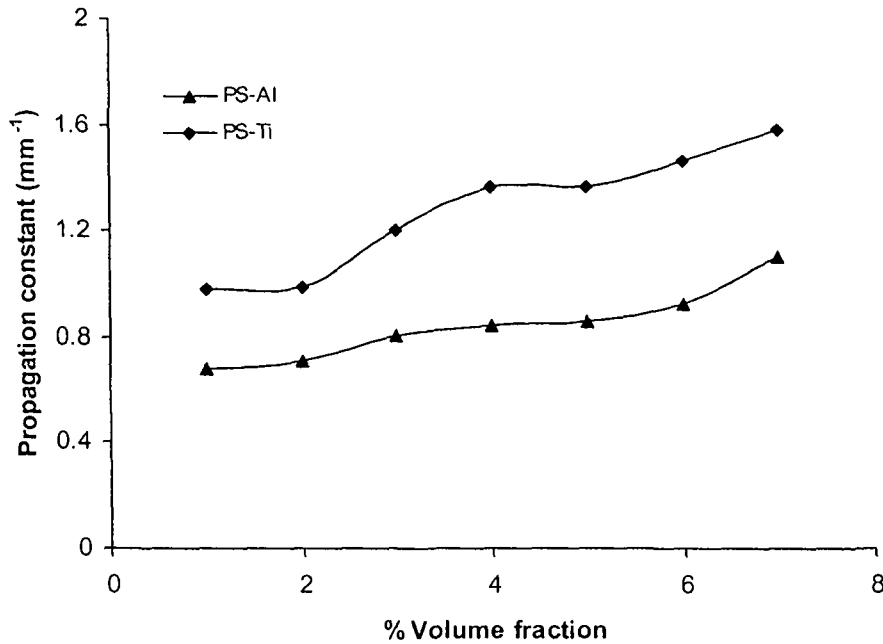
Figure 6.8: Variation of propagation constant with %VF of filler

It is observed that propagation constant increases with the increase in percentage volume fraction in both the composite systems. The increase in propagation constant reduces the phase velocity of wave in microstrip with increase in frequency which explains the influence of frequency on permittivity of composites mentioned in chapter IV.

The results for propagation constant are analyzed using SDTMC technique developed in chapter V. The experimental results of propagation constant and that computed by SDTMC in PS-alumina and PS-titania composites for zero order approximation are shown in figures 6.9 (a-b) and 6.10(a-b) respectively. The results computed by spectral domain technique are also given for comparison.

Figures 6.9 and 6.10 show that the propagation constant (β) increases with the increase in frequency. The increase in propagation constant reduces the phase velocity of the waves in microstrip with increase in frequency. It is observed from the figures that the computed value of β is more in PS-titania composite than the PS-alumina composite for the same percentage increase in the volume fraction. The higher dielectric constant of the
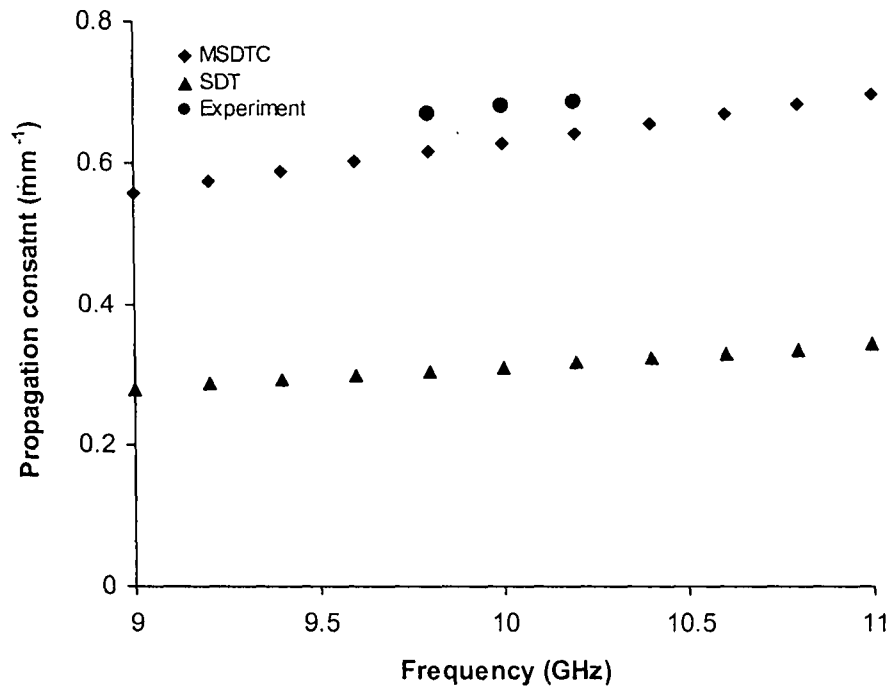
Figure 6.9a: Comparison of experimental and theoretical propagation constant of (PS-1%VF of alumina)
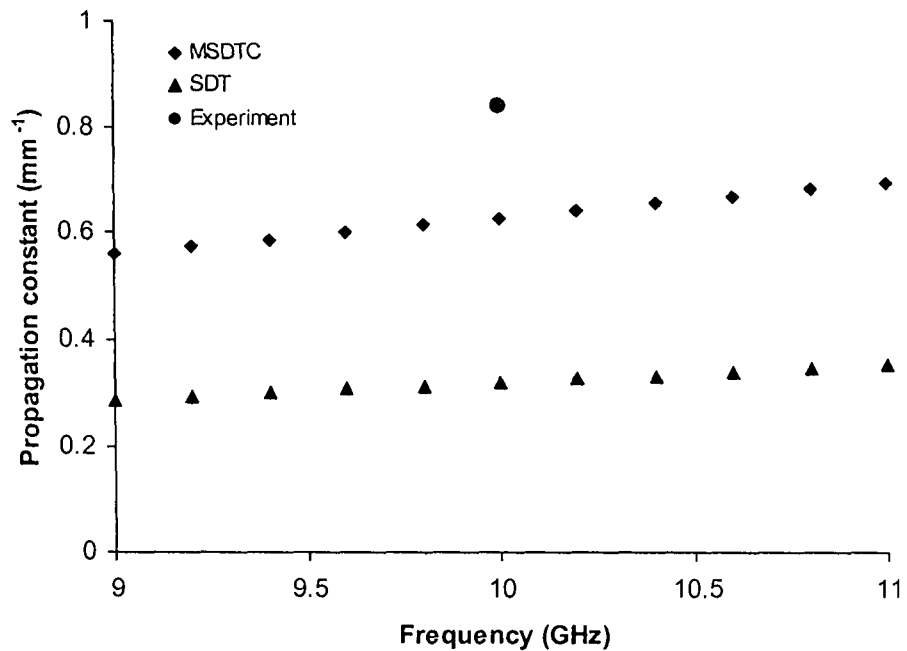

Figure 6.9b: Comparison of experimental and theoretical propagation constant of (PS-4%VF of alumina)
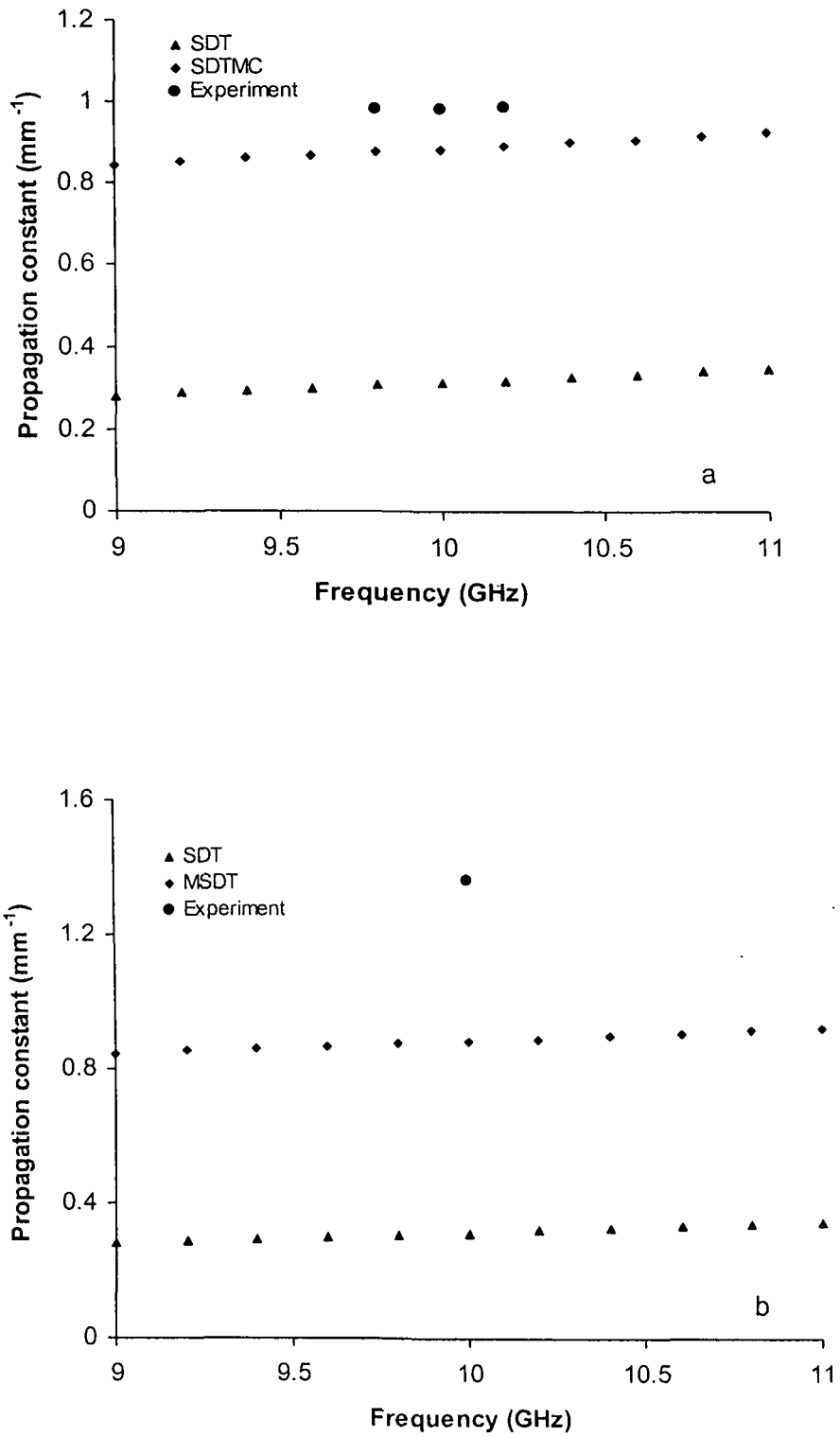
132

Figure 6.10: Comparison of experimental and theoretical propagation constant of a) PS-1%VF and b) PS-4%VF of Titania

titania particle indicates that phase velocity in the microstrip on PS-titania composite is lesser than that in the PS-alumina composites.

MSDTC technique shows better agreement with the experimental results as compared to that shown by conventional SDT where composites are considered as single layer. With increase of %VF of filler a deviation of MSDTC technique is observed. Experimentally, same quantity of surfactant is added to all the sample sets to reduce the interphase layer. For higher quantity of filler the interphase layer need not necessarily vanishes completely. Hence instead of two layers model a three layers model, polymer-interphase-polymer should be considered. Moreover, the polymer filler cell is considered to be square in shape of whose length is considered as the average diameter of the filler particle, but practically, filler is spherical in shape, which may leave more space for polymer in the polymer filler unit. With increase of filler quantity, from the approximation polymer space is further reduced.

6.7 CONCLUSION

In this chapter design and fabrication process of microstrip line on the PS-alumina and PS-titania composites is presented. It is seen that masking tape fabrication method used to fabricate microstrip line is able to print microstrip line with high accuracy. This process is less costly than the photolithography technique generally used to fabricate microstrip line. This method is cost effective but also reduces the fabrication time. A maximum shift of ±0.2 GHz is observed in design frequency and transferring of artwork to the substrate.

IL results obtained in C-band for PS-alumina and PS-titania shows that this composite system is not suitable as substrate in 3-6 GHz range. Propagation measurement shows an increase in propagation constant with the increase in filler percentage. Propagation constant simulated with SDTMC technique shows closer agreement with experimental results.

References:

[1] C. Brosseau, P. Queffelec and P. Talbot, "Microwave Characterization of Filled Polymer," Journal of Applied Physics, vol. 89, pp- 4532, 2001.

[2] H. M. Musal Jr., H. T. Hahn and G. G. Bush, "Validation of Mixture Equation for Dielectric-Magnetic Composite," Journal of Applied Physics, vol. 63, pp- 3768, 1988.

[3] B. Sareni, L. Krahenbuhl, A. Beroual and C. Brosseau, "Effective Dielectric Constant of Periodic Composite Materials," Journal of Applied Physics, vol. 80, pp- 1688, 1996.

[4] Z. Yutao, C. Cheng, J. Weifang, X. Hengkun and L. Yaonan, "Relationship Between Dielectric Loss and Interphase Structure of Filled-types Polymer Composite," State Key Lab Of Electrical Insulation For Power Equipments, pp- 77.

[5] M. G. Todd and F. G. Shi, "Characterization of the Interphase Dielectric Constant of Polymer Composite Materials: Effect of Chemical Coupling Agents," Journal of Applied Physics, vol. 94, pp- 4551, 2003.

[6] R. Garg, "A Microstrip Design Guide," Int. Journal of Electron, vol. 46, pp- 178, 1979

[7] S. J. Fiedziuszko, I. C. Hunter, T. Itoh, Y. Kobayashi , T. Nishikawa, S. N. Stitzer and K. Wakino, "Dielectric Materials, Devices and Circuits," IEEE Trans Microwave Theory and Techniques, vol. 50, pp- 706, 2002.

[8] R. P. Owens, J. E. Aitken and T. C. Edwards, "Quasi-Static Characteristics of Microstrip on an Anisotropic Sapphire Substrate," IEEE Trans Microwave Theory and Techniques, vol. 24, pp- 499, 1976.

[9] R. A. Pucel and D. J. Masse, "Microstrip Propagation on Magnetic Substrate", Part I: Design Theory," IEEE Trans Microwave Theory and Techniques, vol. 20, pp- 304, 1972.

[10] H. A. Wheeler, "Transmission Line Properties of Parallel Strips Separated by Dielectric Sheet," IEEE Trans Microwave Theory and Techniques, vol. 13, pp-172, 1965.

[11] T. S. Laverghetta, "Microwave Materials and Fabrication Techniques," Third Edition, Artech House, 2002.

[12] P. A. Rizzi, "Microwave Engineering Passive Circuits," Prentice Hall of India, 1999.

CHAPTER VII

DESIGN AND FABRICATION OF MICROSTRIP

REFLECTION TYPE RADIAL STUB RESONATOR

7.1 INTRODUCTION

Circular microstrip disc resonators find wide applications in filters, junction circulators, planar antenna elements and power dividers [1-3]. Microstrip stubs on the circumference of such resonators not only influences the resonance frequency but significantly reduces the dimensions [4]. The conventional straight stub reduces the band width and exhibits very low characteristic impedance. The width of the stub is a significant fraction of the wavelength and therefore higher order modes can easily be excited at high frequencies leading to uncertainty in characteristic impedance value at the stub input point and structure behavior differing significantly.

The layout of microstrip reflection-type radial stub resonator (RRSR) is shown in figure 7.1. The center of the disc is coaxially fed, which is both the input and output port. The radial stubs are symmetrically located around the periphery of the circular disc.
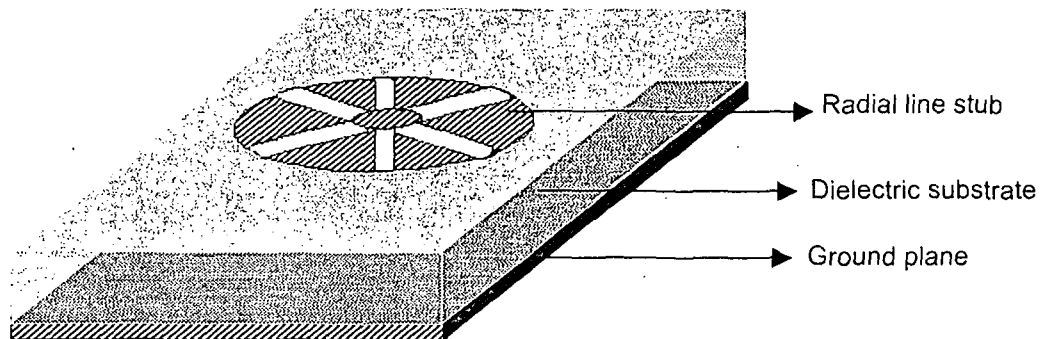
Figure 7.1: Reflection-type radial stub resonator (RRSR) structure for increased band width

The design geometry of the circular disc and radial stubs are discussed in the following section. The masking tape technique used for fabrication of microstrip line in chapter VI could not be used because it was difficult to layout the complex artwork by the high precision tool. Hot press lamination method is used to layout the computer generated artwork on the metallized material and subsequently etched.

137

Following reflection coefficient (S_{11}) measurements were carried out in X-band on PS-alumina and PS-titania composite systems.

i.   when all the radial stub ends are open

ii.   shorting one of the stubs end at $\lambda_g/2$ and $\lambda_g/3$

iii.   coupling adjacent radial stubs

iv.   for samples with different percent volume fraction of filler

7.2 DESIGN OF A MICROSTRIP REFLECTION-TYPE RADIAL STUB RESONATOR

A reflection-type radial stub resonator (RRSR) structure is designed using following methods

a) Microstrip circular disc resonator of radius 'R'

b) Microstrip radial stub of length $d = \lambda_g/2$ from the centre of the resonator

7.2.1 Dimensions of the Circular Disc Resonator

Figure 7.2 gives the geometry of uniform part of the RRSR without stubs. Magnetic wall model is used to design a microwave circular disc at resonance frequency (f). As the height h of substrate material is small the field excited is only TM mode.

(a)   (b)
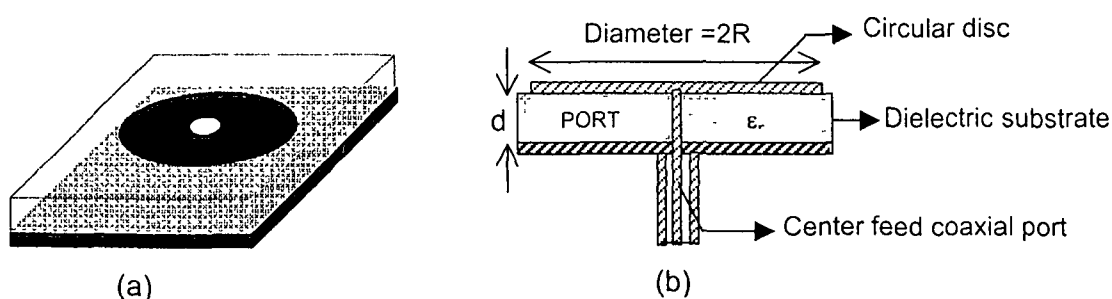
Figure 7.2: a) Geometry of uniform part of the RRSR without stubs
b) Coaxially fed port at the centre of a circular disc

138

To determine the effective radius (a_e) at the design frequency, the resonance frequency for excited TM_{mn} mode for first order circular patch [5] it must satisfied the following relation

$$f = \frac{X_{nm}c}{2\pi a_e \sqrt{\varepsilon_r}}$$ 7.1

f = resonance frequency

c= velocity of light

ε_r = relative permittivity of the substrate material

a_e = effective radius of the circular disc

X_{nm}= m^{th} zero of the derivative of Bessel's function of order n

n = angular mode number and

m = radial mode number

For m=1, the zeros are [6]

X_{nm} = 3.832   for n =0

   = 1.841   for n=1

   = 3.054   for n=2

   = 4.201   for n=3

For the lowest order mode TM_{110} mode of the circular disc on substrate of height h, the effective radius (a_e) [6] is

$$a_e = R\left\{1 + \frac{2h}{\pi R \varepsilon_r}\left[\ln\left(\frac{\pi R}{2h}\right) + 1.7726\right]\right\}^{1/2}$$ 7.2

$$R = \frac{a_e}{\sqrt{1 + \frac{2h}{\pi R \varepsilon_r}\left[\ln\left(\frac{\pi R}{2h}\right) + 1.7726\right]}}$$ 7.3

7.2.2 Microstrip Radial Stub

Figure 7.3 shows the sketch of the radial stub where 'L' (= $\lambda_g/2$) is the length of radial stub from the center, 'w₁' is angular distance between two stubs and 'w₂' is the angular width of stub end at L. The radial angle 'θ' of a stub is

$$\theta = \sin^{-1}\left(\frac{l}{L}\right) \text{ in degree} \qquad\qquad 7.4$$

For design of a symmetric structure,

Number of stubs with metallization = space without metallization

For non symmetric structure, if 'n' is the number of stubs, space without metallization (l') is

$$l' = L\sin\left(\frac{360-n\theta}{n}\right) \qquad\qquad 7.5$$

In the design equation when $\theta \sim 0$ the radial stub becomes a straight stub.
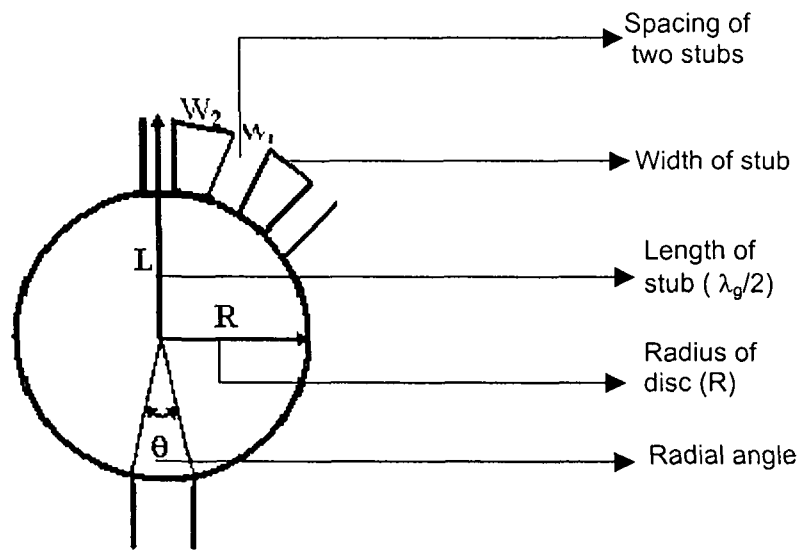
Figure 7.3: Detail sketch of a microstrip radial stub

Table 7.1 gives the different design parameter of radial stub at 10 GHz on the periphery of a microstrip circular disc of substrate height 0.6 mm.

Table 7.1: Design parameter of radial stub at 10 GHz on composite substrate

Sample		ϵ_r	Length of stub (L=λ_g/2)mm	Radius of circular disc(r) mm
PS-Al$_2$O$_3$	1%VF	2.55	9.393	5.228
	2%VF	2.614	9.277	5.166
	3%VF	2.671	9.178	5.113
PS-TiO$_2$	1%VF	2.6	9.302	5.180
	2%VF	2.68	9.162	5.105
	3%VF	2.78	8.996	5.016

7.3 FABRICATION OF MICROSTRIP RADIAL STUB RESONATOR CIRCUIT WITH HOT PRESS LAMINATION METHOD

The main motivation for hot press lamination method for fabrication of microstrip circuit is to get microstrip circuits, which exhibit a higher efficiency than conventional ones, minimize errors and can be fabricated using inexpensive large quantity production techniques. The approach is to make maximum use of the existing/available instrument and facility of the laboratory. Fabrication and etching of the above circuit is done using the following processes

❖ Metallization of copper on the substrate

❖ Preparation of microwave artwork

❖ Transferring artwork to the metal surface

❖ Etching with acidic ferric chloride

❖ Removal of mask

7.3.1 Metallization of Copper on the Substrate

The metallization process was performed in two steps by rolling technique

(a) Surface treatment of copper

A thin uniform copper foil of thickness 20 mils is taken. At first, traces of oil and contamination from the surface of the composite substrate and copper sheet is removed by cleaning them thoroughly with acetone.

The desired thickness of 152 mils which is 6 times the skin depth of copper foil is obtained by electrolysis. The copper foil is then treated with nitric acid. The treatment with acid removes the oxide layer and roughens the surface of copper to provide good adhesion with the substrate materials. The sheet is then washed in a double distilled water bath to remove traces of acids and water soluble contamination. Precaution is taken not to touch the treated substrate and copper foil with finger to avoid transfer of grime and oil. The copper sheet is dried at 40°C in an oven.

(b) Pasting of copper sheet on the sample surface

A thin layer of cyanoacrylate epoxy resin, an adhesive of thickness less than 20 micron, is brushed on both sides of the sample surface. It is observed with the cavity resonator method described in chapter IV that the loaded frequency of the sample does not shift its position on inserting adhesive on both sides of the sample. The surface treated nascent copper sheet is then placed on both sides of the substrate. For excellent adhesion of copper and the sample the system is kept under vice for 1 hour.

7.3.2 Preparation of Microwave Artwork

A positive artwork of 10 times enlarged layout of microstrip circuit is made in MS Word software. To realize the exact dimension of the circuit on the sample with higher accuracy a square boundary of (25mm x 25mm) size is given to the circuit pattern. The precise printout of this is taken on bond paper in a very high quality laser printer at 10%

reduction to get the actual dimension and accuracy. The printouts are examined thoroughly through a magnifying glass so that there should not be any exposed portion in the microstrip dimension. The printouts are examined thoroughly through a microscope to ensure its uniformity and freedom from edge distortion.

7.3.3 Transferring Artwork to the Metal Surface

Proper placement of the mask (artwork) plays vital role in exact transfer of circuit to the copper sheet attached with the sample. The paper with the masked is held properly on one side of the metallized substrate. The alignment of the artwork is checked with a microscope. The paper is made moist with a wet tissue paper for better transfer of the circuit pattern. Then hot press (at temperature 80°C and pressure 6 torr) is rolled over it. After every 3 minutes the level of circuit transfer is monitored. By hit and trial methods it is found that complete transference of the circuit pattern takes place at around 5 -7 minutes. The sample is then allowed to cool at room temperature. When the sample gets cool, it is kept in a water bath to remove the paper from the circuit pattern.

7.3.4 Etching with Ferric Chloride

A masking tape is placed on the bottom side of the metallized sample system exposing a circular hole of diameter 3 mm on the centre. To remove the unwanted copper from the circuit pattern the sample system is dipped in a slightly acidic ferric chloride ($FeCl_3$ + HCl) bath. A spinning movement to the ferric chloride solution is made for uniform etching of the copper. To prevent the sample from over etching, which may cause bad edging of the microstrip line, the concentration of ferric chloride solution is reduced with time. The whole system is then taken out from the solution and washed with distilled water to remove any traces of ferric chloride solution.

7.3.5 Removal of Mask

The mask of the microstrip circuit is removed by smoothly rubbing with tissue paper

dipped in kerosene oil. The tape on the bottom side is lifted carefully to release ground plane side. The edge of the microstrip circuit is confirmed under a traveling microscope. The photograph of the circuit pattern is shown in figure 7.4.
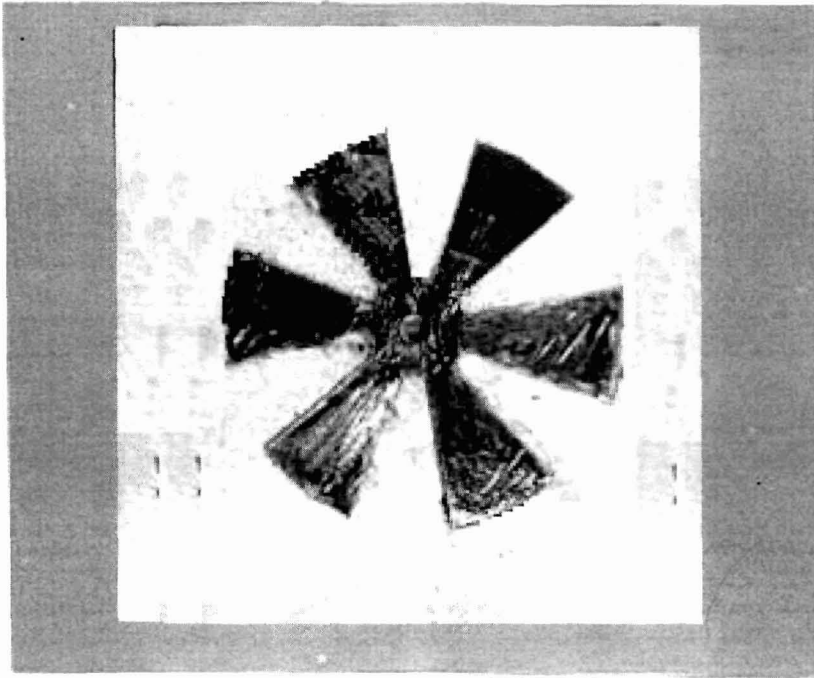
Figure 7.4: Photograph of the RRSR circuit configuration

7.4 RESULTS AND DISCUSSION

The resonator is designed to give reflection type characteristics. The basic parameters investigated are return loss, 3 dB band widths and the Q factor. The performance of the device is studied when all the radial stub ends are open, one of the stubs end is shorted at $\lambda_g/2$ and $\lambda_g/3$ and coupling pair of adjacent radial stubs.

The centre of the disc is coaxially fed port which acts as both input and output port. On sweeping frequency from 9.0 to 12.0 GHz, the resonant frequency of the device is found for two composite systems up to 3%VF. From the resonant frequency f_0 and the 3 dB band width (Δf) of the resonant peak, the loaded Q- factor is determined as

$Q = f_0/\Delta f$

144

7.4.1 Return Loss of Device for Open Stub, Shorting One Stub End at $\lambda_g/2$ and $\lambda_g/3$

Figures 7.5(a-c) and 7.6 (a-c) show the reflection behaviour of the circuit on PS-alumina and PS-titania composites. At the resonant frequency return loss is found to be minimum for 3%VF of filler (alumina/titania). This is because of the higher dielectric constant of the composite in comparison to others, which decreases the radiation from the sample. The symmetrical geometry provides balance in amplitude or phase of the output signal at any frequency.

The design frequency of the resonator is 10 GHz. Inspection of the plot shows that there is a ± 0.1 GHz shifting of the resonant frequency position. The variation may be due to the radiation loss associated with the fringing field at the circular edge of the disc.
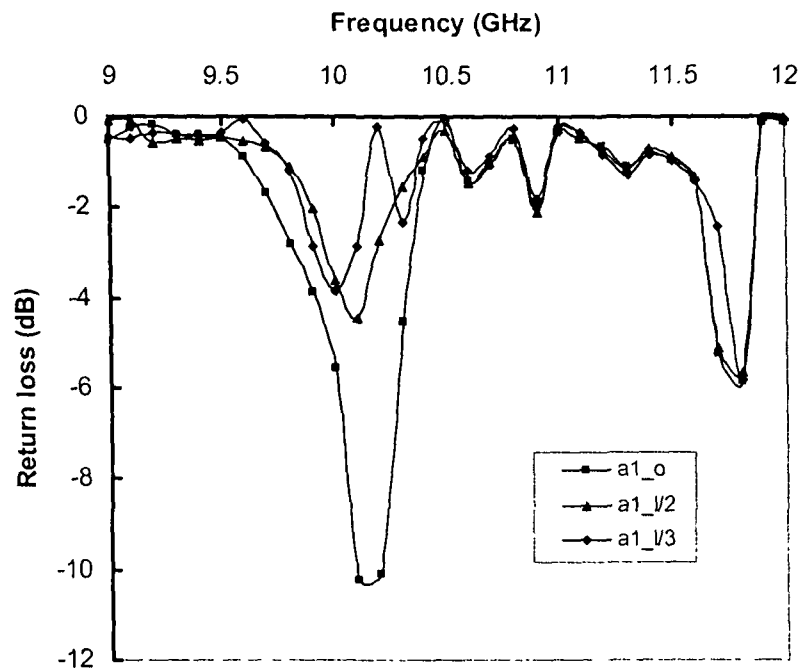

Figure 7.5a: Return loss plot of RRSR on 1%VF PS-alumina composite
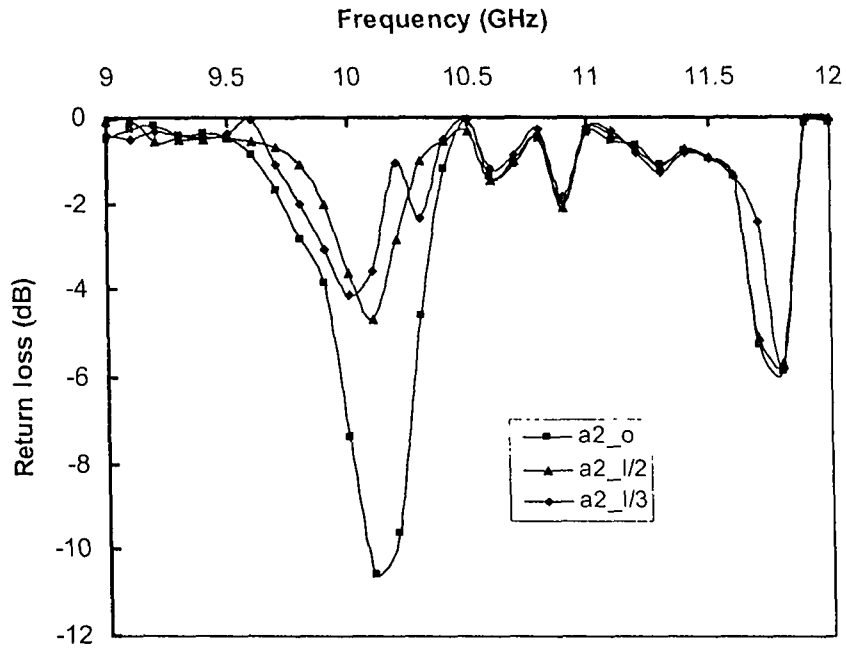
Figure 7.5b: Return loss plot of RRSR on 2%VF PS-alumina composite
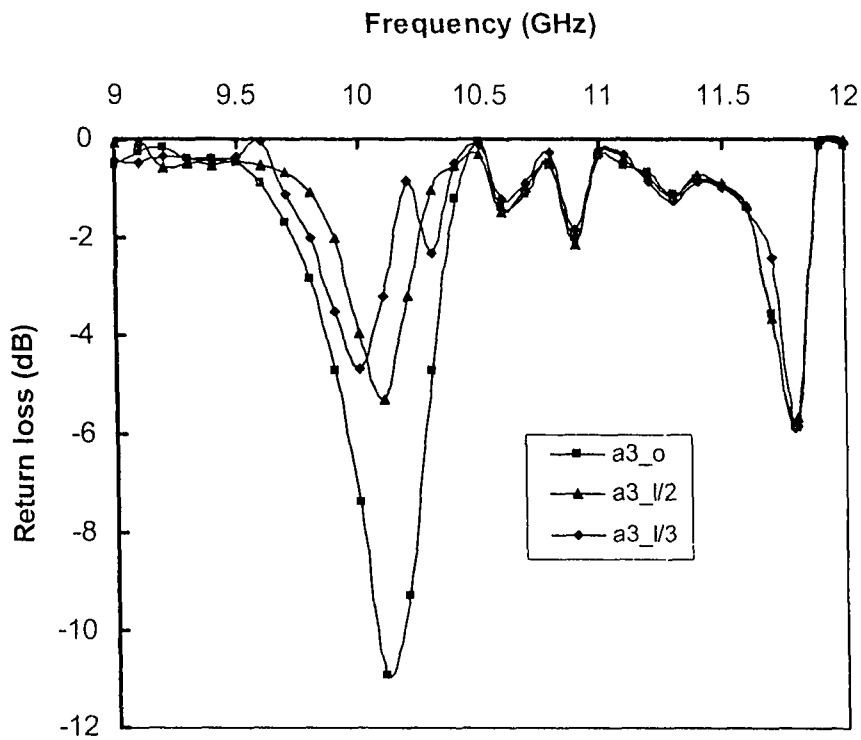
Figure 7.5c: Return loss plot of RRSR on 3%VF PS-alumina composite
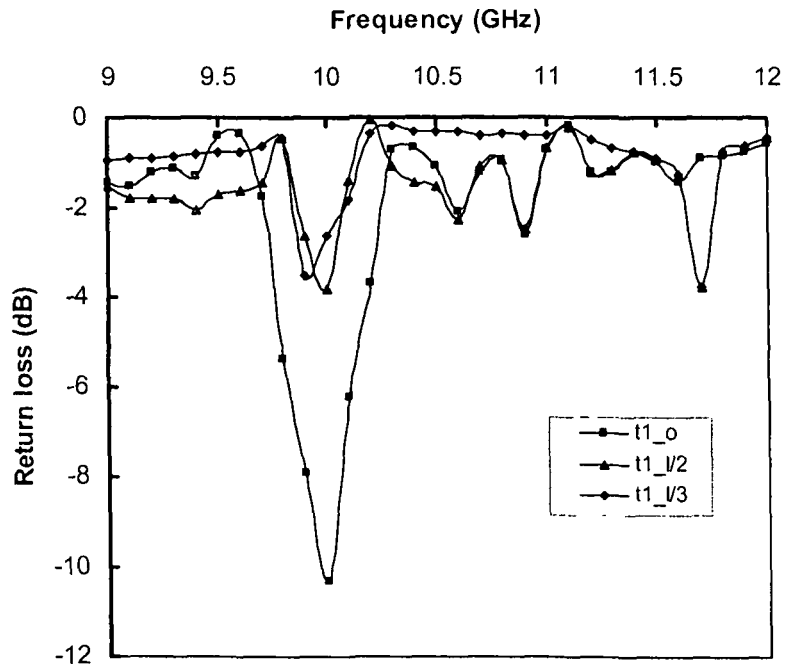
Figure 7.6a: Return loss plot of RRSR on 1%VF PS-titania composite
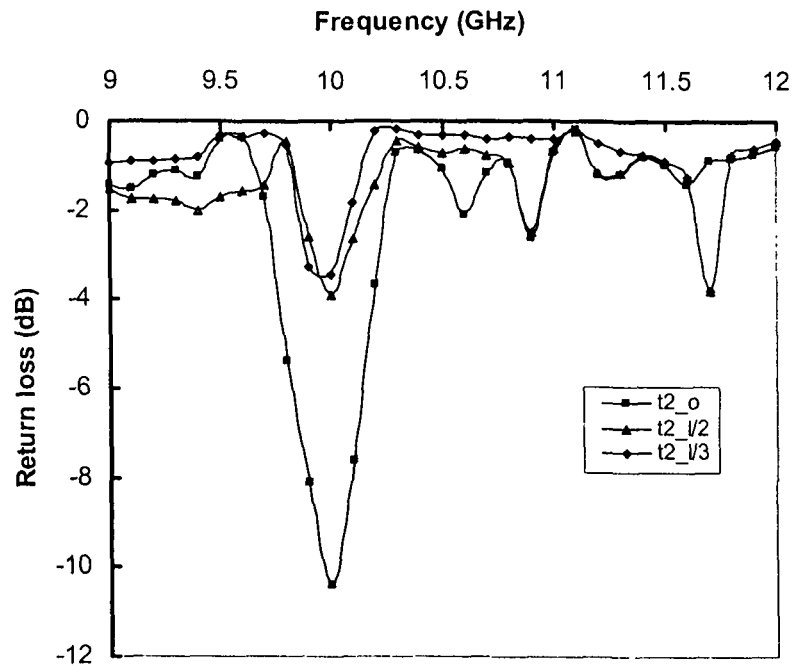
Figure 7.6b: Return loss plot of RRSR on 2%VF PS-titania composite
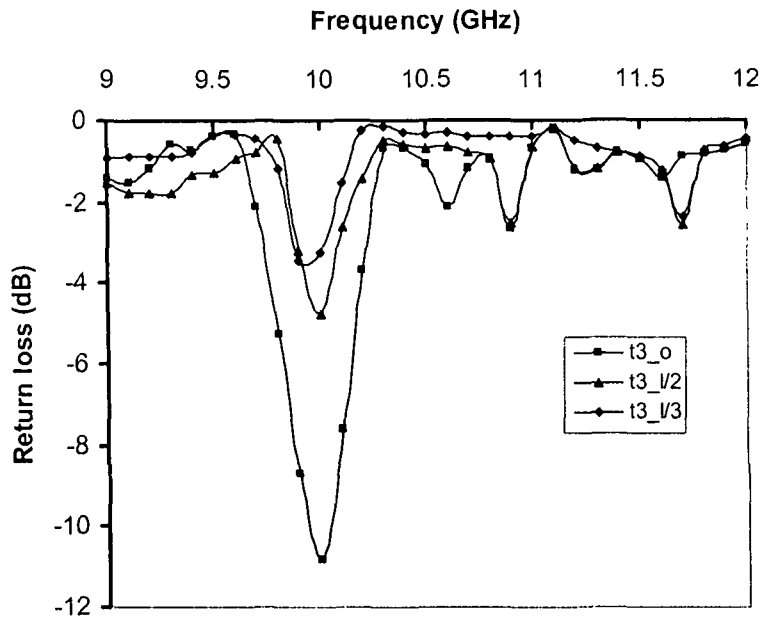
Frequency (GHz)

Figure 7.6c: Return loss plot of RRSR on 3%VF PS-titania composite

When one of the stubs end of the device is shorted at $\lambda_g/2$ and connected to a 50 Ω feeding point, it is observed from plots that the return loss increases. A shift in resonance frequency of 0.1GHz towards the higher frequency side is observed.

When one of the stubs end of the device is shorted at $\lambda_g/3$ and connected to a 50 Ω feeding point, a shift in resonance frequency of 0.2 GHz towards the lower frequency side is observed. It is observed from figure 7.5 and 7.6 that 3 dB band width of the device increases when one of the stubs is shorted at $\lambda_g/2$ in comparison to the device when stubs end are open. The band width is found to be maximum for the device where one end of the stubs is shorted at $\lambda_g/3$ for the same composite. With the increase in permittivity of the - substrate 3 dB band width of the resonator increases whereas the Q factor decreases as the radial line stubs can maintain low characteristic impedance for a wider range of frequency thus increasing the bandwidth of operation.

When the stubs ends are open it acts as the series reactance. The increase in band width of the device is obtained as a result of the interaction between the modes of resonance in circular disc structure [7]. This is due to excitation of higher order modes in

width direction of resonator. Table 7.2 shows the variation of return loss (RL), Q-factor and band width (BW) of RRSR with the increase in filler percentage when stubs are open. Variation of RL, BW and Q-factor of the device when stub is shorted at $\lambda_g/2$ and $\lambda_g/3$ are shown in table 7.3 and table 7.4 respectively.

Table 7.2: Return loss, band width and Q factor of RRSR when stubs are open

Sample		Resonant frequency (GHz)	Return loss (dB)	Q factor	Band Width (MHz)
PS-Alumina	1%VF	10.15	-10.40	44	230
	2%VF	10.12	-10.65	37	270
	3%VF	10.1	-11.10	34	290
PS-Titania	1%VF	10.0	-10.52	45	220
	2%VF	10.0	-10.6	40	250
	3%VF	10.0	-11.0	37	264

Table 7.3: Return loss, band width and Q factor of RRSR when one stub is shorted at $\lambda_g/2$

Sample		Resonant frequency (GHz)	Return loss (dB)	Q factor	Band Width (MHz)
PS-Alumina	1%VF	10.1	-4.25	28	360
	2%VF	10.1	-4.62	25	400
	3%VF	10.01	-5.00	23	424
PS-Titania	1%VF	10.0	-4.12	31	320
	2%VF	10.0	-4.15	27	360
	3%VF	10.0	-4.50	26	376

Table 7.4: Return loss, band width and Q factor of RRSR when one stub is shorted at $\lambda_g/3$

Sample		Resonant frequency (GHz)	Return loss (dB)	Q factor	Band Width (MHz)
PS-Alumina	1%VF	10.0	-3.89	22	440
	2%VF	10.0	-4.00	18	550
	3%VF	10.0	-4.4	18	555
PS-Titania	1%VF	9.9	-3.90	24	400
	2%VF	9.9	-3.90	24	400
	3%VF	9.9	-4.00	24	410

7.4.2 Return Loss of Device when Adjacent Radial Stubs are Coupled

Figures 7.7 (a - b) and 7.8 (a - b) show computed behavior of return loss versus frequency for microstrip radial stubs resonator on two composite systems when adjacent radial stubs of the device are coupled at $\lambda_g/2$ and connected to a 50 Ω feeding point. From the plot it is observed that return loss decreases when adjacent stubs are coupled at the resonant frequency but it starts increasing in the higher frequency side.
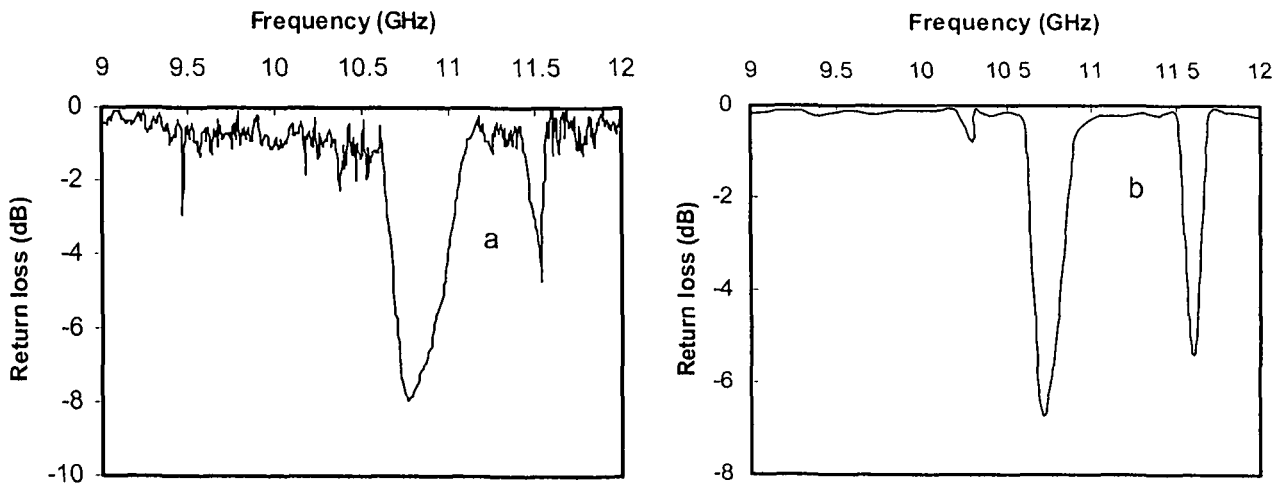
Figure 7.7: Return loss of RRSR on a) 1%VF, b) 2%VF PS-alumina composite when adjacent radial stubs are coupled
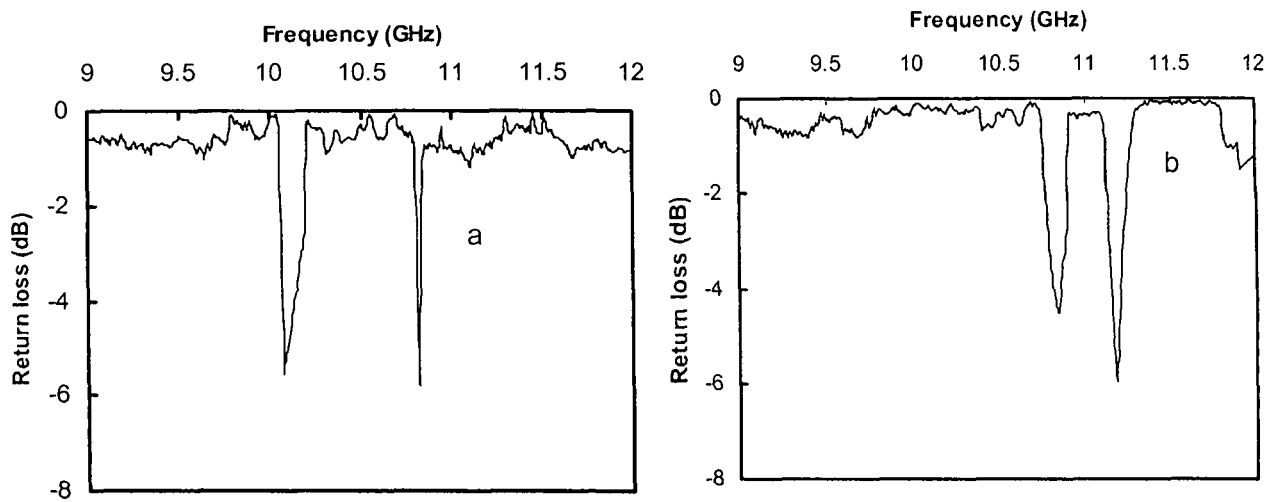
Figure 7.8: Return loss of RRSR on a) 1%VF, b) 2%VF PS-titania composite when adjacent radial stubs are coupled

Table 7.5 shows the variation of Q, return loss, Q-factor and band width with the increase in filler percentage. The band width of the structure is higher in resonant frequency side.

Table 7.5: Return loss, Band width and Q factor of devices when adjacent stubs are coupled at $\lambda_g/2$

Sample		Resonant frequency (GHz)	Return loss (dB)	Q factor	Band Width (MHz)
PS-Alumina	1%VF	10.72	-6.55	63	170
	2%VF	10.6	-5.42	58	180
PS-Titania	1%VF	10.07	-5.56	77	130
	2%VF	10.85	-4.52	77	140

Results show that band width can be varied by changing the material characteristics and shorting the radial stubs at different lengths. The radial structure reduces the existence of excessive spurious losses. RRSR works better than straight stubs when an accurate localization of zero-point impedance is needed. The device can be used as fine tuning element.

151

SDTMC, spectral domain technique modified for composite developed in chapter V, will be modified in spherical co-ordinate to analyze the field distribution in the microstrip reflection type radial stub resonator.

7.5 CONCLUSION

It can be observed from the experiments that reflected resonator fabricated on different substrates of thickness 0.6 mm, a resonator like characteristic which can be used as a tuning element is observed. The resonator shows higher return loss when all stubs are shorted at $\lambda_g/3$ with higher band width. A simple design has been used in fabrication of reflection type resonator which does not have end effects. Shorting of the stubs at different lengths, give less return loss. It can be used for a broad band application which can be tuned at different frequency.

References:

[1] F. Giannini and R. Sorrentino, "Planar Circuit Analysis of Microstrip Radial Stub," IEEE Trans Microwave Theory and Techniques, vol. 32, pp- 1652, 1984.

[2] K. C. Gupta and M. D. Abouzahra, "Analysis and Design of Four-Port and Five-Port Microstrip Disc Circuits," IEEE Trans Microwave Theory and Techniques, vol. 33, pp- 1422, 1985.

[3] M. D. Abouzahra and K. C. Gupta, "Multiple-Port Power Divider/Combiner Circuits Using Circular Microstrip Disk Configurations," IEEE Trans Microwave Theory and Techniques, vol. 35, pp- 1296, 1987.

[4] V. A. Dmitriev and C. A. João Weyl Costa, "Theoretical Investigation of Compact Microstrip Resonators with Stubs for Patch Antennas," IEEE Trans Microwave Theory and Techniques, vol. 50, pp- 27, 2002.

[5] K. Chang, I. Bahl and V. Nair, "RF and Microwave Circuit and Component Design for Wilreless Systems", Wiley Interscience, USA, 2002.

[6] I. Wolff and N. Knoppik, "Rectangular and Circular Microstrip Disk Capacitors and Resonators," IEEE Trans Microwave Theory and Techniques, vol. 22, pp- 857, 1974.

[7] K. C. Gupta and M. D. Abouzahra, "Analysis and Design of Four-Port and Five-Port Microstrip Disc Circuits," IEEE Trans Microwave Theory and Techniques, vol. 33, pp- 1422, 1985.

CHAPTER VIII

ACHIEVEMENTS, LIMITATIONS AND FUTURE DIRECTIONS

The present research puts forth the various aspects of ceramic particle reinforced polymer composite by regulating the filler percentage and its micro structural properties to develop polymer composites which can be used as substrate material for microwave applications. It also exemplifies the diverse properties which can be tailored to get a good microwave device performance on such a substrate. The key findings of the present work are mentioned below.

New microwave transmission media polystyrene-alumina and polystyrene–titania, polymer composite systems are fabricated for better suitability in microwave device applications. Microwave properties of the composites are studied in C- and X-bands by varying the reinforce particles from 1-7%VF.

Microstructural studies of PS-alumina and PS-titania systems show that the composite systems are homogenous. Alumina and titania particles get confined in the polystyrene matrix and the size of the filler particles are 3 micron and 1 micron respectively which is quiet smaller than the minimum probing wavelength thus reducing attenuation due to scattering. An enhanced thermal conductivity and improved dimensional stability is observed with increase in reinforced particle content. Both the composite systems show increase compactness and no water absorbance.

Complex permittivity of the PS-alumina composite system increases from 2.5 to 2.785 at X-band as the filler percentage increases from 0%VF to 7%VF. An increase of permittivity of 2.5 to 3.338 is observed in PS-titania composite for same change in %VF of the filler. A dispersion of 0.31 to 0.39% in permittivity is observed in PS-alumina composite on sweep frequency measurement from 8.4 to 12.0 GHz. A dispersion of 0.60 to 0.69% in real part of permittivity of PS-titania composite is observed.

In PS-alumina composite the loss factor varies in the range 0.004-0.016 and in PS-titania it varies from 0.0036 to 0.005. The loss factor measurements show a nominal increase with the increase in filler percentage in both the composite systems.

154

Using dispersion model, microstrip line is designed at 10 GHz on both the composite systems. Propagation constant, attenuation constant and insertion loss of the device fabricated are determined. The measurement conducted in C-band show that the material is not suitable for devices designed in 3 to 6 GHz. From the propagation constant measurement, it is observed that with the increase in filler percentage propagation constant in the both the composites increase. The insertion loss of the device on both the composites substates decreases with increase in filler percentage.

Spectral domain technique modified for composites (SDTMC) shows better agreement for composite materials where the substrate is taken as a combination of two dielectric media with largely different dielectric constant as compare to conventional spectral domain technique (SDT) where substrate is taken with one permittivity.

Microstrip reflection-type radial stub resonator (RRSR), a novel geometry for efficient signal transition between circuit layers on the composite, is designed and fabricated on both the composite systems. RRSR can maintain low characteristic impedance for a wider range of frequency thus increasing the band width of operation. The resonator shows good reflection type characteristics with high band width and nominal Q-values. A simple mechanism of shorting the resonator at different stub length affirmed its comprehensive utility for different band width and fine tuning.

Investigation on the two composite systems illustrates the possibility of using these materials as substrate for microwave devices and also gives a possibility of using particulate composite systems for microwave devices.

Optimizing the filler percentage and surfactant quantity composites of higher permittivity can be fabricated. The desired properties of the composite substrates can be obtained by controlled mixing of alumina and titania. Experimental investigation of shape and size dependent complex permittivity will provide further scope for research.

By changing the matrix, instead of polystyrene, whose dielectric constant is higher than PS and losses are smaller, the permittivity of the composite can be increased. There is a plan to study these polymer composites for MMIC's. For this semiconductor fillers will be used as the reinforced particle in the polymer matrix. Investigation of the effect of magnetic fillers like ferrites in the polymer matrix, plastoferrites has tremendous future aspect. SDTMC will be modified in spherical co-ordinate to analyze the field distribution in the microstrip reflection type radial stub resonator.

The present investigation provides a wide scope for improvement of the materials and design for microstrip devices. As evident from the studies on microstrip devices that the microstrip losses lowering the Q-value. The main contributions in the losses are the surface loss and conductor loss. Since gold is good conductor than copper which is used in present investigation, an improvement on Q-factor can be made by using gold conducting strips. Better techniques of using connectors with thermal compression bonding will further improve the insertion loss than the pressure contacts as used in the present investigation.

PC BASED MICROWAVE MEASUREMENT SETUP SOFTWARE
by
Juti (5.5.2003)

```c
#include<stdio.h>
#include<conio.h>
#include<math.h>

main()
{
FILE *physics,*physics1,*physics2;
float digit,mm,freq,mmcal[128],fcal[128],rr,rr1,r,fstart,micmt,fend;
float stepno,freqnew,freqstep,fprev,fincr=0.05;
int result,digit1,digit2,digit3,digit4,divider,sign;
int k,movenext,steptot,stepint,stepinit,p,stepf[9],motstep,stepnext;
int porti = 889;  /* input port address */
int porto=0X378;  /* output port address */
int x=3;   /*delay*/
/********** motor sequence *********/
stepf[1]=1;
stepf[2]=3;
stepf[3]=2;
stepf[4]=6;
stepf[5]=4;
stepf[6]=12;
stepf[7]=8;
stepf[8]=9;
/*********open input-output files*****************/
clrscr();
physics1=fopen("juti8.dat","w+");
physics2=fopen("calf1.dat","r");
/************read calibration data from file********/
for(p=1;p<=126;p++)
    {
```

```c
    fscanf(physics2,"%f%f",&mmcal[p],&fcal[p]);
 }
fclose(physics2);
/************input measurement freq range**********/
   printf("enter start frequency:" ,fstart);
   scanf("%f",&fstart);
   printf("enter end frequency:" ,fend);
   scanf("%f",&fend);
/**************go to start frequency*****************/
freq=fcal[1];
fprev=fstart-fincr;
for(p=1;p<=126;p++)
 {
   if(fprev<=fcal[p] )
       /*********** micrometer reading **********/
   {
       micmt=(fprev-fcal[p-1])*(mmcal[p-1]-mmcal[p])/(fcal[p-1]-fcal[p])+mmcal[p-1];
       stepno=(510.0*2.0)*(16.5-micmt);
       stepinit=stepno;
        if ((stepno-stepinit)>=0.5)
         {
           stepinit=stepinit+1;
           }
          p=127;
        }
   }


/***************rotate motor to fstart*****************/
   outport (porto,stepf[8]);
   k=0;
   for (motstep=1;motstep<=stepinit;motstep++)
   {
       k=k+1;
       if (k==9)
       {
         k=1;
         }
```

```c
        outport(porto,stepf[k]);
        delay(x);
    }
    steptot=stepinit;
                    /*** motor status = k ******************/
                    /*** steps to start freq = stepinit******/
sound(300);
delay(200);
nosound();
delay(3000);


/*******************************************************************/
/****************MAIN MEASUREMENT MODULE**************************/
/*******************************************************************/
for (freq=fstart;freq<=fend+fincr;freq=freq+fincr)
{
  /**********find next motor position************************/
  for(p=1;p<=126;p++)
    {
      if(freq<=fcal[p] )
          /*********** micrometer reading **********/
          {
            micmt=(freq-fcal[p-1])*(mmcal[p-1]-mmcal[p])/(fcal[p-1]-fcal[p])+mmcal[p-1];
            stepno=(510.0*2.0)*(16.5-micmt);
            stepint=stepno;
            if ((stepno-stepint)>=0.5)
             {
               stepint=stepint+1;
             }
            p=127;
          }
    }
    /********* calculate freq from integral step no *********/
      mm=16.5-(stepint/(2.0*510.0));
        for(p=1;p<=126;p++)
          {
          if(mm>=mmcal[p])
```

```
        {
        rr= (fcal[p]-fcal[p-1]);
        rr1=(mmcal[p]-mmcal[p-1]);
        r=(rr/rr1);
        freqnew=(r*(mm-mmcal[p-1]))+fcal[p-1];
        p=127;
        }
    }


/*********** rotate motor to next measurement freq ***********/
    stepnext=stepint-stepinit;
    steptot=steptot+stepnext;
    stepinit=stepint;
    for (movenext=1;movenext<=stepnext;movenext++)
    {  k=k+1;
        {
        if (k==9)
        {
        k=1;
        }
        outport(porto,stepf[k]);
        delay(x);
        }
    }
    /***"stepint" and "steptot" are basically the same-check*****/
sound(500);
delay(300);
nosound();


/***************** start power meter reading *********************/
    delay(1000);
    outport(porto,48+stepf[k]);
    delay(x);
    result = inport(porti);
    if (result==0xC70)
      digit1=0;
    if (result==0xC00)
```

iv

```
     digit1=1;
  if (result==0xC68)
    digit1=2;
  if (result==0xC48)
    digit1=3;
  if (result==0xC18)
    digit1=4;
  if (result==0xCD8)
    digit1=5;
  if (result==0xCF8)
    digit1=6;
  if (result==0xC40)
    digit1=7;
  if (result==0xC78)
    digit1=8;
  if (result==0xC58)
    digit1=9;
    delay(x);
  outport(porto,32+stepf[k]);
  delay(x);
  result = inport(porti);
   if (result==0xC70)
     digit2=0;
   if (result==0xC00)
     digit2=1;
   if (result==0xC68)
     digit2=2;
   if (result==0xC48)
     digit2=3;
   if (result==0xC18)
     digit2=4;
   if (result==0xCD8)
     digit2=5;
   if (result==0xCF8)
     digit2=6;
   if (result==0xC40)
     digit2=7;
```

```
if (result==0xC78)
  digit2=8;
if (result==0xC58)
  digit2=9;
outport(porto,16+stepf[k]);
 delay(x);
 result = inport(porti);
 if (result==0xC70)
  digit3=0;
 if (result==0xC00)
  digit3=1;
 if (result==0xC68)
  digit3=2;
 if (result==0xC48)
  digit3=3;
 if (result==0xC18)
  digit3=4;
 if (result==0xCD8)
  digit3=5;
 if (result==0xCF8)
  digit3=6;
 if (result==0xC40)
  digit3=7;
 if (result==0xC78)
  digit3=8;
 if (result==0xC58)
  digit3=9;
outport(porto,0+stepf[k]);
 delay(x);
 result = inport(porti);
 if (result==0xCB8)
 {
  sign=(-1);
  digit4=1;
  divider=1000;
 }
 if (result==0xC18)
```

```
   {
    sign=-1;
    digit4=1;
    divider=100;
     }
  if (result==0xCD8)
   {
    sign=-1;
    digit4=1;
    divider=10;
     }
  if (result==0xCA8)
   {
    sign=-1;
    digit4=0;
    divider=1000;
     }
  if (result==0xC08)
   {
    sign=-1;
    digit4=0;
    divider=100;
     }
  if (result==0xCC8)
   {
    sign=-1;
    digit4=0;
    divider=10;
     }
  if (result==0xCB0)
   {
    sign=1;
    digit4=1;
    divider=1000;
     }
  if (result==0xC10)
   {
```

```c
  sign=1;
  digit4=1;
  divider=100;
   }
if (result==0xCD0)
 {
  sign=1;
  digit4=1;
  divider=10;
   }
if (result==0xCA0)
 {
  sign=1;
  digit4=0;
  divider=1000;
   }
if (result==0xC00)
 {
  sign=1;
  digit4=0;
  divider=100;
   }
if (result==0xCC0)
 {
   sign=1;
   digit4=0;
   divider=10;
    }
digit=digit1+(10*digit2)+(100*digit3)+(1000*digit4);
digit=(sign*digit/divider);
/********PRINT DATA TO FILE***************/
printf("%.3f\t%.3f\t%.3f\t%d\n",freq,freqnew,digit,sign);
fprintf(physics1,"%.3f\t%.3f\n",freq,digit);


}


/*****************************************************************/
```

```c
/****close files********************/
fclose(physics1);
sound(500);delay(300);nosound();
sound(500);delay(300);nosound();

/*****return micrometer to initial position**********/
for (movenext=1;movenext<=steptot;movenext++)
 { k=k-1;
   {
    if (k==0)
     {
      k=8;
         }
     outport(porto,stepf[k]);
     delay(2);
     printf("Step No=%d\t%d\n",(steptot-movenext),stepf[k]);
    }
  }

outport(porto,0);
sound(500);
delay(500);
nosound();
getch();
return(0);
}
```

PROGRAM FILE- MSDT.C FOR NUMERICAL DETERMINATION OF PROPAGATION CONSTANT ON A MICROSTRIP LINE ON COMPOSITE SUBSTRATE

by

Juti (Feb, 2004)

```c
#include<stdio.h>
#include<math.h>
#include<conio.h>
main()
{
  float G11, G12, G21,G22, N21, N22, N41,N42;
  float DEL, K11,S,C,AL,OMEGA,BETA,GAMAP;
  float X11,X12,X13,X14,X21,X22,X23,X24,X31,X32,X33,X34,X41,X42,X43,X44;
  float Y11,Y12,Y13,Y14,Y21,Y22,Y23,Y24,Y31,Y32,Y33,Y34,Y41,Y42,Y43,Y44;
  float Z11,Z12,Z13,Z14,Z21,Z22,Z23,Z24,Z31,Z32,Z33,Z34,Z41,Z42,Z43,Z44;
  float L11,L12,L13,L14,L21,L22,L23,L24,L31,L32,L33,L34,L41,L42,L43,L44;
  float a11,a12,a13,a14,a21,a22,a23,a24,a31,a32,a33,a34,a41,a42,a43,a44;
  float A11,A12,A13,A14,A21,A22,A23,A24,A31,A32,A33,A34,A41,A42,A43,A44;
  float p11,p12,p13,p14,p21,p22,p23,p24,p31,p32,p33,p34,p41,p42,p43,p44;
  float pc11,pc12,pc13,pc14,pc21,pc22,pc23,pc24,pc31,pc32,pc33,pc34,pc41,pc42,pc43,
        pc44, DET,p2, T, kp,p1,ep,s,c, A, KA, GAMAA,Y, EPSILONA, FREQUENCY;
  float q1,q2, g, gx, ef, GAMAF, kpf, jz, sjz, w,GAMA,sum, pc, GAMAC,kpc;
  int N;
  /************************ Data input *******************/
  FREQUENCY=10.2; /* operating frequency*/
  EPSILONA =1.0;
  A=8.0;
  Y=100.0;
  T=0.6; ,  /* thickness of the substrate*/
  p1=0.001; /* inter particle distance*/
  ep=2.5;   /* dielectric constant of polymer */
  p2=0.001; /* size of the filler particle*/
  ef=99.0; /* dielectric constant of filler */
```

```
N=1067;      /* number of filler particle*/

w=1.668;    /* width of the microstrip line*/

pc=2.6;    /* dielectric constant of the composite */
/*****************************************************************************/
/*********************************MAIN MODULE*********************************/
for( BETA=0.89,BETA<=0.9;BETA=BETA+0.001)

{
AL=(0.5*3.141/A);   /********* A IS THE LENGTH OF THE SAMPLE*********/

OMEGA=(2*3.141*FREQUENCY/300);

KA=sqrt(OMEGA*OMEGA*EPSILONA);

GAMAA=sqrt((AL*AL)+(BETA*BETA)-(KA*KA));

kp=sqrt((OMEGA*OMEGA*ep));

GAMAP=sqrt(((AL*AL)+(BETA*BETA)-(kp*kp)));

kpf=sqrt(OMEGA*OMEGA*ef);

GAMAF=sqrt((kpf*kpf)-((AL*AL)+(BETA*BETA));

/**************Determination of coefficient for polymer layer*********/

A11=((kp*kp)-(BETA*BETA))*(sinh(GAMAP*p1));

A23=a11;

A12=((kp*kp)-(BETA*BETA))*(cosh(GAMAP*p1));

a24=a12;

a31=(-1)*(AL)*(sinh(GAMAP*p1));

a43=a31;

a32=(-1)*(AL)*(cosh(GAMAP*p1));

a32=a44;

a33=(-1)*(OMEGA*GAMAP/BETA)*(cosh(GAMAP*p1));

a34=(OMEGA*GAMAP/BETA)*(sinh(GAMAP*p1));

a41=((OMEGA*GAMAP*ep)/BETA)*(cosh(GAMAP*p1));

a42=((OMEGA*GAMAP*ep)/BETA)*(sinh(GAMAP*p1));

/**************Determination of coefficient for filler layer**********/

p11= ((kp*kp)-(BETA*BETA))*(sinh(GAMAP*p2));

p23=p11;

p12=((kp*kp)-(BETA*BETA))*(cosh(GAMAP*p2));

p24=p12;

p31=(-1)*(AL)*(sinh(GAMAF*p2));

p43=p31;

p32=(-1)*(AL)*(cosh(GAMAF*p2));

p32=p44;
```

```
p33= (-1)*(OMEGA*GAMAF/BETA)*(cosh(GAMAF*p2));
p34=(OMEGA*GAMAF/BETA)*(sinh(GAMAF*p2));
p41=((OMEGA*GAMAF*ef)/BETA)*(cosh(GAMAF*p2));
p42=((OMEGA*GAMAF*ef)/BETA)*(cosh(GAMAF*p2));
/***********Determination of determinant for one polymer filler unit********/
DET=(((p12*p31)-(p11*p32))*((p23*p44)-(p24*p43)))+(((p11*p42)-(p12*p41))*((p23*p34)-
    (p24*p33)));
/**************** Determination of cofactor for inverse calculation******/
pc11=(-1)*(p23*p32*p44)+(p23*p34*p42)+(p24*p32*p43)-(p24*p33*p42);
pc12=p23*((p31*p44)-(p34*p41))-(p24*((p31*p43)-(p33*p41)));
pc13=p24*((p31*p42)-(p32*p41));
pc14=(-1)*p23*((p31*p42)-(p32*p41));
pc21=(-1)*p12*((p33*p44)-(p34*p43));
pc22=p11*((p33*p44)-(p34*p43));
pc23=p12*((p31*p44)-(p34*p41))-p11*((p32*p44)-(p34*p42));
pc24=p11*((p32*p43)-(p33*p42))-p12*((p31*p43)-(p33*p41));
pc31=p12*((p23*p44)-(p24*p43));
pc32=(-1)*p11*((p23*p44)-(p24*p43));
pc33=p24*((p12*p41)-(p11*p42));
pc34=p23*((p11*p42)-(p12*p41));
pc41=p12*((p24*p33)-(p23*p34));
pc42=p11*((p23*p34)-(p24*p33));
pc43=p24*((p11*p32)-(p12*p31));
pc44= p23*((p12*p31)-(p11*p32));
/****************Determination of matrix element of the inverse matrix*****************/
A11=(pc11/DET); A12=(pc21/DET); A13=(pc31/DET); A14=(pc41/DET);
A21=(pc12/DET); A22=(pc22/DET); A23=(pc32/DET); A24=(pc42/DET);
A31=(pc13/DET); A32=(pc23/DET); A33=(pc33/DET); A34=(pc43/DET);
A41=(pc14/DET); A42=(pc24/DET); A43=(pc43/DET); A44=(pc44/DET);
/***************Calculation of the element of the transpose matrix********/
L11=((a11*A11)+(a12*A21));
L12=((a11*A12)+(a12*A22));
L13=((a11*A13)+(a12*A23));
L14=((a11*A14)+(a12*A24));
L21=((a23*A31)+(a24*A41));
L22=((a23*A32)+(a24*A42));
L23=((a23*A33)+(a24*A43));
```

```
L24=((a23*A34)+(a24*A44));
L31=(a31*A11)+(a32*A21)+(a33*A31)+(a34*A41);
L32=(a31*A12)+(a32*A22)+(a33*A32)+(a34*A42);
L33=(a31*A13)+(a32*A23)+(a33*A33)+(a34*A43);
L31=(a31*A14)+(a32*A24)+(a33*A34)+(a34*A44);
L41= (a41*A11)+(a42*A21)+(a43*A31)+(a44*A41);
L42= (a41*A12)+(a42*A22)+(a43*A32)+(a44*A42);
L43= (a41*A13)+(a42*A23)+(a43*A33)+(a44*A43);
L44= (a41*A14)+(a42*A24)+(a43*A34)+(a44*A44);


/*********************Determination of the final matrix***************/
kpc=sqrt(OMEGA*OMEGA*pc);
GAMAC=sqrt(((AL*AL)+(BETA*BETA)-(kpc*kpc)));
S=sinh((GAMAC)*T);
C=cosh((GAMAC)*T);
K11=(((kpc)*(kpc))-(BETA*BETA));
X11=(K11*N*L11*S)+(K11*N*L21*C);
X12=(K11*N*L12*S)+(K11*N*L22*C);
X13=(K11*N*L31*S)+(K11*N*L23*C);
X14=(K11*N*L34*S)+(K11*N*L24*C);
X21= (K11*N*L31*S)+(K11*N*L41*C);
X22=(K11*N*L32*S)+(K11*N*L42*C);
X23=(K11*N*L33*S)+(K11*N*L43*C);
X24=(K11*N*L34*S)+(K11*N*L44*C);
X31=(AL*(N*L11*S+N*L21*C)-((OMEGA*GAMAF/BETA)*(N*L31*C+N*L41*S)));
X32=(AL*(N*L12*S+N*L22*C)-((OMEGA*GAMAF/BETA)*(N*L32*C+N*L42*S)));
X33=(AL*(N*L13*S+N*L23*C)-((OMEGA*GAMAF/BETA)*(N*L33*C+N*L43*S)));
X34=(AL*(N*L14*S+N*L24*C)-((OMEGA*GAMAF/BETA)*(N*L34*C+N*L44*S)));
X41=(AL*(N*L31*S+N*L41*C)+((OMEGA*GAMAF*ep/BETA)*(N*L31*C+N*L41*S)));
X42=(AL*(N*L32*S+N*L42*C)+((OMEGA*GAMAF*ep/BETA)*(N*L32*C+N*L42*S)));
X43=(AL*(N*L33*S+N*L43*C)+((OMEGA*GAMAF*ep/BETA)*(N*L33*C+N*L43*S)));
X44=(AL*(N*L34*S+N*L44*C)+((OMEGA*GAMAF*ep/BETA)*(N*L34*C+N*L44*S)));
Y12= ((KA*KA)-(BETA*BETA));
Y24= ((KA*KA)-(BETA*BETA));
Y32= exp((-1)*GAMAA*T);
Y34= (-1)*(OMEGA*GAMAA/BETA)*exp((-1)*GAMAA*(Y-T));
Y42= (OMEGA*GAMAA*EPSILONA/BETA)*exp((-1)*GAMAA*(Y-T));
```

```
Y44= (AL exp((-1) GAMMA (1-1)));
Q1=((X11*X24*Y32*Y44)+(X11*X34*Y24*Y42)+(X14*X21*Y34*Y42)+(X14*X41*Y24*Y32)
   +(X21*X34*Y12*Y44)+(X24*X41*Y12*Y34)+(X31*X44*Y12*Y24));
Q2=((X11*X24*Y34*Y42)+(X11*X44*Y24*Y32)+(X14*X21*Y32*Y44)+(X31*X14*Y42*Y24)
   +(X21*X44*Y12*Y34)+(Y12*Y44*X24*X31)+(X34*X41*Y12*Y24));
DEL= Q1-Q2;

/************************* Generation of the Greens function*************/
Z21=((-1)*X14*(Y32*Y44-Y34*Y42))-(Y12*((X44*Y34)-(X34*Y44)));
Z22=(X11*((Y32*Y44)-(Y42*Y34)))-(Y12*(X31*Y44)+(X41*Y34));
Z41=((X14*Y24*Y32)-(Y12*((X34*Y24)-(X24*Y34))));
Z42=(Y12*((X31*Y24)-(X21*Y34))-(X11*Y24*Y32));
N21=(Z21/DEL);
N22=(Z22/DEL);
N41=(Z41/DEL);
N42=(Z42/DEL);
G11=(-(N21*X11+N22*X34));
G12=(N41*X11+N42*X34);
G21=(-(N21*X31+N22*X34));
G22=(N41*X32+N42*X34);

/******************** Fourier transform of the current density******/
jz=((2/AL)*(sin((AL*w)/2)));
sjz=(jz*jz);
sum=((G12*sjz));
printf("sum=%f\tBETA=%f\n",sum,BETA);
}
getch();
return(0);
```

Publications List

Published in Journals

1. Juti R. Deka and Nidhi S. Bhattacharyya, "Measurement of Complex Permittivity of Polymer Sample with Cavity Resonator Using Perturbation Technique", Indian Journal of Pure & Applied Physics (In Press).

2. Juti R. Deka, N. S. Bhattacharyya and S. Bhattacharyya, "Development of a Low Cost Automated PC-Based Insertion Loss Measurement Setup Using a Simple Source and Detector in X-Band", Journal of Measurement Science and Technology (Communicated).

3. Juti R. Deka and N. S. Bhattacharyya "Thermal Conductivity and Thermal Stability Studies of Alumina Reinforced Polystyrene for Microwave Applications", Physica Stata Solidi (Communicated).

4. Juti R. Deka and N. S. Bhattacharyya, "Improvement in Thermal Properties on Addition of Titania-Filler in Polystyrene Matrix", European Polymer Journal (Communicated).

Published in Conference Proceedings

1. Juti R. Deka and Nidhi S. Bhattacharyya, "Microwave sensing of moisture in wood tissue," Proc. 3rd Regional Conference on Physics Research in the North-East, pp. 38-43, Nov 9, 2002.

2. Juti R. Deka and Nidhi S. Bhattacharyya "Microwave Permittivity Studies on a Novel Composite Material–Polyester/alumina for application as Substrate in MIC/MMIC", Proc. National Symposium on Antennas and Propagations, 9-11 Dec., 2002, Kochi.

3. Juti R. Deka and Nidhi S. Bhattacharyya, "Microwave Frequency Dispersion in Polymer –Ceramic Composite", Proc. 14th AGM & Theme Symposium on Novel Polymeric Materials, 11-13 Feb., 2003, BARC, Mumbai.

4. Juti R. Deka and Nidhi S. Bhattacharyya, "Microwave Characterisation of New Composite-Alumina Graded Polystyrene Samples", Proc. National Conference on Materials, Components and Applications (MCA-2003), 15-16 Feb., 2003, Bhubaneswar, Orissa.

5. Juti R. Deka and Nidhi S. Bhattacharyya, "Novel Polymer Composite Material for Application as Substrate in Microwave Integrated Circuits", International Conference on Computers and Devices for Communication (CODEC 04), 1-3 January, 2004.